U.S. DEPARTMENT OF ENERGY

Office of ENERGY EFFICIENCY & RENEWABLE ENERGY

Operating Lifetime Study of Ultraviolet (UV) Light-Emitting Diode (LED) Products

U.S. Department of Energy—Lighting R&D Program

April 2022

(This page intentionally left blank)

Disclaimer

Authors

The authors of this report are all from RTI International:

J. Lynn Davis

Kelley Rountree

Roger Pope

Clint Clayton

Abdal Wallace

Karmann Riter

Andrew Dart

Michelle McCombs

Acknowledgments

This material is based upon work supported by the U.S. Department of Energy's Office of Energy Efficiency and Renewable Energy (EERE) under the National Energy Technology Laboratory (NETL) Mission Execution and Strategic Analysis (MESA) contract, award number DE-FE0025912.

List of Acronyms

5090	storage test conducted at 50°C and 90% RH
°C	degree Celsius
λ_{max}	nominal maximum emission wavelength
Ω	ohm
A	amps
A/cm^2	amps per square centimeter
AFM	atomic force microscopy
Ag	silver
Al	aluminum
AlGaN	aluminum gallium nitride
AlN	aluminum nitride
ANSI	American National Standards Institute
Au	gold
D1	diode with higher turn-on voltage in the test circuit
D2	diode with lower turn-on voltage in the test circuit
dc	direct current
DLTS	deep-level transient spectroscopy
DOE	U.S. Department of Energy
DUT	device under test
EERE	Office of Energy Efficiency and Renewable Energy
ft	feet, foot
GaN	gallium nitride
GUV	germicidal UV
hr, hrs	hour, hours

IES	Illuminating Engineering Society
I_f	forward current
In	indium
InGaN	indium gallium nitride
IR	infrared
I-V	current-voltage
K	Kelvin
LED	light-emitting diode
LPMV	low-pressure mercury vapor
LSRC	LED Systems Reliability Consortium
MΩ	megaohm
m	meter
mA	milliampere
MC-PCB	metal-core printed circuit board
MESA	Mission Execution and Strategic Analysis
mp-LED	mid-power LED
mW	milliwatt
MW	megawatt
NETL	National Energy Technology Laboratory
nm	nanometer
RFM	radiant flux maintenance
RH	relative humidity
R_{serial}	serial resistance
RTOL	room-temperature operating life
RTOL-1	RTOL study conducted on all products at I_f values approaching the specified maximum for the product

RTOL-2	RTOL study conducted on all products at mid-range values of I_f for each product
SARS-CoV-2	severe acute respiratory syndrome coronavirus 2
SIMS	secondary ion mass spectrometry
SRH	Shockley-Read-Hall
SSL	solid-state lighting
T_a	ambient temperature
TAT	trap-assisted tunneling
TC	thermocouple
TEM	transmission electron microscopy
T-H	temperature-humidity
T_{hs}	heat sink temperature
T_j	junction temperature
T_{sp}	solder point temperature
UV	ultraviolet radiation
UV-A	a band of UV radiation with wavelengths between 315 nm and 380 nm
UV-B	a band of UV radiation with wavelengths between 280 nm and 315 nm
UV-C	a band of UV radiation with wavelengths between 100 nm and 280 nm
UV-x	identification code for UV products used in this report; x is a number between 1 and 14
V	volt
V_{dc}	direct current volt
V_{th}	threshold voltage
W	watt
XRD	X-ray diffraction

Executive Summary

Light-emitting diodes (LEDs) can emit radiation that spans the range from near infrared (IR) to all three bands of ultraviolet (UV) radiation: UV-A, UV-B, and UV-C. This report focuses on LEDs that emit in one of the three UV bands because they have the potential to displace low-pressure mercury vapor (LPMV) lamps in a variety of industrial processes, including ink and adhesive curing, medical procedures, and germicidal disinfection. However, before emerging UV LED technologies can displace LPMV lamps, the efficiency and reliability of these sources must meet the user's expectations in each application. An earlier report focused on the construction and initial performance of commercial UV LED products in radiometric and current-voltage (I-V) tests [1]. This report focuses on the long-term performance and reliability of the same set of commercial products. The intent of this report is to provide to the lighting industry a benchmark of the state of UV LEDs as of mid-2021 when these products were purchased. Understanding the failure modes and failure rates of UV LEDs is important in improving UV product reliability at the LED, lamp, and luminaire level and is critical to developing products with higher efficiency, lower carbon footprint, and significantly reduced environmental impact than LPMV lamps.

The lifetime testing results for a series of 13 commercial UV LED products, spanning the range from UV-A to UV-C, are provided in this report. These products were chosen from commercially available UV LEDs in conjunction with the LED Systems Reliability Consortium (LSRC). All products were tested as packaged die, soldered to a metal-core printed circuit board (MC-PCB), and mounted on a heat sink. Three stress tests were used during this study to examine the reliability of each product when subjected to current, temperature, and humidity stressors that may be encountered during normal operation. Separate, independent populations of devices were used for each product during the three tests, and no device under test (DUT) experienced more than one stress test. The three stress tests are as follows:

- A room temperature operating life (RTOL) test conducted near the maximum forward current (I_f) for each product as given by the manufacturer's specifications. This test is termed RTOL-1, and there were 10 DUTs for each product used in this test matrix.
- A second RTOL test conducted at a lower I_f value that was 15% to 65% of that used during RTOL-1. This test is termed RTOL-2, and there were 10 DUTs for each product used in this test matrix.
- A temperature-humidity (T-H) storage test conducted in an environmental chamber set to 50 degrees Celsius (°C) and 90% relative humidity. This T-H storage test was performed with the LEDs in an unpowered state. A subset of three products from the test matrix was chosen for the T-H storage tests, and there were three DUTs for each product tested.

The 13 UV LED products were divided into two groups: the RTOL-1 test lasted for 1,000 hours (hrs) for Group-1 and 500 hrs for Group-2. Between the two groups, a total of 57 failures (which is 44% of the total product population) occurred during RTOL-1 that were classified as either abrupt failures (i.e., produced no UV radiation) or parametric failures (i.e., radiant flux

maintenance [RFM] was 0.50 or lower). Four products (i.e., UV-3, UV-5, UV-9, and UV-11) did not experience any failures during RTOL-1, but the other nine products had failure rates ranging from 10% to 100%. The most common failure mode was a parametric failure, which accounted for 50 failures during the test. Only seven DUTs failed abruptly, and four out of these seven devices were UV-2 DUTs. These findings demonstrate that there is a wide range of reliability in commercially available UV LED products.

Different DUTs of the 13 UV LED products were divided into two groups for RTOL-2 based on their power rating. Group-B, which had I_f values less than 55 milliampere (mA), was operated for 2,500 hrs during RTOL-2, whereas Group-A, which had I_f values greater than 100 mA, was operated for 3,000 hrs during RTOL-2. Even though product operation times were longer in RTOL-2 compared with RTOL-1, the cumulative failure rate was lower, as might be expected for the milder stress conditions (i.e., lower I_f values). A total of 32 failures occurred during RTOL-2 (which is 25% of the total product population): 11 abrupt failures and 21 parametric failures. This finding corresponds to a cumulative failure rate of 25%. Most of the failures during RTOL-2 were concentrated in fewer products; this observation was in contrast to findings from RTOL-1, during which failures were more widespread. For example, during RTOL-2, 7 abrupt failures occurred in the UV-2 DUTs and a greater than 50% parametric failure rate was measured for the UV-8 and UV-14 DUTs. These three products accounted for 22 out of the 32 failures recorded in RTOL-2.

Based on this work and combined with an extensive literature review, the following failure mechanisms could be identified across these UV LEDs:

- Abrupt failure caused by macroscopic defects in the semiconductor material. This failure mode was most prevalent in UV-2, but appeared sporadically in a couple other products that were tested.
- Contributions to parametric failure caused by the growth of parasitic diode circuits that reduce radiant carrier recombination through modification of Shockley-Read-Hall (SRH) mechanisms. The parasitic diode emerges early in the operational life of the UV LED and can be identified through a characteristic hump in the I-V profile. This mechanism was especially prominent in the aluminum gallium nitride (AlGaN) LEDs with nominal maximum emission wavelength (λ_{max}) at either 275–280 nanometers (nm) or at 310 nm. This mechanism occurred to a smaller extent in indium gallium nitride (InGaN) LEDs with λ_{max} of 365 nm.
- Contributions to parametric failure likely caused by the degradation of silicones (e.g., cracking, discoloration) used in encapsulation of the UV-A LEDs. This failure mechanism only occurred in the InGaN LEDs with λ_{max} of 365 nm because the AlGaN LEDs do not use silicones. This failure mechanism may account for the poor RFM performance of UV-12 and UV-14 during RTOL-1 and UV-14 during RTOL-2.

- Contributions to parametric failure caused by package effects likely arising from organic residues from lid seal processes and processes that use conductive adhesives (e.g., protective diode attach). The existence of this failure mechanism was supported by T-H storage tests, during which the radiant flux declined even though the DUTs were unpowered during test and their I-V curves did not change during the 148 hrs of this test.

In addition to identifying some of the failure mechanisms occurring in commercial UV LED products, one of the most significant findings from this research was that not all of the LEDs of a given product exhibited the same behavior within the test duration. For example, 60% of the UV-8 DUTs during both RTOL-1 and RTOL-2 were parametric failures by the end of each test. The DUTs that exhibited parametric failures also displayed a rise in leakage current flowing through a parasitic parallel diode circuit as shown by the changes in the I-V curve presented in **Figure ES-1**. In contrast, 40% of the UV-8 DUTs during RTOL-1 and 20% of the DUTs during RTOL-2 exhibited no changes in the I-V curve at test completion. In short, these DUTs showed no evidence of the emergence of a significant parallel diode circuit during operation. During the milder RTOL-2 experiment, there was an addition sample sub-population in-between these two extremes. During RTOL-2, 20% of the UV-8 DUTs exhibited significant leakage current that was less than that of the parametric failures; however, these DUTs exhibited acceptable RFM values that were lower than those of DUTs with minimal leakage current. Radiometric studies of the sub-populations indicated that the RFM values were significantly higher for DUTs that did not exhibit the parallel diode circuit. This finding suggests that a burn-in test of 500-hr duration followed by I-V measurements can be used to quickly identify UV LED products that are prone to significant RFM loss through the formation of a parasitic diode circuit during operation.

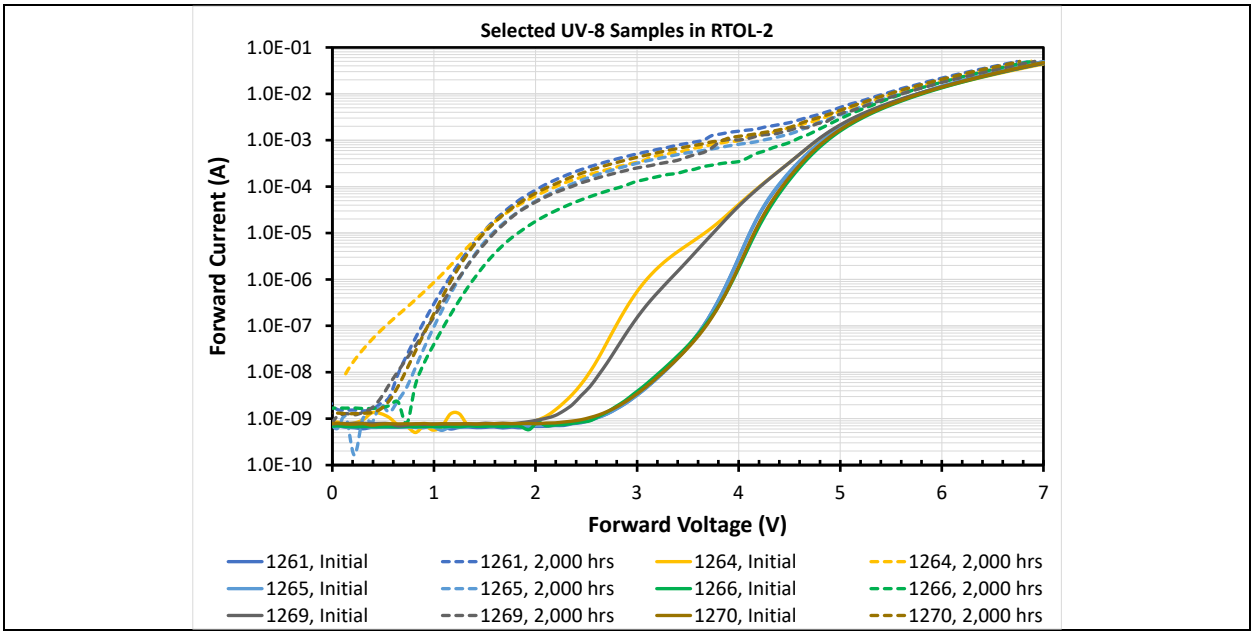

Figure ES-1. I-V curves for six DUTs of UV-8 as initially received (solid lines) and after 2,000 hrs of RTOL-2 (dashed lines). The emergence of the parasitic diode in parallel with the UV LED is demonstrated by the hump in the I-V curve between 0.5 volts (V) and 4 V.

The wide variation in behavior in radiometric and I-V tests observed for UV-8 and other UV LEDs during this study was likely the consequence of process variability during semiconductor manufacturing. Reducing this process variability across the wafer will likely produce a more consistent lifetime and efficiency for UV LED products. Such process consistency would reduce or eliminate the formation of parallel diode circuits during UV LED operation, a leading failure mechanism found in the products examined in this study.

Improving the packaging of UV LEDs by developing better encapsulation polymers and reducing or eliminating outgassed organic residues from adhesives and solder fluxes would likely also improve the RFM performance of UV LEDs. Encapsulation polymers are important to improve light extraction efficiency and to provide environmental protection. Silicones are a common encapsulant and can be found in three UV-A products that were tested during this study. Unfortunately, two out of the three products quickly displayed large RFM losses during testing likely because of silicone degradation. The other product (i.e., UV-11) exhibited RFM values greater than 0.95 under all test conditions, demonstrating that some silicones can be used as encapsulants in UV-A LEDs. In general, the materials and processes currently used for fabricating blue and white LEDs may not be appropriate for UV LEDs because of their different emission wavelengths and semiconductor chemistries.

More research is needed by the industry to improve the efficiency and long-term performance of InGaN and AlGaN materials and their LED packages. The findings from this research will be critical to delivering on the promise of high efficiency and a long lifetime for UV LED products The findings from this research will also be helpful in creating new UV technologies for building systems, personal safety, and industrial and medical application that will be energy efficient, low carbon producing, and environmentally friendly and will improve human well-being and health.

Table of Contents

List of Figures

List of Tables

1 Introduction

1.1 Applications and Sources for Ultraviolet Radiation

Electromagnetic radiation in the form of light is widely used in illumination applications throughout the world. The band of visible radiation known as light is defined by the response of the photoreceptors in the human retina and occurs at wavelengths between 380 nanometers (nm) and 780 nm. Ultraviolet (UV) radiation occurs at shorter wavelengths between 100 nm and 380 nm, and this radiation is not directly imaged by the human eye. Commercially, UV radiation has many useful applications, including curing of inks, medical procedures, and deactivation of biological species [2, 3].

UV radiation is typically divided into three bands: UV-A, which spans the wavelengths between 315 nm and 380 nm; UV-B, which spans the wavelengths between 280 nm and 315 nm; and UV-C, which spans the wavelengths between 100 nm and 280 nm. Of the industrial applications, UV curing, which mainly involves UV-A radiation, has reached the broadest commercial use at this time. UV-B radiation is used in medical phototherapy for treatment of specific skin diseases (e.g., severe cases of eczema, moderate psoriasis). UV-C radiation is receiving a significant amount of attention because of its germicidal capabilities, especially against viruses such as severe acute respiratory syndrome coronavirus 2 (SARS-CoV-2). Because the potential use of UV radiation for germicidal activity could significantly impact the energy use in buildings and increase its carbon footprint, it is important to optimize UV sources for electrical efficiency, application efficiency, safety, germicidal effectiveness, and low environmental impact [4].

The most common source of UV radiation is the low-pressure mercury vapor (LPMV) lamp, which offers high efficiency (30–40%), is low cost, and has been used for many years in the field [1, 4]. Although these LPMV lamps are relatively efficient, they have many known limitations, including lamp breakage, causing mercury to leak into the environment [5]; tendency to produce ozone; limited form factors; and low luminaire efficiency [4]. Recently, UV-producing light-emitting diodes (LEDs) have emerged as an alternative to LPMV sources. UV LEDs have the potential to eliminate some of the limitations of LPMV lamps (e.g., LEDs are amenable to many form factors, and lamp breakage does not release harmful substances into the environment). However, UV-B and UV-C LED sources currently have significantly lower source efficiencies (1–5%) than LPMV lamps [1]. The inefficiency could be counterbalanced to some degree by their directional emission profile. There is also significant headroom for improving UV LEDs across all three bands, whereas the potential for improvement of LPMV lamps is limited [4].

Improving the energy efficiency of UV LEDs involves addressing key technical challenges in the development roadmap that broadly fall into electrical and optical technology needs [1, 4, 6–11]. Because the bandgap of gallium nitride (GaN) corresponds to an emission wavelength of 362 nm, UV-A LEDs can be made by doping indium (In) into GaN to create indium gallium nitride (InGaN) alloys [1, 4, 6–11]. This same materials system, albeit at higher In doping levels, is also used to make blue LEDs that are widely applied as sources in solid-state lighting (SSL) devices.

Consequently, there is a significant body of knowledge in fabricating InGaN LEDs that is already known in the SSL industry and can be applied to improving UV-A LEDs.

However, making LEDs in the UV-B and UV-C bands requires the use of the aluminum gallium nitride (AlGaN) alloys to achieve sufficient band gaps for emission at these wavelengths. Doping aluminum (Al) into GaN produces alloys with progressively larger band gaps (emissions start at 362 nm [pure GaN] and decrease to approximately 200 nm [pure aluminum nitride (AlN)] as the concentration of Al in the alloy increases). The processibility of the AlGaN material system with current tools (usually designed for InGaN) combined with the intrinsic physical properties of AlGaN alloys (e.g., high melting temperatures, low UV transmittance) are partially responsible for the low performance observed in the current generation of UV LEDs [7–11]. It is expected that advancements in materials, processes, fabrication tools, and packaging technologies will produce significant improvements in UV LED technology within the next 5–10 years so that the energy efficiencies of UV-C LEDs are comparable to LPMV sources. The development of these higher efficiency sources, combined with improved luminaire designs and control systems, is expected to provide germicidal UV (GUV) systems that are energy efficient and highly efficacious against biological threats in buildings and provide a boost to industrial, horticultural, and medical applications of UV radiation.

1.2 Previous Studies About UV LED Reliability

Although previous studies of the reliability of UV LEDs are more limited in scope than this report, there have been notable studies spanning the UV-A [12–14], UV-B [15, 16], and UV-C [10, 16–22] bands. The forward current (I_f) densities in these studies ranged from 27 amps per square centimeter (A/cm^2) to 140 A/cm^2. Several general trends have emerged from these studies, and perhaps the most significant finding involved increased leakage currents at voltages well below the threshold voltage (V_{th}). The parasitic shunt circuits that give rise to such low voltage leakage currents appeared to reduce active carrier concentration through modifications of Shockley-Read-Hall (SRH) mechanisms and are thought to be directly tied to aging-induced reductions of emissions from UV-A, UV-B, and UV-C devices [10, 12–20, 22]. Evidence for parallel shunt circuits is provided in the current-voltage (I-V) measurements of an LED by a growing feature at voltages below V_{th}. Other major findings from these studies were that low current radiometric studies were likely to be most sensitive to increased SRH behavior [10, 15, 20], device efficiency and reliability could be improved by reducing threading defect densities [21], and higher temperatures and/or higher I_f values tend to reduce device lifetimes [23].

1.3 Study Goal

The goal of this study was to compare the initial performance and long-term reliability of UV LEDs for a group of 13 commercial UV LED products that spanned the three UV bands: UV-A, UV-B, and UV-C. This current report is the second in a series of reports, and it focuses on the evaluation of the operational lifetime of the test matrix of 13 different UV LED products. The initial study focused on the construction and initial performance of each product. Twenty-five

samples of each product were examined during this analysis to provide statistical power to the findings. The current study focuses on the performance of these LED products over several thousand hours of room temperature operating life (RTOL) testing. During both studies, the behavior of the UV LEDs was compared across the different bands to provide insights into opportunities to improve energy efficiency and reliability. The intent of this work was to provide information to facilitate the use of energy-efficient, lower carbon emitting, UV technologies for use in combination with lighting systems for commercial and residential buildings.

2 LED Samples

Based on feedback from the U.S. Department of Energy (DOE) LED Systems Reliability Consortium (LSRC), a sample matrix of 13 different UV LED products was developed for this study. The sample matrix contained representative examples of UV-A, UV-B, and UV-C products spanning both low-power and high-power products. For convenience, the identity of each product was anonymized, and labels of the format UV-x (where x is a number between 1 and 14 that uniquely identifies the product) are used in this report. Basic properties of the 13 products are presented in **Table 2-1**. The average V_{th} value, which is the minimum voltage required to create a conductive path, is also included in **Table 2-1**.

Table 2-1. Basic Properties of the UV LEDs Examined During This Study

Product Number	Nominal UV Band	Nominal Peak Wavelength[a] (nm)	V_{th} [b] (V)	Maximum dc Current[a] (mA)	Maximum Radiant Flux[a] (mW)	Initial Radiant Efficiency[c] (%)	Maximum Use Temperature[a] (°C)
UV-1	UV-C	275	6.066	30	2.8	2.3	$T_a < 60$
UV-2	UV-C	275	5.991	30	2.5	2.0	$T_{sp} < 80$
UV-3	UV-C	275	5.428	40	4.7	5.1	$T_a < 60$
UV-4	UV-C	275	5.462	200	15.0	2.0	$T_a < 60$
UV-5	UV-C	280	4.612	500	119	5.0	$T_a < 85$
UV-6	UV-C	275	4.905	500	47	4.1	$T_a < 60$
UV-7	UV-C	275	5.071	800	88	2.7	$T_j < 100$
UV-8	UV-B	310	5.426	30	1.2	2.0	$T_a < 60$
UV-9	UV-B	310	5.560	30	2.7	2.2	$T_{sp} < 80$
UV-11	UV-A	365	3.279	500	1,000	55.7	$T_j < 90$
UV-12	UV-A	365	3.203	700	1,050	10.5	$T_a < 85$
UV-13	UV-A	365	3.160	4,000	3,800	13.4	$T_j < 125$
UV-14	UV-A	365	3.172	1,000	1,375	57.0	$T_{sp} < 70$

[a] Reported values are based on manufacturer's specifications.

[b] Initial V_{th} values were reported in the earlier benchmarking study [1] and are reproduced here for convenience.

[c] Initial radiant efficiency was measured at 5 mA as reported elsewhere [1].

Note: °C = degree Celsius; dc = direct current; mA = milliampere; mW = milliwatt; T_a = ambient temperature; T_j = junction temperature; T_{sp} = solder point temperature; V = volt.

Photographs of each UV LED are presented in **Appendix A**, and representative electrical and radiometric measurements are provided in the initial benchmarking report [1]. Details about the experimental techniques used in this study are discussed in **Section 3** of this current report. At least 25 samples of each product were obtained from outside distribution vendors except for Product UV-1 of which only 22 samples could be purchased because of supply limitations. Product UV-10 was not included in this study because sufficient quantities of the product could not be purchased in time because of supply limitations.

Most of the products examined during this current study were purchased with a single LED package already mounted on a metal-core printed circuit board (MC-PCB). Five products (i.e., UV-3, UV-6, UV-7, UV-8, and UV-14) could only be purchased as LED packages. A local design and prototyping company was contracted to design custom MC-PCBs for each of these five products according to the manufacturer's specifications. For these five products, one LED was soldered to each custom MC-PCB by using solder thicknesses and stencil patterns recommended by each LED manufacturer.

The MC-PCBs of all samples, regardless of operational current, were mounted on extruded Al heat sinks such as the ones shown in **Figure 2-1**. Each heat sink measured 1.813 inches × 2 inches × 1.25 inches and weighed approximately 89 grams. The heat sink contained six tapered fins measuring 0.95 inches in length. A single MC-PCB containing one LED package was attached to each heat sink by using a combination of thermally conductive tape (thermal conductivity of 1.5 watts [W]/meter (m) Kelvin [K]) and mounting screws. This size of heat sink was chosen in part because it is approximately the same size as the sample stage in the integrating sphere used for most of the radiometric measurements in this study, and there was concern that a larger heat sink could interfere with the reflection of radiation inside the integrating sphere.

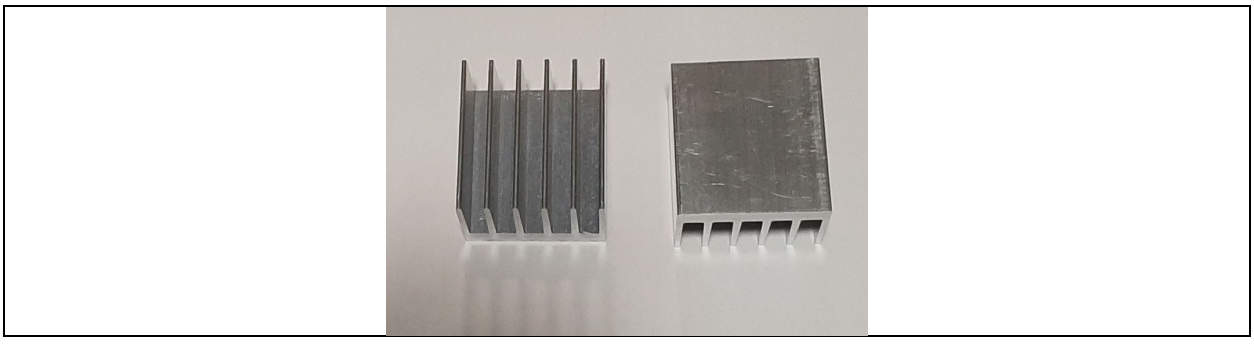

Figure 2-1. Extruded Al heat sinks used for all UV LEDs included in the study.

Additional classification of the products was conducted to determine the LED package properties and construction methods used in the UV and white LED products. These findings are summarized in **Appendix A** of this report and are discussed in detail in a previous report [1].

3 Experimental Methods and Procedures

In this current report, and in a previous report [1], a series of electrical and radiometric measurements were collected on each device under test (DUT) to determine the level of performance. These tests were performed on the samples only after placing the packaged LED and MC-PCB combination on a heat sink, and then this assembly was tested without further modifications after each round of RTOL. Depending on the experimental conditions, the RTOL test duration of each cycle could range from 24 hours (hrs) to 1,000 hrs, although most RTOL test cycle durations were 500 or 1,000 hrs. In all cases, measurements were taken after each DUT had cooled to room temperature, which is typically 22 ± 2 degrees Celsius (°C). Room temperature was monitored during all tests to track the impacts of any temperature change on electrical and radiometric properties of the LEDs. These measurement methods are briefly summarized in the remainder of **Section 3.3** and **Section 3.4**, and additional details can be found in an earlier report [1].

3.1 Testing Environments

There were three principal testing environments that were used for this study, and separate populations of samples were used for each environment. The test environments were as follows:

1. RTOL studies conducted on all products at I_f values approaching the specified maximum for the product (termed RTOL-1)
2. RTOL studies conducted on all products at mid-range values of I_f for each product (termed RTOL-2)
3. Unpowered temperature-humidity (T-H) storage tests conducted on only products UV-4, UV-5, and UV-6 (termed T-H storage test).

The samples of each product were divided into separate populations for the various RTOL and storage tests, and no sample was subjected to more than one test environment. A total of 10 different samples were used for each product in RTOL-1 and RTOL-2, whereas only 3 samples were used for products UV-4, UV-5, and UV-6 in the T-H storage test. Both RTOL-1 and RTOL-2 were conducted in an open-air, large room. To avoid any issues with inadvertent UV exposure to staff, a plan was approved by RTI's Radiation Officer in which the samples were placed on the tops of the wall-mounted laboratory storage cabinets which made the UV LEDs approximately 7.3 feet [ft] above the floor. The laboratory has an open ceiling, and the LEDs were directed toward the building's roof, which is 16 ft above the floor. In the space between the cabinets and the roof, the typical building infrastructure exists (e.g., metal heat ventilation and cooling ducts, metal supports). This infrastructure was covered with brown paper and cardboard to act as an absorber of UV radiation. Without this covering, a significant amount of UV radiation (principally UV-A) was reflected into the laboratory space off the metal infrastructure from the RTOL samples. With the covering of the metal structures in the upper portion of the room, the amount of radiation measured in the laboratory space was negligible.

3.1.1 RTOL-1

This initial test consisted of operating a population of 10 DUTs of each product in the test matrix (130 DUTs total) near the maximum current value specified by the manufacturer. In many ways, the fact that the DUTs were operated near their specification limits made this test similar to the Hammer Test that was performed on LED luminaires approximately 10 years ago [24].

The test conditions for each product in RTOL-1 were varied slightly according to the manufacturer's specification. Each group of 10 DUTs for a given product was kept together during testing, and the individual heat sinks used with each DUT were placed on a common heat spreader (i.e., metal sheet) for that product. There was one heat spreader dedicated to each product, except for the UV-13 DUTs that required two water-cooled heat spreaders to keep the solder point temperature (T_{sp}) value within specifications because of the higher I_f values. The manufacturer's specified maximum I_f value, the I_f value used during RTOL-1 testing for each product, the resulting current density (based on overall chip size), and the test configuration of the DUTs are presented in **Table 3-1**.

To achieve the I_f values given in **Table 3-1**, either one or two dedicated dimmable LED drivers was used for each product. The decision to either have one group with 10 DUTs in series or two parallel groups with 5 DUTs in series was determined by the voltage required to deliver the targeted I_f values and the rated maximum voltage of the selected driver. If a configuration of two parallel groups of five DUTs in series was used, then the maximum power rating of the driver had to be checked. If a single driver could provide the necessary power to two parallel strings of DUTs, then only one driver was used. If not, two drivers were used. In **Table 3-1**, the latter configuration is denoted as "two independent sets of five DUTs in series" whereas the former is denoted as "two parallel sets of five LEDs in series." A special driver was required for UV-13 to reach the specified current limit. When necessary, a 0–10 volt (V) dimmer was used to set the output power delivered by the driver, and current-limiting resistors were used for all products to set maximum current values. Currents were verified before the start of each RTOL-1 cycle and the DUTs were regularly inspected for the occurrence of abrupt failures.

Table 3-1. Manufacturer's Specifications and Operational Conditions for RTOL-1

Product Number	Rated Maximum dc Current (mA)	RTOL-1 I_f (mA)	RTOL-1 Current Density (A/cm²)	Configuration	Driver[a]	Dimmer	RTOL-1 Test Duration (hrs)
UV-1	30	25	10	2 Parallel sets of 5 DUTs in series	1	Yes	1,000
UV-2	30	27 and 29	7.5 and 8.1	2 Parallel sets of 5 DUTs in series	1	Yes	1,000
UV-3	40	35	23	2 Parallel sets of 5 DUTs in series	1	Yes	500
UV-4	200	154	27	2 Parallel sets of 5 DUTs in series	1	No	1,000
UV-5	500	474	49	10 DUTs in series	1	No	1,000
UV-6	500	490	34	2 Independent sets with 5 DUTs in series	1	No	500
UV-7	800	760	70	2 Independent sets with 5 DUTs in series	2	No	500
UV-8	30	24	12	2 Parallel sets of 5 DUTs in series	1	Yes	500
UV-9	30	26 and 27	8.6 and 8.9	2 Parallel sets of 5 DUTs in series	1	Yes	1,000
UV-11	500	495	50	10 DUTs in series	2	No	1,000
UV-12	700	705	71	10 DUTs in series	2	No	500
UV-13	4,000	3,484	49	2 Independent sets of 5 DUTs in series	3	No	1,000
UV-14	1,000	968	93	10 DUTs in series	2	No	500

[a] Driver 1 has an output voltage range of 20–56 V_{dc} and a maximum power output of 39 W. Driver 2 has an output voltage range of 27–54 V_{dc} and a maximum power output of 54 W. Driver 3 has an output voltage range of 9 to 27 V_{dc} and a maximum power output of 96 W.

Note: dc = direct current; mA = milliampere; V_{dc} = direct current volt.

During RTOL-1, the DUTs were divided into two distinct groups: Group-1 consisted of UV-1, UV-2, UV-4, UV-5, UV-9, UV-11, and UV-13, and Group-2 consisted of UV-3, UV-6, UV-7, UV-8, UV-12, and UV-14. This difference arose simply because of the availability of the individual DUTs. Specifically, the Group-1 products could be ordered with the LEDs already mounted on MC-PCBs, but the Group-2 products could only be ordered as individual LED packages and had to be placed on MC-PCB prior to test. Because of the added assembly step for the Group-2 products, the Group-1 products were tested for 1,000 hrs, and the Group-2 products were tested for 500 hrs. After each 500 hrs of RTOL-1 exposure, the performance of the DUTs was characterized by using the I-V methods (see **Section 3.3** of this report) and the radiometric methods (see **Section 3.4**). These data were used to determine the number of DUTs that

exhibited abrupt failure (i.e., did not produce radiant flux) and the number of DUTs that produced parametric failures (e.g., DUTs that produced less than 50% of their initial radiant flux).

3.1.2 RTOL-2

RTOL-2 consisted of operating a population of 10 DUTs of each product in the test matrix at lower currents than in RTOL-1. In general, the I_f values used during RTOL-2 were 15% to 65% of those in RTOL-1, with the lower power products being operated near 50% of the maximum specified I_f values and the higher powered products being operated at 15% to 30% of the maximum I_f values. UV-7 was operated at an I_f value that was the lowest percentage of the maximum rated current for any of the products in the test matrix, but was operated at the same overall current as other comparable high-powered UV-C LEDs (e.g., UV-5, UV-6). Current densities used during RTOL-2 were generally lower than those found in most literature studies [14, 15, 17, 20].

Each group of 10 DUTs for a given product was kept together during test, and the individual heat sinks used with each DUT were placed on a common heat spreader (i.e., metal sheet) for that product. The manufacturer's specified maximum I_f value, the I_f value used during RTOL-2 for each product, the resulting current densities (based on overall chip size), and the DUT configuration during testing are shown in **Table 3-2**. To achieve the I_f values presented in **Table 3-2**, either one or two dedicated dimmable LED drivers were used for each product, and the configuration was determined by using the same procedure as for RTOL-1 as outlined in **Section 3.1.1** of this report. When necessary, a 0-10 volt (V) dimmer was used to set the output power delivered by the driver, and current-limiting resistors were used for all products to set maximum current values.

The DUTs were divided into two distinct groups based solely on power requirements: the high-power Group-A consisted of UV-5, UV-6, UV-7, UV-11, UV-12, UV-13, and UV-14, and the lower power Group-B consisted of UV-1, UV-2, UV-3, UV-4, UV-8, and UV-9. Although the designations of higher power and low power was arbitrary, for this test, the higher power LEDs were those operated at I_f values of 100 mA and above, and the lower power DUTs were those operated at currents below 55 mA. After every 500 hrs of RTOL-2 exposure, the performance of all of the DUTs was characterized by using the I-V methods (described in **Section 3.3** of this report) and radiometric methods (discussed in **Section 3.4**). Measurements were also taken at other times, including 24, 48, 100, 250, and 750 hrs, but these measurements were only collected on a sampling (typically three DUTs) of the test population, and the same samples were measured each time.

Table 3-2. Manufacturer's Specifications and Operational Conditions for RTOL-2

Product Number	Rated Max dc Current (mA)	RTOL-2 I_f (mA)	RTOL-2 Current Density (A/cm^2)	Configuration	Driver[a]	Dimmer	RTOL-2 Test Duration (hrs)
UV-1	30	15.8	6.3	2 Parallel sets of 5 DUTs in series	2	Yes	2,500
UV-2	30	15.1	4.2	2 Parallel sets of 5 DUTs in series[b]	2	Yes	1,000
UV-3	40	19.3 and 20.0	12.9 and 13.3	2 Parallel sets of 5 DUTs in series	2	Yes	2,500
UV-4	200	50.0 and 51.0	8.9	2 Parallel sets of 5 DUTs in series	2	Yes	2,500
UV-5	500	102	10.6	10 DUTs in series	2	No	3,000
UV-6	500	102	7.1	2 Independent sets with 5 DUTs in series	2	No	3,000
UV-7	800	100	9.2	2 Independent sets with 5 DUTs in series	2	Yes	3,000
UV-8	30	15.0	7.4	2 Parallel sets of 5 DUTs in series	2	Yes	2,500
UV-9	30	15.5	5.1	2 Parallel sets of 5 DUTs in series	2	Yes	2,500
UV-11	500	102	10.2	10 DUTs in series	2	No	3,000
UV-12	700	211	21.1	10 DUTs in series	2	No	3,000
UV-13	4,000	965	13.4	2 Independent sets with 5 DUTs in series	2	No	3,000
UV-14	1,000	397	38.2	10 DUTs in series	2	No	3,000

[a] Driver 2 has an output voltage range of 27–54 V_{dc} and a maximum power output of 54 W.

[b] The configuration for UV-2 was changed to 7 LEDs in series after 500 hrs of testing because of failures. The I_f value for each LED was unchanged.

Note: dc = direct current; mA = milliampere; V_{dc} = direct current volt.

3.1.3 T-H Storage Tests

A short T-H storage test was also performed with the LEDs in an unpowered state. This test was intended to assess the impact of environment exposure to elevated ambient temperatures (50°C) and high humidity (90% relative humidity [RH]). This test, which was termed 5090, was performed in the unpowered state because UV reflections off the stainless-steel walls of the environmental chamber could potentially be absorbed by the UV LEDs and create new failure modes. Only three UV-C products with similar properties (i.e., UV-4, UV-5, and UV-6) were subjected to the T-H storage test, and there were only three samples for each product. The main difference between these three products was that UV-5 was in a hermetically sealed LED package, but UV-4 and UV-6 were not. A hermetically sealed package may increase product

reliability because it provides increased resistance to moisture ingress and prevents corrosion. The T-H storage test was conducted in cycles of approximately 48 hrs of continuous exposure to 5090, and I-V and radiometric measurements were collected after each cycle. The total test time in the 5090 environment was 144 hrs (i.e., three cycles).

3.2 Temperature Measurements

The temperatures of DUTs in RTOL-1 and RTOL-2 were monitored by using a combination of thermocouples (TCs) and thermal imaging. Heat sink temperatures (T_{hs}) of the DUTs during RTOL-1 and RTOL-2 are presented in **Table 3-3**. T_{hs} values should be similar to T_{sp} in the long experimental times used during this study.

Table 3-3. T_{hs} Values for the DUTs During RTOL-1 and RTOL-2

Product	RTOL-1 T_{hs} (°C)	RTOL-2 T_{hs} (°C)
UV-1	25	21
UV-2	25	23
UV-3	29	22
UV-4	35	23
UV-5	40	20
UV-6	42	21
UV-7	62	21
UV-8	28	20
UV-9	28	23
UV-11	43	20
UV-12	47	20
UV-13	103, 40[a]	20
UV-14	40	20

[a] The T_{hs} values for UV-13 was originally 103°C for the first 167 hrs of RTOL-1. Then, the heat sinks were moved to two water-cooled plates; the T_{hs} value dropped to 40°C.

3.3 I-V Measurements

During the study, I-V measurements were performed on all DUTs by using a programmable source meter operating under computer control. The computer program changed V_f of the DUT in a linear ramp between an preset initial and final value. For this study, a calibrated Keithley 2400 source meter was used for all I-V measurements. This source meter can measure currents as low as 10^{-12} amps (A). I-V measurements were performed with biases as low as 2 V; however, because most products have a protective diode in the package, negative bias measurements are generally dominated by the behavior of this diode and are, therefore, not presented in this report.

3.4 Radiometric Measurements

Measurements of the radiometric properties of the LEDs examined in this study were taken with integrating spheres by using the procedures outlined in American National Standards Institute (ANSI) and Illuminating Engineering Society (IES) standard LM-79-19 and ANSI/IES LM-85-20 [25, 26]. For these measurements, two integrating spheres were used, both of which were coated with Teflon as required for UV-B and UV-C measurements. Descriptions of both integrating spheres are found in a previous report [1]. Most of the measurements were collected in a 10-inch Teflon-lined integrating sphere (see **Figure 3-1**) that was equipped with a xenon lamp calibration source with calibration range from 210 nm to 800 nm. The xenon lamp, which is a 2π source, served as both the calibration source and the auxiliary lamp for all measurements and allowed calibrated measurements of radiant flux, traceable to standards at the National Institute of Standards and Technology. All samples were mounted on a stage in the center of the integrating sphere, and all measurements were taken in the 4π geometry.

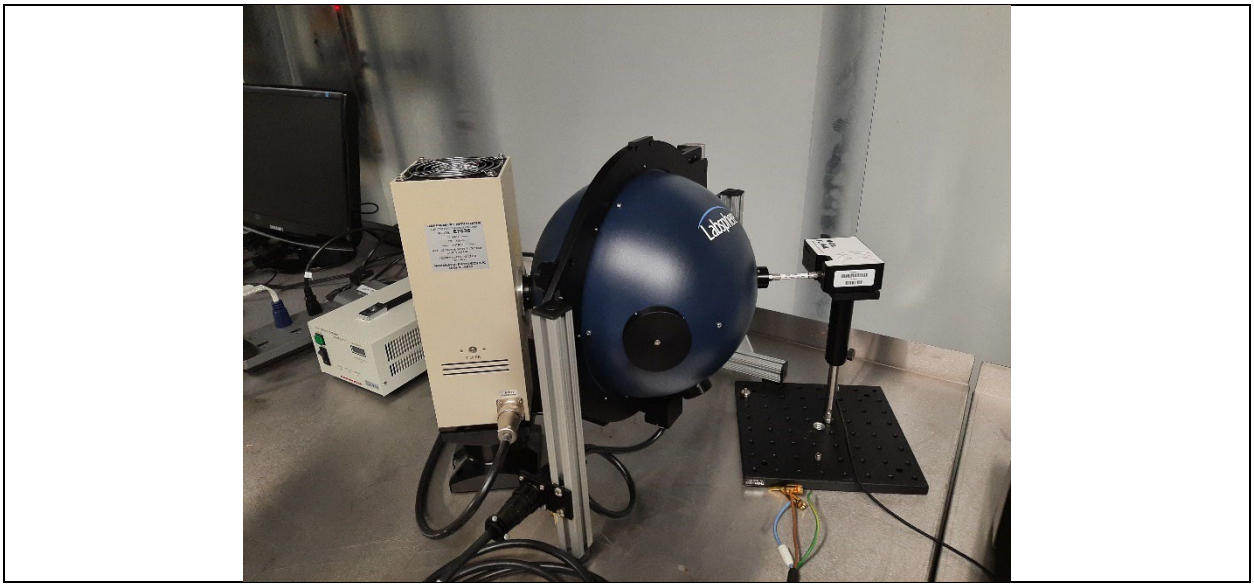

Figure 3-1. Large integrating sphere (10 inches in diameter) used to collect these measurements.

When performing radiometric measurements, all samples were measured in continuous mode at an I_f value of 5 mA. This current was chosen to minimize heating of the samples and to keep the junction temperature (T_j) values near room temperature during radiometric testing. For all DUTs examined during this study, T_j was 22°C ± 3°C during radiometric testing, although higher T_j values occurred during life testing when higher I_f values were used. One coincidental advantage of performing radiometric tests at low I_f values was that parasitic luminescence generally accounts for a higher percentage of the total radiation at low currents. Parasitic luminescence, if present, arises from deep-level defects (e.g., vacancies, impurities, dislocations) and can reduce quantum yield [18].

4 I-V Measurements of Simple Diode Circuits

Previous studies have shown that the change in I-V measurements of the UV LED products provides insights into the degradation of the DUTs [10–24]. When combined with radiant flux maintenance (RFM) measurements, a clearer picture of the mechanisms that may be responsible for abrupt and parametric failure emerges. To understand the changes occurring in I-V measurements, several simple circuits were constructed and tested, following the guidance outlined in one publication [6], to study the impacts of serial and parallel circuit changes involving the UV LED. The addition of serial resistance to a UV LED diode was found to affect the slope of the I-V curve after V_{th} but had minimal effect before V_{th} in agreement with previous results [6]. In contrast, the most noticeable changes in the I-V curves occurred when there was a second circuit in parallel with the UV LED diode. Understanding how these parallel (i.e., shunt) circuit changes impact the shape of the I-V curves is important to understanding how the electrical properties of UV LEDs change during their lifetime as demonstrated by I-V measurements.

To provide examples of possible circuit changes that could happen in UV LEDs, two simple circuits were constructed to characterize the resulting I-V curves under different parallel circuit conditions. The first circuit (Circuit-1) is a UV LED in parallel with a resistor and the second circuit (Circuit-2) is a UV LED in parallel with a diode of lower V_{th} value and a serially connected resistor (**Figure 4-1**). Having a lower V_{th} value is critical for the two diodes in parallel configuration because that means that the diodes will start conducting current at different voltages. Any UV LED in the test matrix could have been chosen for D1 (i.e., diode with higher V_{th} values in the test circuit). However, for simplicity, an untested UV-5 LED was used as component D1 in all circuits because UV-5 LEDs have the lowest V_{th} value of the UV-B and UV-C LEDs. The V_{th} value of the UV-5 LED was 4.59 volts (V). A white high-power LED in a ceramic package (V_{th} = 2.57 V) was used as component D2 (i.e., diode with lower turn-on voltage in the test circuit) in the Circuit-2 configurations.

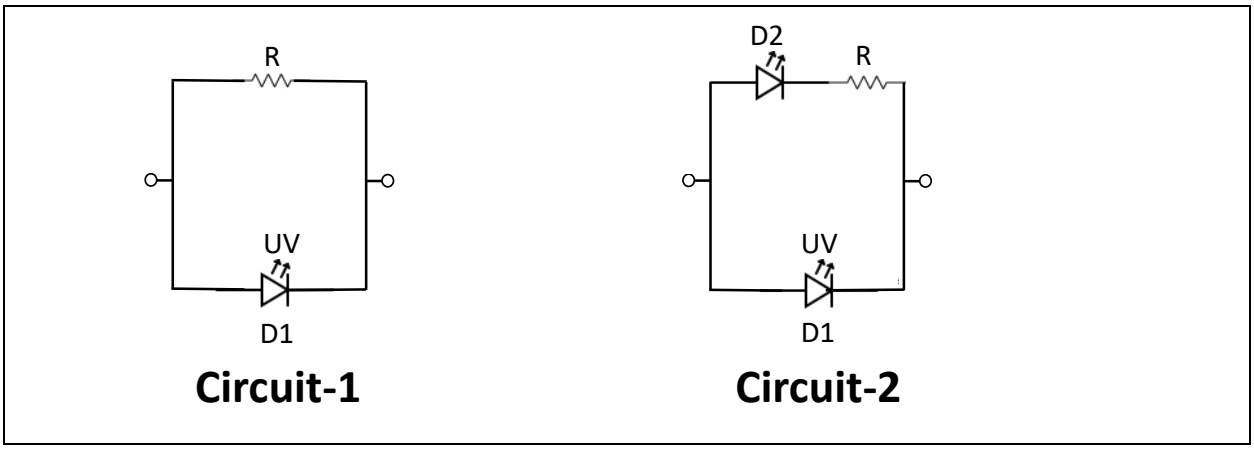

Figure 4-1 Schematic drawings of circuits used to model I-V characteristics of UV LEDs.

Circuit-1 has a parasitic resistance in parallel with the main diode, and this type of structure was found in some early GaN LEDs [6]. When measured alone, the UV-5 diode exhibited an I-V curve similar to what would be expected for an LED (**Figure 4-2**). However, changing the value of R in Circuit-1 had a significant impact on the I-V curves **(Figure 4-2**). At all values of R that were tested, the current exhibited a continuous linear increase, as expected from Ohm's Law[1], until the UV LED (i.e., D1) reached its V_{th} value. At that point, nearly all current flowed through D1, in agreement with the measurement of the UV diode alone, and the LED provided UV radiation. The key characteristic of the I-V curve for Circuit-1 (i.e., resistance in parallel with a UV LED) is the hump at low voltages (i.e., 0 V to 4 V), and the magnitude of the current flow is set by the resistor. This hump should start at 0 V and exhibits the shape shown in **Figure 4-2** in a semi-log plot. Because Ohm's Law is applicable at low voltages, dividing the voltage by the current of the I-V measurement for Circuit-1 allows calculation of the effective resistance. These data are shown in **Figure 4-3** for the case of a 994-ohm (Ω) resistor in parallel with the UV LED. The voltage where the UV LED (> 4.25 V) is turned on and where its characteristics determine the I-V curve of Circuit-1 is marked by the sudden drop in resistance. For voltages between 0 V and 4.25 V, the parallel (i.e., shunt) resistor dominates the shape of the I-V curve because the UV LED is not conducting at these voltages.

Circuit-2 has a diode (i.e., D2) with a low V_{th} in parallel with the UV diode (i.e., D1) that is operating at a higher V_{th} value. The circuit emulates the condition where a parasitic diode is in parallel with the main diode and has been found in early GaN LED studies [6]. The data measured under these conditions are presented in **Figure 4-4.** Serial resistances (i.e., R in Circuit-2) were also added to illustrate the effects of resistance in this type of circuit. In this case, the total parallel resistance is the sum of the resistance of the LED at a given voltage and that of the fixed resistor. In contrast to Circuit-1 behavior, the value of the total parallel resistance changes with voltage (because the resistance of D2 is not necessarily constant with voltage near V_{th}), which creates a two-step behavior in the resistance as shown in **Figure 4-5**. As a result, the currents for Circuit-2 are lower than those of Circuit-1, even above V_{th} of D2.

[1] Because **Figure 4-2** is a semi-log plot, the linearity of the I-V curve is not as clear. If plotted on a linear graph, the linear nature of the I-V curve would be clear.

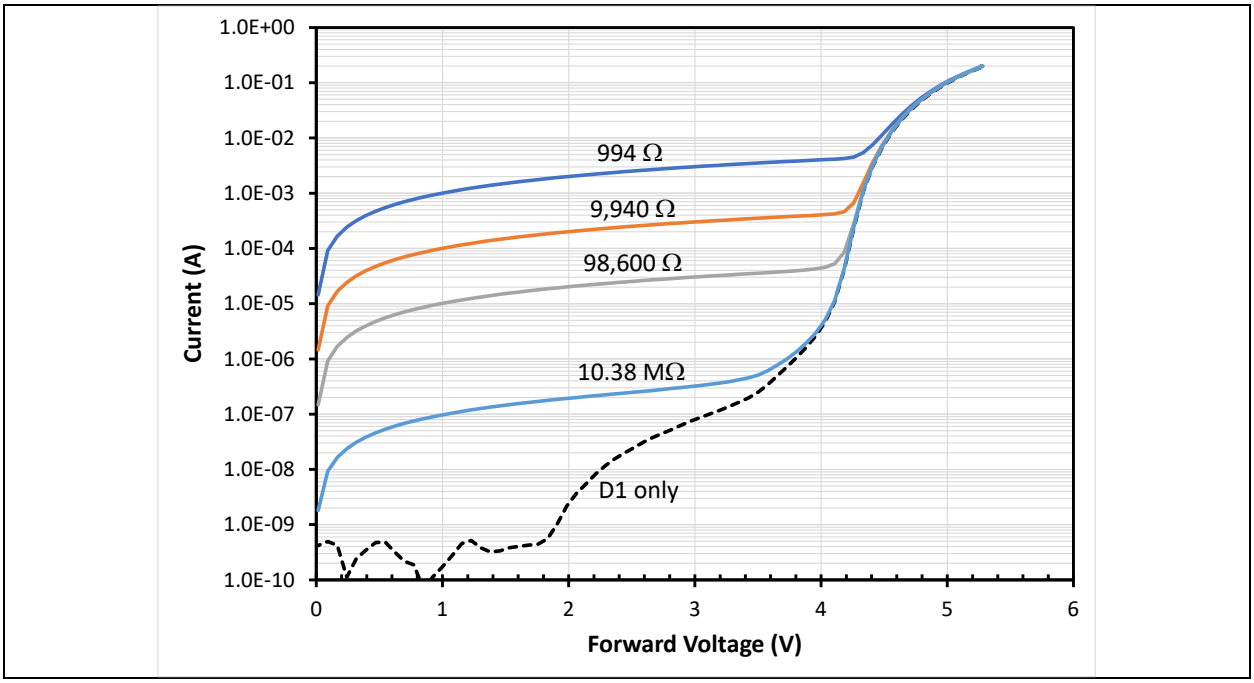

Figure 4-2. I-V measurements of various embodiments of Circuit-1 with the resistor R set to the values indicated in the figure. The dashed line shows the I-V behavior for the UV LED alone.

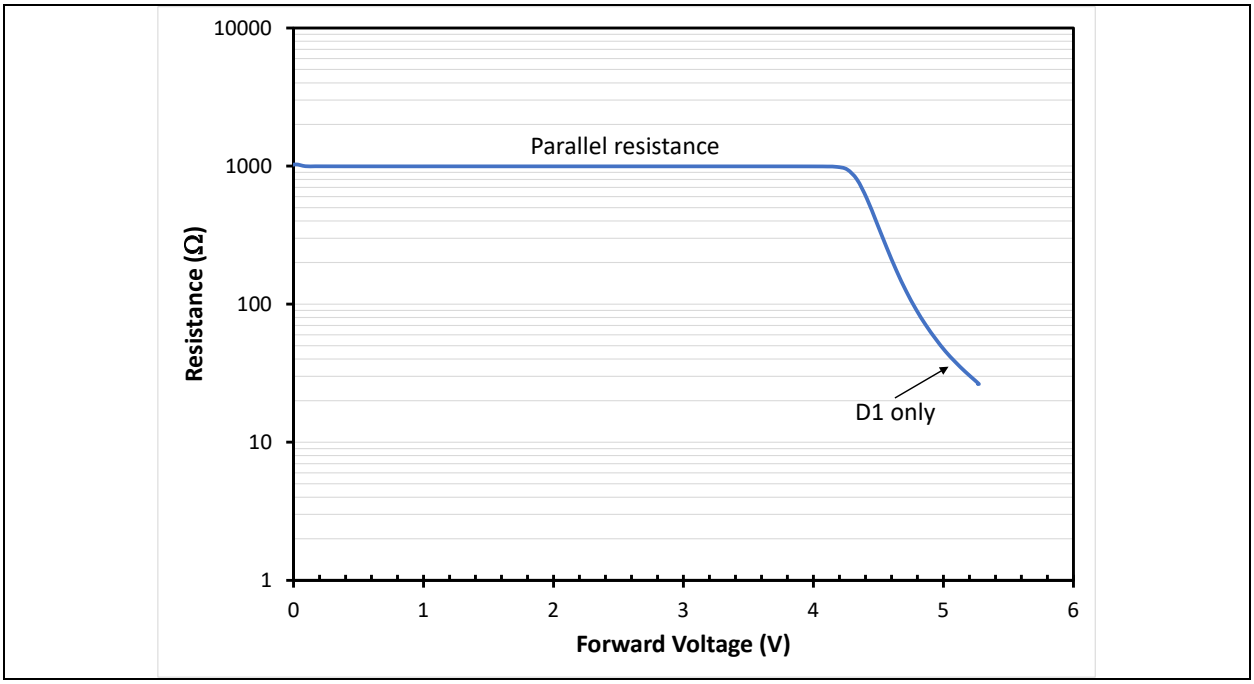

Figure 4-3. Resistance of a Circuit-1 device with a 994 Ω resistor in parallel with the UV LED (D1).

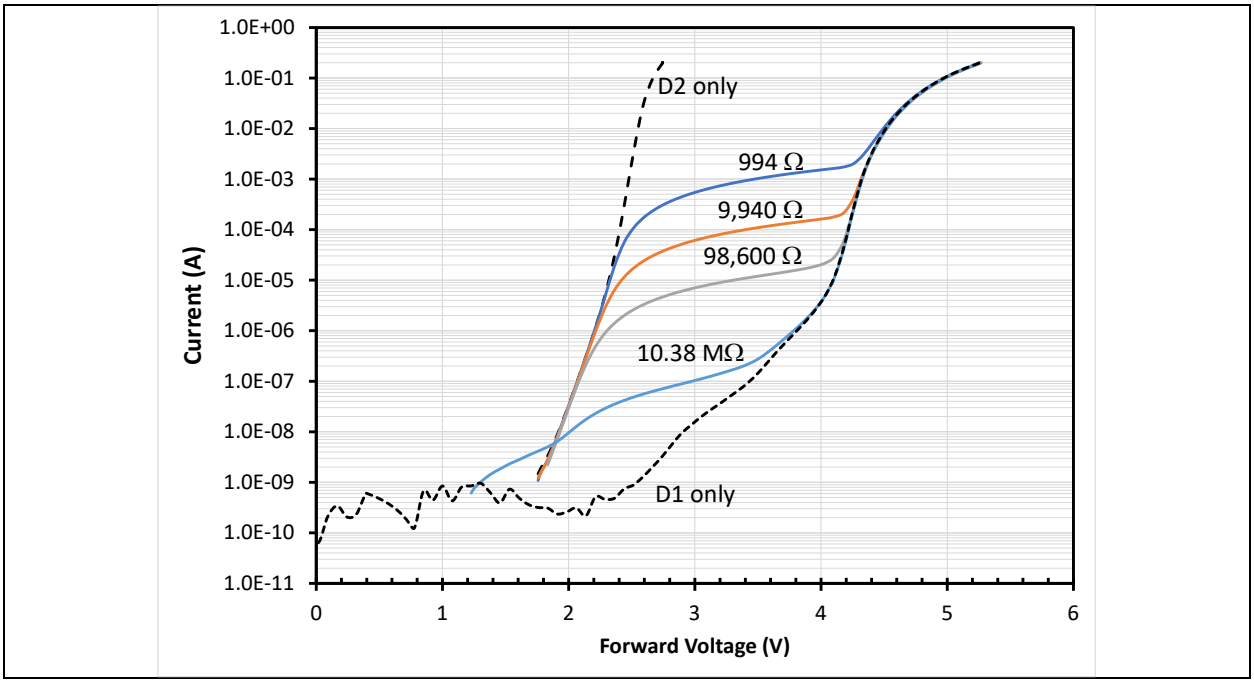

Figure 4-4. I-V measurements of various embodiments of Circuit-2 with the resistor R set to the values indicated in the figure. The I-V characteristics of only D1 and only D2 are given by the dashed lines.

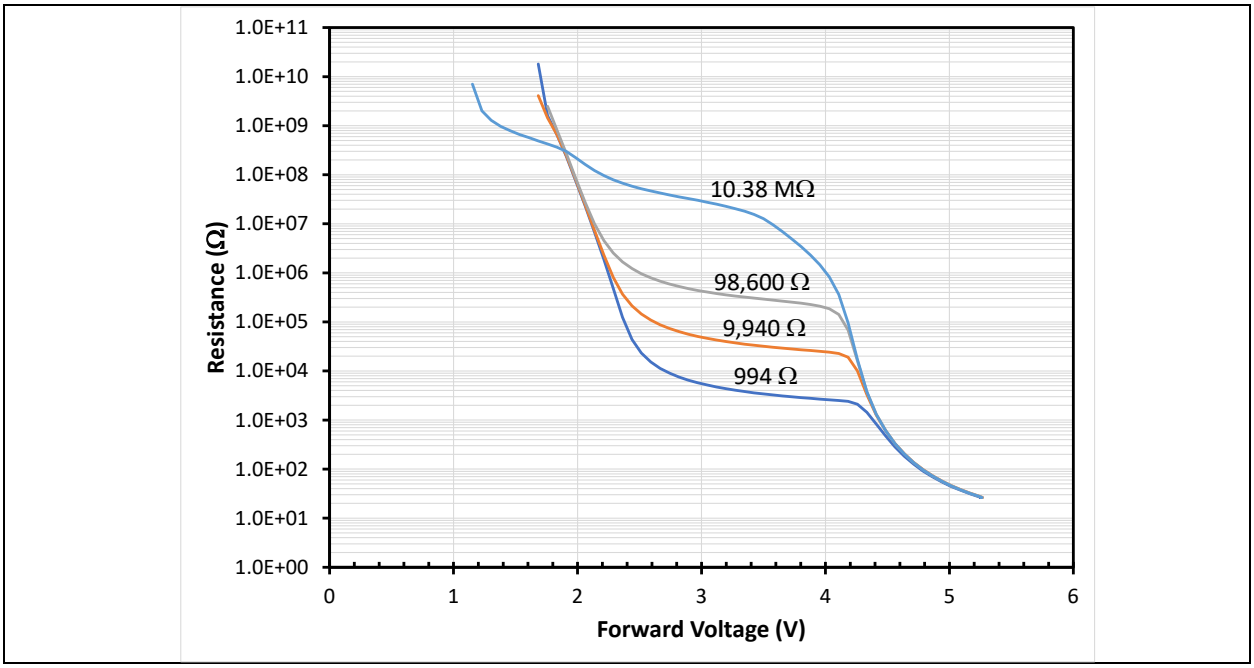

Figure 4-5. Resistance measurements of various embodiments of Circuit-2 with the resistor R set to the values indicated in the figure.

5 Results for UV LEDs

5.1 RTOL-1

RTOL-1 consisted of operating all UV LEDs near their maximum rated current (see **Table 3-1**), with the test population for each product set to 10 DUTs. The date when the products were received determined the length of RTOL-1 for a particular product. LEDs mounted on MC-PCBs that were purchased directly from electronics supply houses and received before August 2021 were operated for 1,000 hrs during RTOL-1. These products included UV-1, UV-2, UV-4, UV-5, UV-9, and UV-11 and are referred to collectively as Group-1. LEDs that were purchased as individual packages and then had to be mounted on MC-PCBs were not ready for testing until after August 2021. As a result, these products were only operated for 500 hrs during RTOL-1. These products included UV-3, UV-6, UV-7, UV-8, UV-12, and UV-14 and are referred to collectively as Group-2. UV-13, which was operated at the highest current (3,484 mA), was stopped after 92 hrs of operation because of the high T_{hs} value **(Table 3-3**). Then, the heat sink of each DUT was placed on one of two water-cooled plates with the circulating water set to 3°C. These water-cooled plates helped keep the T_{hs} value of the UV-13 DUTs to 40°C (**Table 3-3**). After making these changes, the UV-13 DUTs were restarted and continued until their total operating time was 500 hrs.

5.1.1 Failures Observed During RTOL-1

After each 500 hrs of testing, the DUTs were analyzed by using both radiometry and I-V measurements. These measurements provided a basis for classifying the DUTs as (1) still operating, (2) abrupt failure, or (3) parametric failure. The abrupt and parametric failures for the products that experienced 1,000 hrs of RTOL-1 are shown in **Figure 5-1**. Likewise, the abrupt and parametric failures for the products that experienced only 500 hrs of RTOL-1 are shown in **Figure 5-2**. Only four products (i.e., UV-3, UV-5, UV-9, and UV-11) exhibited zero failures during their test periods. In contrast, more than 50% of DUTs failed during the first 500 hrs of testing for UV-6, UV-7, UV-8, UV-12, UV-13, and UV-14.

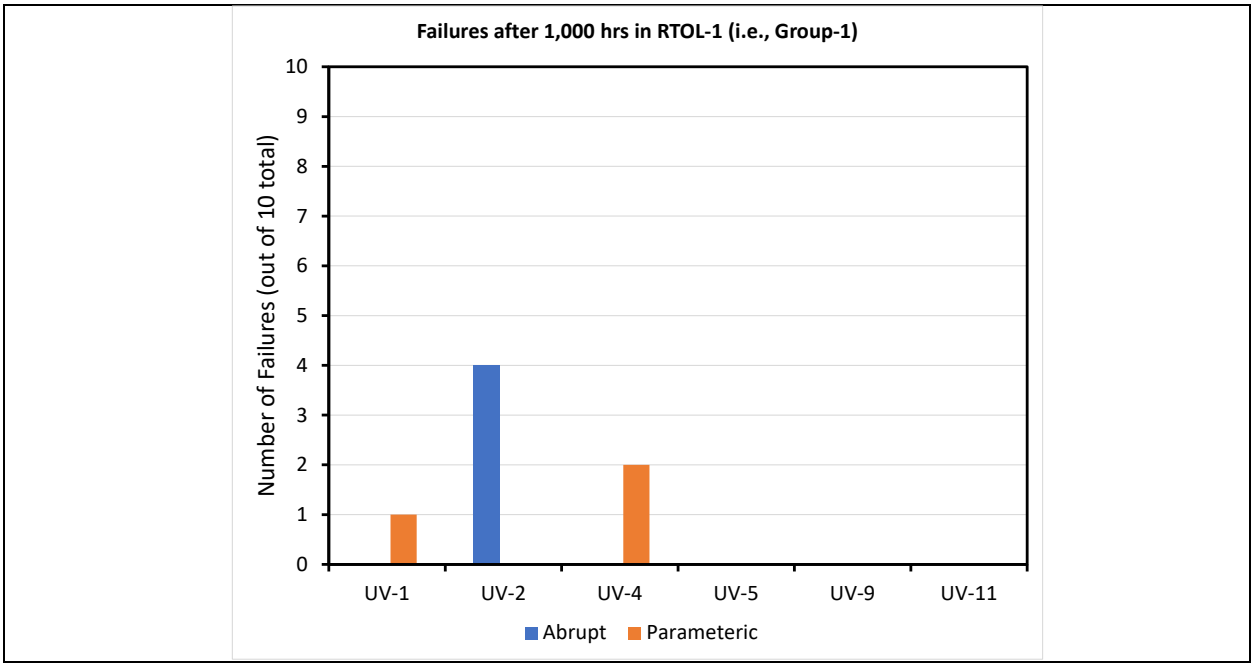

Figure 5-1. Abrupt and parametric failure distribution for products that experienced 1,000 hrs of RTOL-1.

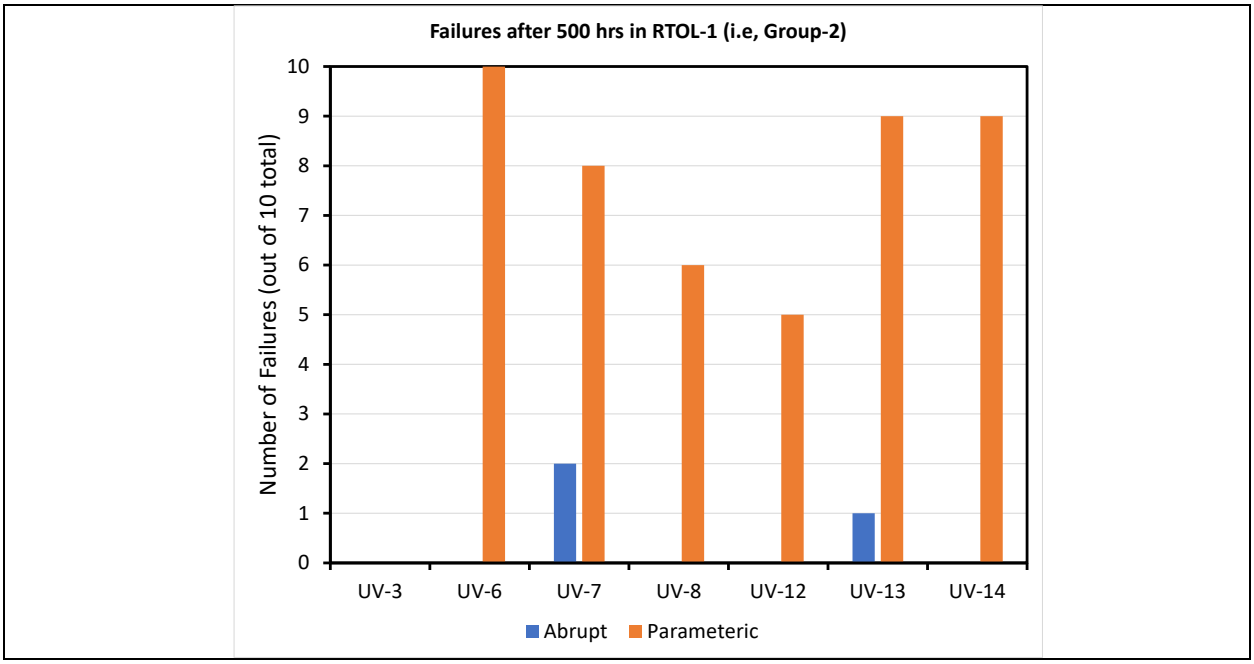

Figure 5-2. Abrupt and parametric failure distribution for products that experienced 500 hrs of RTOL-1.

5.1.2 Radiometric Measurement of RTOL-1 DUTs

The most common failure mode in RTOL-1 was parametric failure (i.e., RFM < 0.50). This failure mode accounted for 50 failures out of the test population of 130 DUTs (i.e., 13 products with 10 samples each), which is 38% of the total population. However, some of the products exhibited RFM values above the parametric failure threshold, when RFM was calculated as an average of all operating DUTs of a given product. The average RFM values for the products with

averages greater than 0.50 are shown in **Figure 5-3**. The products with high parametric failure rates, which led to RFM values below the parametric failure threshold, are omitted from **Figure 5-3** for simplicity. When computing the average RFM values at a given time, any abrupt failures were not included in the calculation; however, individual parametric failures were counted. For example, the four abrupt failures for UV-2 are not included in **Figure 5-3**, and the average was computed by using the six remaining samples. In contrast, the two parametric failures for UV-4 are included in the RFM values shown in **Figure 5-3**. The RFM values of these two UV-4 parametric failures were 0.47 and 0.32 after 1,000 hrs of RTOL-1.

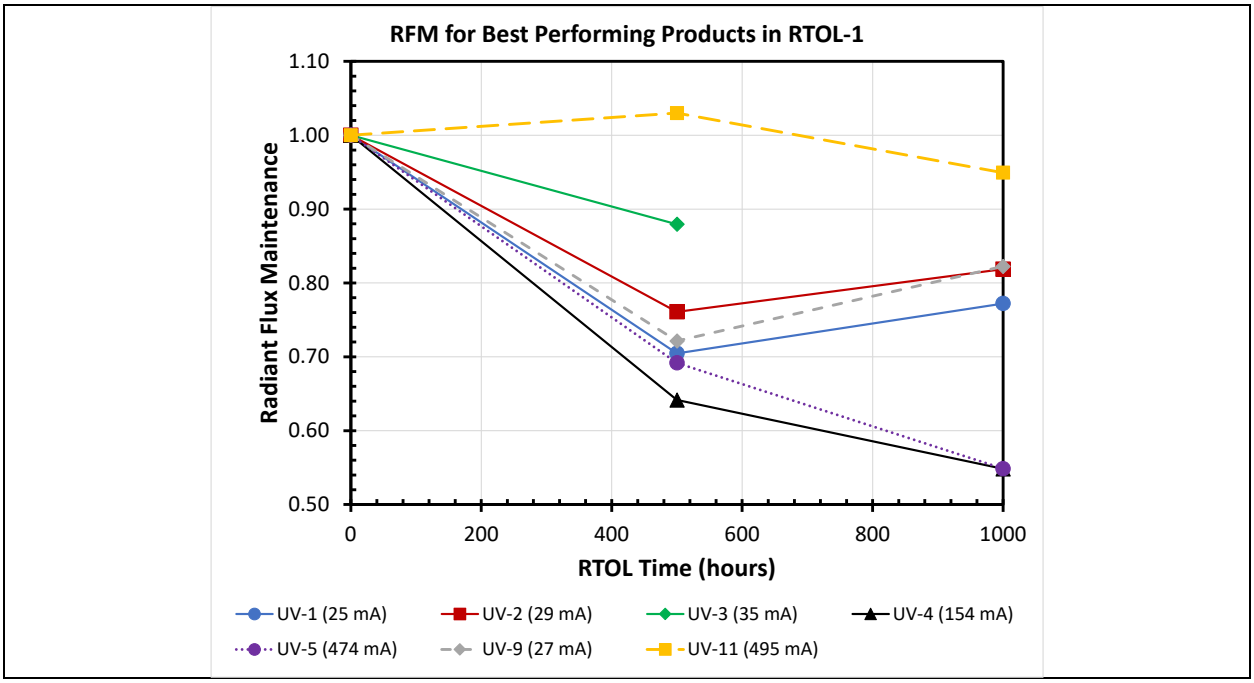

Figure 5-3. Average RFM values with the times for the products, which exhibited RFM > 0.50 during RTOL-1.

UV-11 exhibited the best mean RFM performance over the 1,000 hrs of testing during RTOL-1. The mean RFM of the UV-11 population exceeded 1.0 at the 500-hr measurement and dropped slightly to 0.95 after 1,000 hrs. Products UV-1, UV-2, and UV-9 exhibited a sharp drop in RFM to a value less than 0.80 after the 500-hr measurement, but the RFM value increased slightly when measured after 1,000 hrs of RTOL-1. These products (i.e., UV-1, UV-2, and UV-9) are operating at lower currents (< 30 mA) and lower emission wavelengths than UV-11 as shown in **Table 3-1**. In contrast, products UV-4 and UV-5 exhibited a continuous decline in RFM values at both 500 and 1,000 hrs, and these products were operated at I_f values of 154 and 474 mA, respectively. Both UV-4 and UV-5 had similar emission wavelengths to UV-1 and UV-2. After 1,000 hrs, the RFM values of UV-4 and UV-5 were barely above the parametric threshold; it is anticipated that further testing of these products would cause them to have an RFM below 0.50 during RTOL-1.

In addition to the parametric failures, a total of seven abrupt failures occurred with products UV-2 (four failures), UV-7 (two failures), and UV-13 (one failure). Abrupt failures are easy to

identify by visual inspection because the operational UV LEDs also emit a small amount of visible light. Six of these abrupt failures were because of shorting; the unbiased resistances of these DUTs are shown in **Table 5-1**, along with the expected resistances as measured on the control devices. The exact failure times of these six DUTs are not known, although inspections occurring during testing helped to provide a maximum failure time (e.g., right censored data indicated by < x where x is the first time that the failure was observed) or the time interval when the failure occurred (e.g., interval censored samples such as DUT-1052). The lone UV-13 failure was because the wire bonds broke, which produced an abrupt failure. This failure was noticed after 92 hrs of RTOL-1 testing, and it is speculated that this failure was tied to the high operational temperature of the UV-13 DUTs before the cooling plate was added after 92 hrs.

Table 5-1. Resistance of RTOL-1 Abrupt Failure DUTs and Their Controls

Product Number	DUT Number	Failure Time (hr)	Unbiased Resistance
UV-2 (control)	1075	Not applicable	> 30 MΩ[a]
UV-2	1052	334–358	1.5 Ω
UV-2	1054	< 500	1.3 Ω
UV-2	1055	< 289	1.0 Ω
UV-2	1058	< 289	372 Ω
UV-7 (control)	1250	Not applicable	> 30 MΩ[a]
UV-7	1227	< 500	2,297 Ω
UV-7	1235	< 500	0.6 Ω

[a] The UV-2 DUTs have a protective diode, so resistance is given for zero forward bias when measured with a multimeter. In reverse bias, the resistance is approximately 9.1 megaohms (MΩ) through the protective diode.

5.1.3 I-V Curves of DUTs During RTOL-1

The I-V properties of the DUTs were measured in their initial condition, after 500 hrs of continuous operation during RTOL-1, and after 1,000 hrs of continuous operation during RTOL-1 (when applicable). In a broad sense, the I-V curves of the DUTs in RTOL-1 can be divided into four distinct types based on the circuit examples presented in **Figure 4-1**. These four distinctive types are as follows:

- All DUTs of a given product exhibited no change.
- All DUTs of a given product exhibited the characteristic hump of a parasitic circuit after RTOL-1.
- All DUTs of a given product exhibited low levels of a parasitic circuit but not the distinctive hump.
- The DUTs of a given product exhibited a combination of the three behaviors previously mentioned.

The first of these four distinctive I-V profiles was demonstrated by the behavior of UV-4, which showed very little change in the I-V characteristics as shown in **Figure 5-4**. All 10 UV-4 samples exhibited the same behavior, which permitted the I-V measurements of the samples to be averaged and a mean I-V profile to be calculated for the initial and post-1,000-hr RTOL states.

During initial testing, the mean V_{th} value of the UV-4 DUTs during RTOL-1 was 5.454 V (σ = 0.062), and the mean serial resistance (R_{serial}) value was 6.742 Ω (σ = 0.157). After 1,000 hrs of RTOL-1, the mean V_{th} value was 5.439 V (σ = 0.067), which is statistically indistinguishable from the initial value (p = 0.61). In contrast, the mean R_{serial} value for UV-4 dropped to 5.922 Ω (σ = 0.178), which was found to be statistically different from the initial value at a 95% confidence level ($p < 0.0001$). It is assumed that the influence of annealing during RTOL-1 was responsible for the drop in the R_{serial} value. However, the RFM value after 1,000 hrs of RTOL-1 testing was 0.55 (**Figure 5-3**). Because there was minimal change in the I-V characteristics of the UV-4 DUTs, this finding suggests that other (likely non-electrical) factors may be involved in the RFM decline for these samples. Previously, such behavior was attributed to package degradation [9; 27], which is one possibility here. Another possibility is a change in the transmittance of the p-type layer, which is known to have poor UV transmittance [7–11].

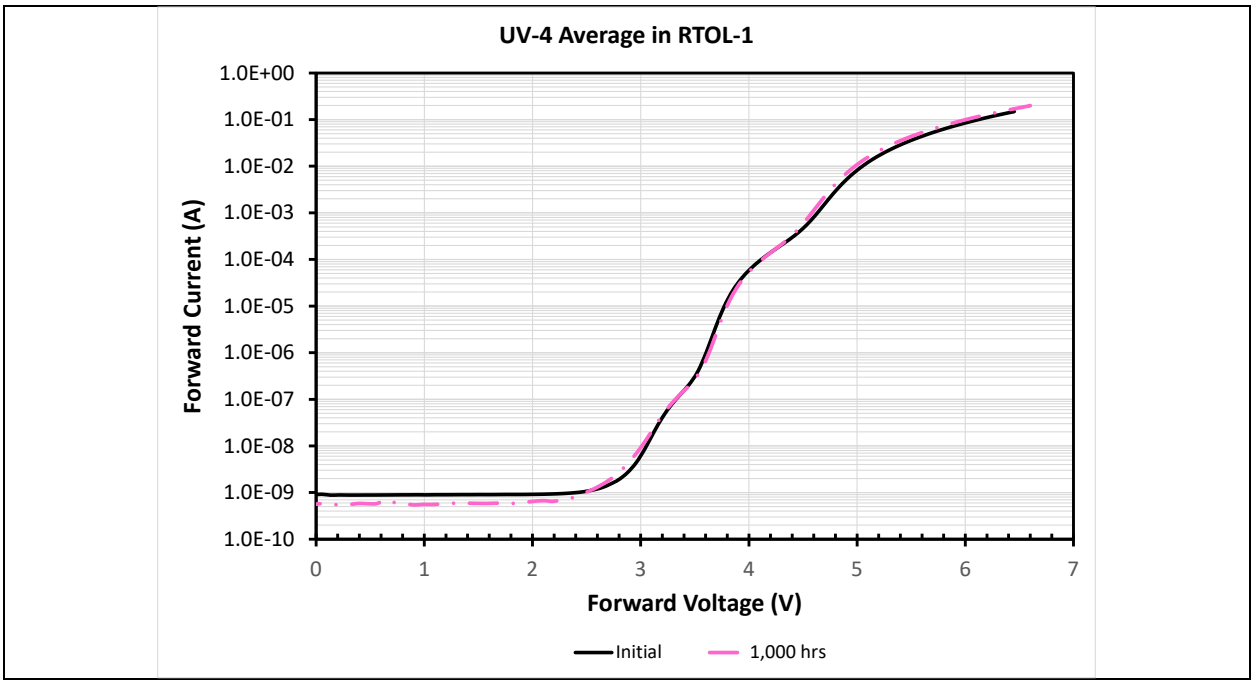

Figure 5-4. Average I-V measurements of 10 UV-4 DUTs in initial condition and after 1,000 hrs of continuous operation in RTOL-1 conditions.

For product UV-6, all 10 DUTs exhibited very similar initial behavior, and after 500 hrs of operation in RTOL-1, their behavior shifted in the same manner for all DUTs. Consequently, an average I-V profile can be calculated, and the average initial and 500 hr I-V measurements are presented in **Figure 5-5**. In the initial condition, the mean V_{th} value was computed to be 5.001 V ($\sigma = 0.029$), and the mean R_{serial} value was 2.312 Ω ($\sigma = 0.110$). After 500 hrs of continuous operation during RTOL-1, there was a large hump in the I-V profile from 0 V to 4.25 V. The corresponding resistance calculated for the 0–4.25 V was not constant (as would be expected for a pure parallel resistance). Instead, the resistance in the 0–4.25 V range decreased from approximately 5×10^9 Ω to 3×10^5 Ω over this interval, which indicates a contribution from a high impedance diode (i.e., Circuit-2). After 500 hrs of RTOL-1, the mean V_{th} value of the UV-6 DUTs was 5.026 V ($\sigma = 0.024$), which was higher by a statistically significant amount from the initial V_{th} value ($p = 0.05$). In addition, the R_{serial} value was 2.879 Ω ($\sigma = 0.285$) after 500 hrs of continuous operation during RTOL-1; this value was higher by a statistically significant amount than the initial value ($p < 0.0001$). This finding suggests the occurrence of additional losses in the semiconductor after RTOL-1, resulting in the need for higher V_f values to achieve V_{th}.

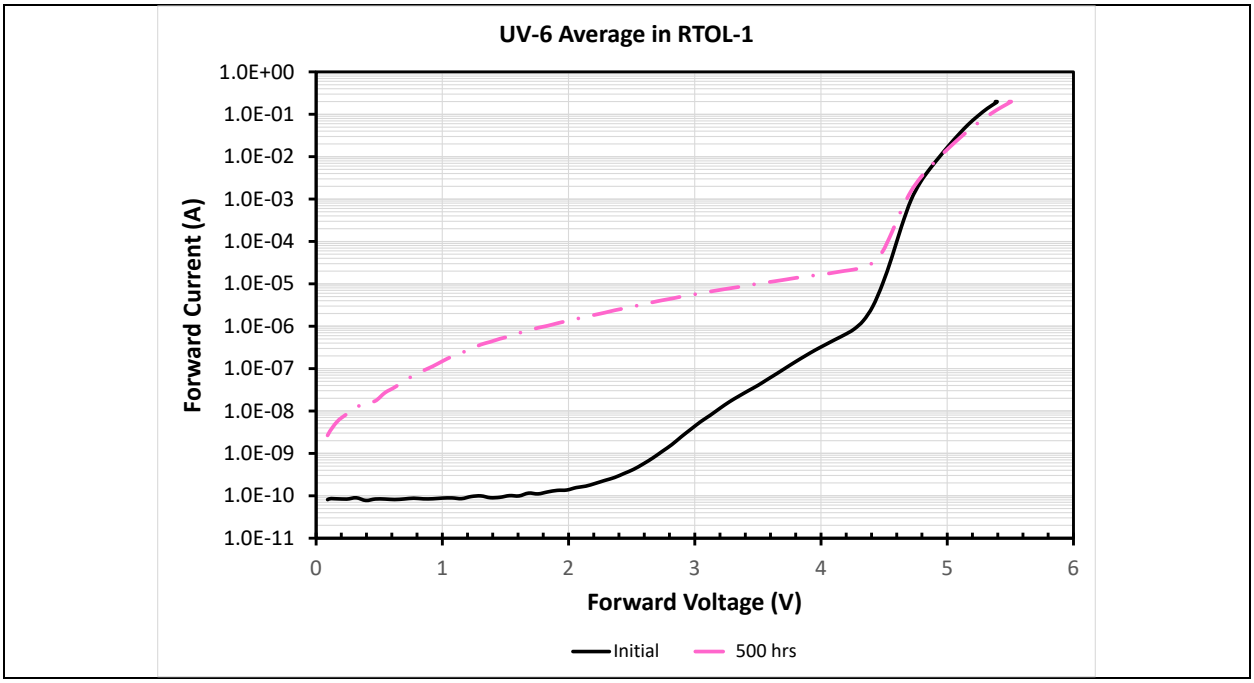

Figure 5-5. Average I-V measurements of the 10 UV-6 DUTs in initial condition and after 500 hrs of continuous operation during RTOL-1. This behavior is characteristic of the I-V profile of a Circuit-2 structure.

The third distinctive I-V profile observed during RTOL-1 was best demonstrated by the behavior of UV-12 DUTs with similar behavior observed for the other UV-A products (i.e., UV-11, UV-13, UV-14). All 10 UV-12 DUTs exhibited the same initial behavior, and after 500 hrs of operation during RTOL-1, their behavior shifted in the same manner with similar magnitude for all DUTs, allowing an ensemble average to be calculated for the population. The average initial and 500 hr I-V measurements are presented in **Figure 5-6**. During the initial testing, the 10 UV-12 DUTs exhibited a typical diode I-V shape, and the values were calculated to be 3.219 V (σ = 0.006) for V_{th} and 1.409 Ω (σ = 0.043) for R_{serial}. However, after 500 hrs of testing, parasitic behavior was evident in all 10 DUTs, resulting in an increase in I_f over the range from 0 V to 3.2 V. The resistance was found to change starting at approximately 10^8 Ω at 0 V and decreasing to approximately 4×10^5 Ω at 3 V with an I-V shape that is indicative of a parasitic diode with high R_{serial} value in parallel with the UV-emitting diode (i.e., Circuit-2). After 500 hrs of testing, the mean V_f had increased slightly to 3.221 V (σ = 0.006), but this difference was not found to be statistically significant (p = 0.452). The mean R_{serial} value after 500 hrs of RTOL-1 increased to 1.447 Ω (σ = 0.046), and the difference between the two mean R_{serial} values was also outside the limits of statistical significance for 95% confidence level (p = 0.07). In this instance, the change in leakage current below 3.2 V did not produce a statistically significant change in V_{th} and R_{serial}.

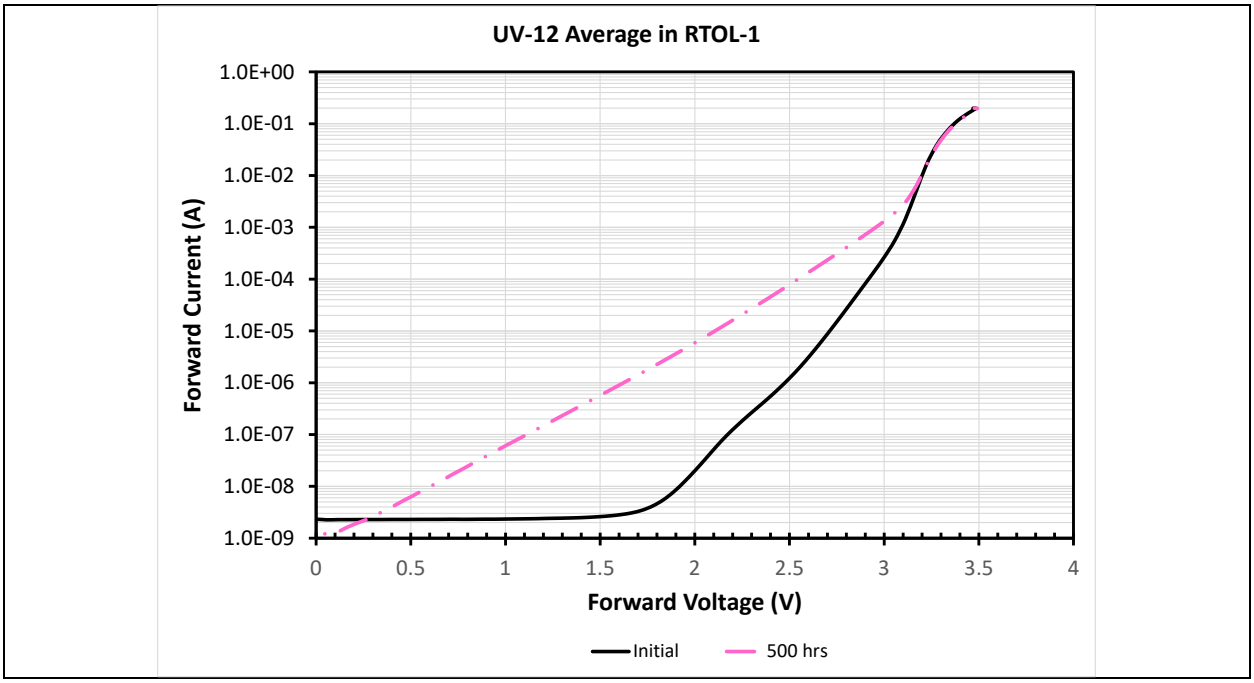

Figure 5-6. Average I-V measurements of 10 UV-12 DUTs in initial condition and after 500 hrs of continuous operation in RTOL-1 conditions. This behavior is characteristic of a Type-3 I-V profile.

For most of the products in RTOL-1, the I-V curves varied from DUT to DUT to the point in which there was not a single behavior that could be assigned for all DUTs of some products. This is the fourth I-V profile, and this behavior occurred for UV-1, UV-2, UV-3, UV-5, UV-7, UV-8, and UV-9. Most commonly, some of the DUTs of a given product exhibited minimal changes between the initial and post-RTOL-1 I-V curves, whereas other products exhibited evidence supporting the formation of a parasitic diode (with high R_{serial} values) in parallel with the UV-emitting diode. The time evolution of this type of I-V behavior at lower stress conditions is investigated in more detail in **Section 5.2**.

5.2 RTOL-2

When conducting RTOL-2, the I_f values and current densities for all DUTs were significantly reduced compared with RTOL-1 as shown in **Table 3-2**. The products were divided into two groups during testing: Group-A and Group-B. Group-A, which consisted of UV-5, UV-6, UV-7, UV-11, UV-12, UV-13, and UV-14, completed 3,000 hrs of RTOL-2. Group-B, which consisted of UV-1, UV-2, UV-3, UV-4, UV-8, and UV-9, completed up to 2,500 hrs of tests. Testing on UV-2 was stopped after 1,000 hrs because of a high failure rate.

5.2.1 Failures Observed During RTOL-2

The DUTs were regularly analyzed after each round of RTOL-2 by using both radiometry and I-V measurements. The measurements of all 10 DUTs for each product occurred at 0; 500; 1,000; 2,000; and 3,000 hrs for Group-A; and 0; 500; 1,000; 2,000; and 2,500 hrs for Group-B. At intermediate times (e.g., 100 hrs, 250 hrs, 750 hrs) only three samples of each product were measured, and the same samples were measured at each intermediate time. These measurements

provided a basis for classification of the DUTs at the end of the RTOL-2 test period as (1) still operating, (2) abrupt failure, or (3) parametric failure. The abrupt and parametric failures for the Group-A products that experienced 3,000 hrs of RTOL-2 are shown in **Figure 5-7**. Likewise, the abrupt and parametric failures for the Group-B products that experienced 2,500 hrs of RTOL-2 are shown in **Figure 5-8**.

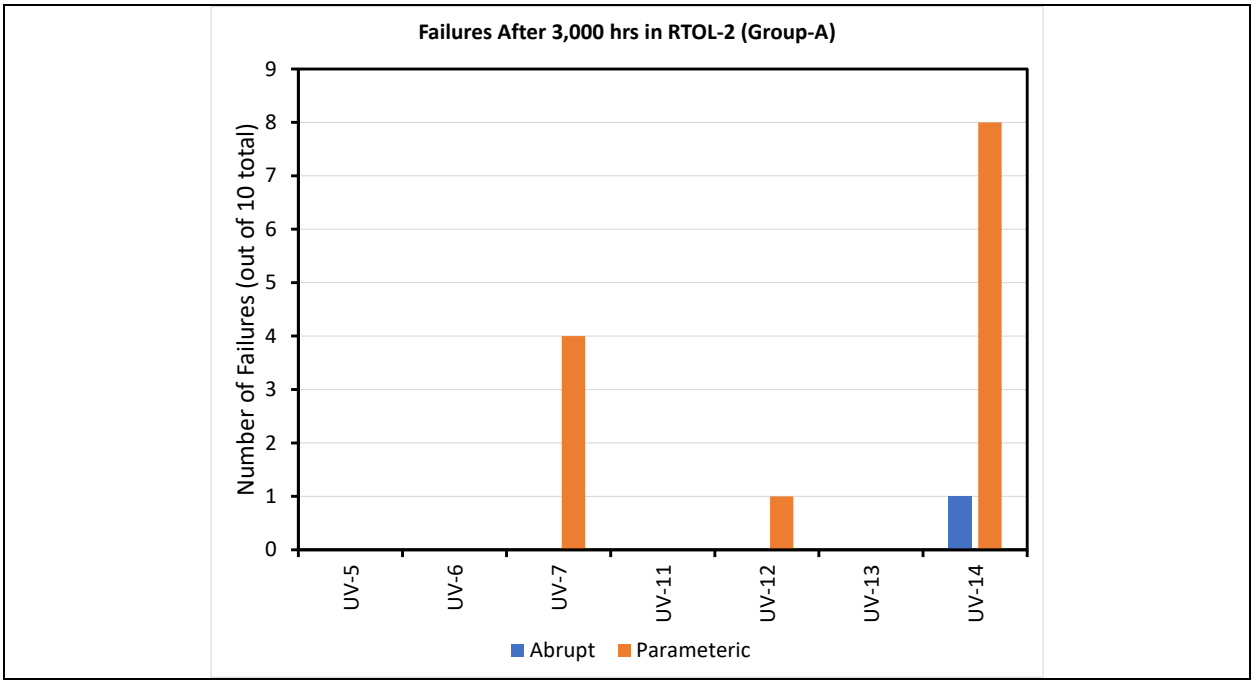

Figure 5-7. Abrupt and parametric failure distribution for products that experienced 3,000 hrs of RTOL-2.

During these milder conditions, there were no abrupt or parametric failures for UV-1, UV-5, UV-6, UV-11, and UV-13, and only one parametric failure was observed for UV-12 and one abrupt failure for UV-9 (see **Figure 5-7** and **Figure 5-8**). In contrast, UV-2 was found to have continued issues with abrupt failures during RTOL-2, and UV-14 had a high rate of parametric failure, along with a single abrupt failure, through 3,000 hrs of RTOL-2. As a result of its high abrupt failure rate during both RTOL-1 and RTOL-2, UV-2 DUTs were dropped from testing after 1,000 hrs. Altogether, a total of 32 failures were observed during RTOL-2. Eleven were abrupt failures, with UV-2 accounting for 64% of the abrupt failures. The other 21 DUTs were classified as parametric failures, with UV-7, UV-8, and UV-14 accounting for 86% of the parametric failures during RTOL-2. Clearly, there is a wide range of reliabilities among the different UV LED products in this test matrix.

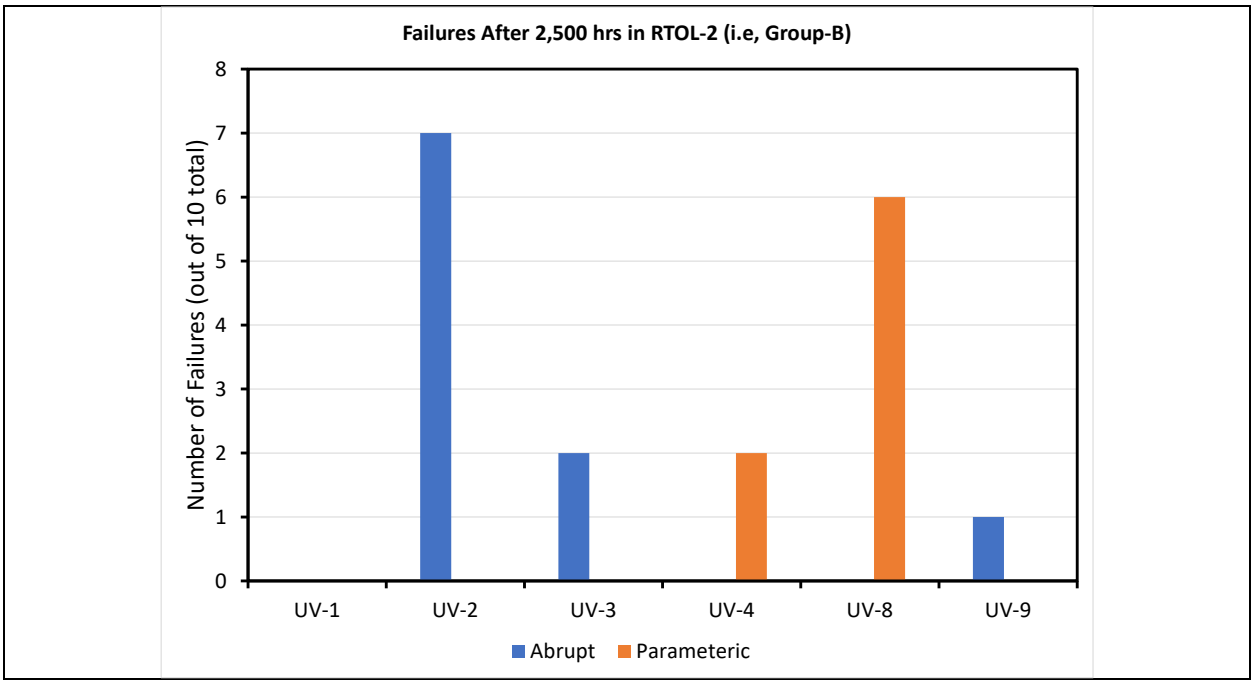

Figure 5-8. Abrupt and parametric failure distribution for products that experienced 2,500 hrs of RTOL-2.

The timing of the failures varied widely from part to part. **Figure 5-9** shows the number of failures measured at each RTOL-2 cycle for the four products with the highest failure rate. One limitation of **Figure 5-9** is that radiometric measurements were only taken on all samples at 0; 500; 1,000; 2,000; 2,500; and 3,000 hrs; therefore, the products with high parametric failure rates (e.g., UV-8, UV-14) will tend to have most failures at these times. However, abrupt failures are readily apparent at any time because a small amount of visible light is produced by all the products in the test matrix and the absence of such visible light emissions is evidence of an abrupt failure. Consequently, the occurrence of an abrupt failure can be recognized for any DUT whenever they are inspected.

The data in **Figure 5-9** demonstrate that the abrupt failure rate of UV-2 was consistent during the experiment, with two abrupt failures observed at 250, 500, and 1,000 hrs, and a single failure observed at 750 hrs. This behavior is suggestive of an intrinsic manufacturing defect that appears throughout its operating cycle. However, for UV-7 and UV-14, the number of parametric failures increased with time. This behavior was consistent with wearout mechanisms such as a gradual decline in RFM for the entire test population. In contrast, UV-8, which also exhibited a high rate of parametric failure, did not demonstrate any additional failures after 500 hrs of testing. This finding suggests that the failure rate of UV-8 stabilized after a sub-population with high failure rates had been screened out. This behavior is suggestive of different sub-populations among the test samples for this product, possibly resulting from variabilities in the processes used for manufacturing. Based on this outcome, a screening test of between 200 hrs and 500 hrs may be useful in identifying UV products with sub-populations that are likely to show high parametric failure rates.

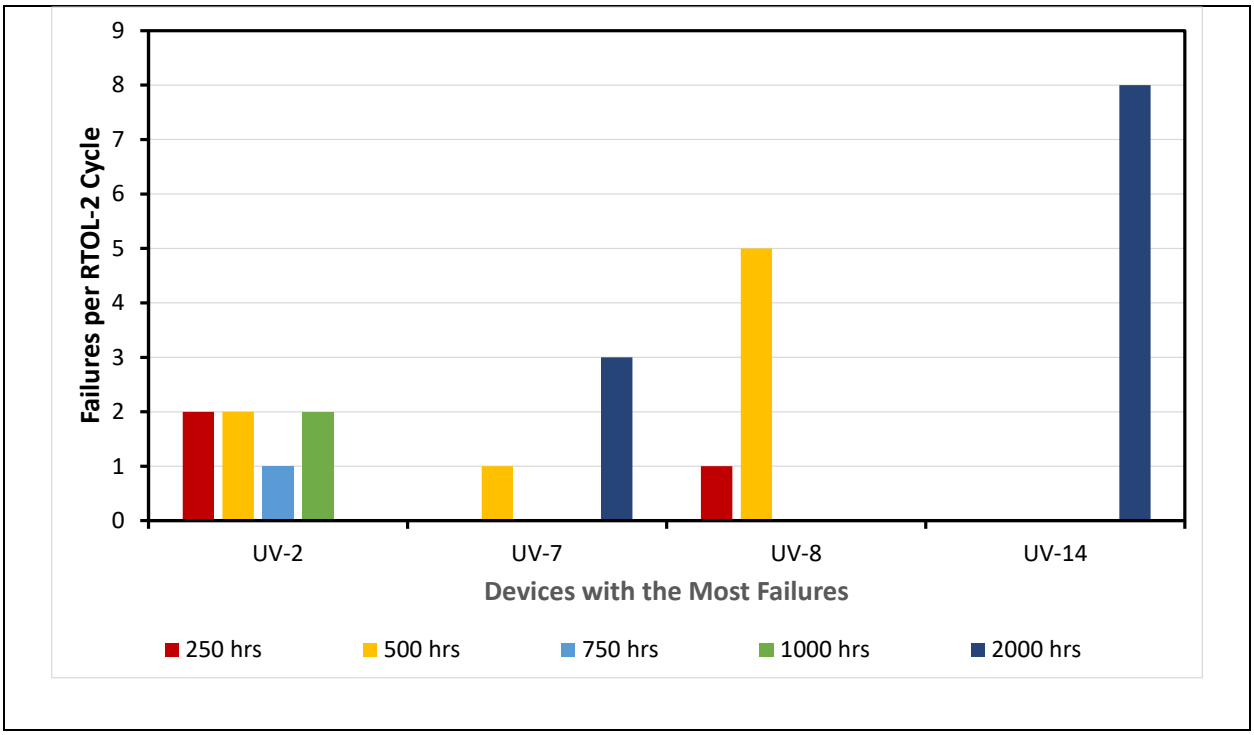

Figure 5-9. Distribution of failures of select products for each RTOL-2 cycle.

5.2.2 Radiometric Measurement of DUTs During RTOL-2

The RFM of products in the test matrix was often better during RTOL-2 than RTOL-1 because of the milder experimental conditions. For example, the average RFM values for all products except for UV-8 was greater than 0.5 at the end of RTOL-2 compared with RTOL-1 during which six products had RFM values less than 0.5. The RFM data for the Group-A products are shown in **Figure 5-10**, and the data for the Group-B products are shown in **Figure 5-11**. In general, a gradual decline in RFM with time was found for most products.

In agreement with the results from RTOL-1, UV-11 exhibited the best average RFM performance, with values of 1.0 or greater at all measurement intervals. The average RFM values for UV-1, UV-3, UV-5, and UV-12 were also greater than 0.75 at the completion of RTOL-2. The average RFM values for UV-4, UV-7, UV-9, and UV-14 all declined more rapidly over the test period and exhibited RFM values of 0.60 or less at the conclusion of this test. The products with nominal maximum emission wavelengths (λ_{max}) of 310 nm or 275–280 nm in the test matrix exhibited a sharp drop in RFM during the first 100 hrs of operation. This drop in RFM ranged from approximately 0.11 (UV-1, UV-5, and UV-6) to 0.26 (UV-7). After this initial drop in RFM, there was a more gradual decline for products with nominal λ_{max} of 310 nm or 275–280 nm. In contrast, the products with nominal λ_{max} of 365 nm all exhibited RFM values > 0.97 after 100 hrs of testing; however, after this amount of time, the average RFM values for UV-12, UV-13, and UV-14 showed a gradual decline, whereas the average RFM value for UV-11 remained above 1.0.

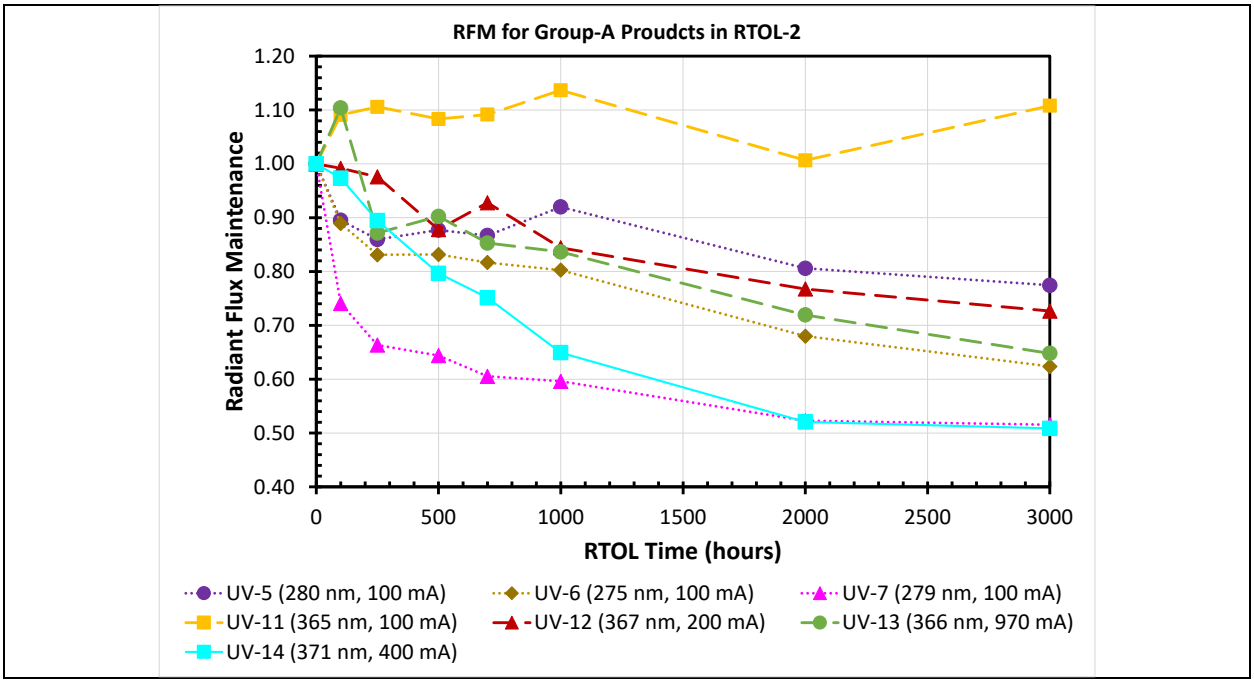

Figure 5-10. Average RFM values with time for the Group-A products during RTOL-2.

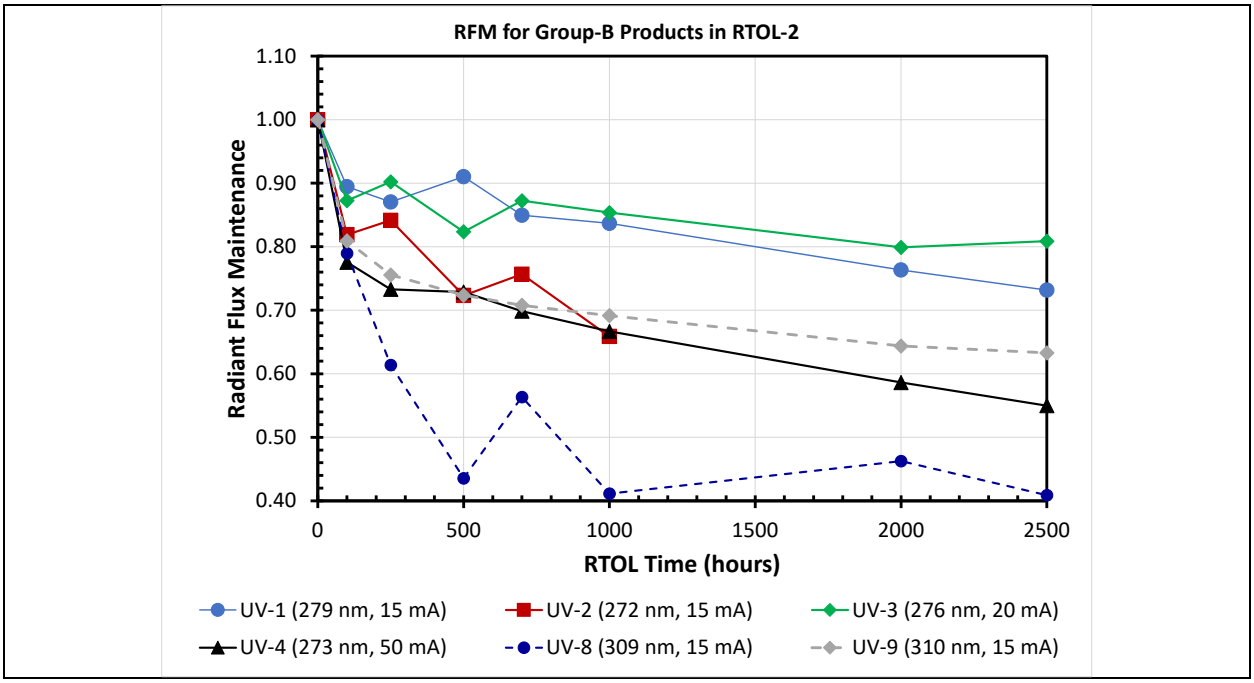

Figure 5-11. Average RFM values with time for the Group-B products during RTOL-2.

5.2.3 I-V Curves of DUTs During RTOL-2

The I-V properties of the DUTs during RTOL-2 were measured in their initial condition, and at periodic intervals during testing. I-V measurements were taken on all Group-A DUTs after 500; 1,000; 2,000; and 3,000 hrs, and measurements were taken on a sampling of the Group-A DUTs at 100, 250, and 750 hrs. For Group-B, I-V measurements were taken on all samples after 500; 1,000; 2,000; and 2,500 hrs, and intermittent sampling of select Group-B DUTs took place at

100, 250, and 750 hrs of RTOL-2. The initial I-V curves and the I-V measurements after the completion of RTOL-2 are presented in **Appendix B** for all products in this study.

Some of the products exhibited the same I-V behavior during RTOL-1 and RTOL-2 testing. UV-4, which was operated at one-third the I_f value in RTOL-2 than in RTOL-1, continued to exhibit minimal change in the I-V curve between the beginning and ending of test (**Figure 5-4** for RTOL-1 and **Figure B-4** for RTOL-2). Most of the UV-4 DUTs exhibited I-V curves that are typically expected for LEDs. The current in the samples is small at low voltages and gradually increases up to V_{th} and beyond. The resistance exhibits the opposite pattern with high resistance values followed by a continual decline. The lone exception to this behavior among the UV-4 DUTs that were tested was DUT-1120 (**Figure B-4**), and the first 750 hrs of the time evolution of the I-V curve for DUT-1120 is shown in **Figure 5-12**. A parasitic diode can be seen to make a small contribution to the initial I-V curve, as indicated by small hump between 2.5 V and 3.5 V. After 100 hrs during RTOL-2, this small hump had grown substantially and appeared over the range from 1 V to 3.5 V; however, with additional testing through 2,500 hrs, only small changes in the serial resistance of the parasitic diode were observed, as indicated by the small changes in the characteristic hump between 1 V and 3.5 V.

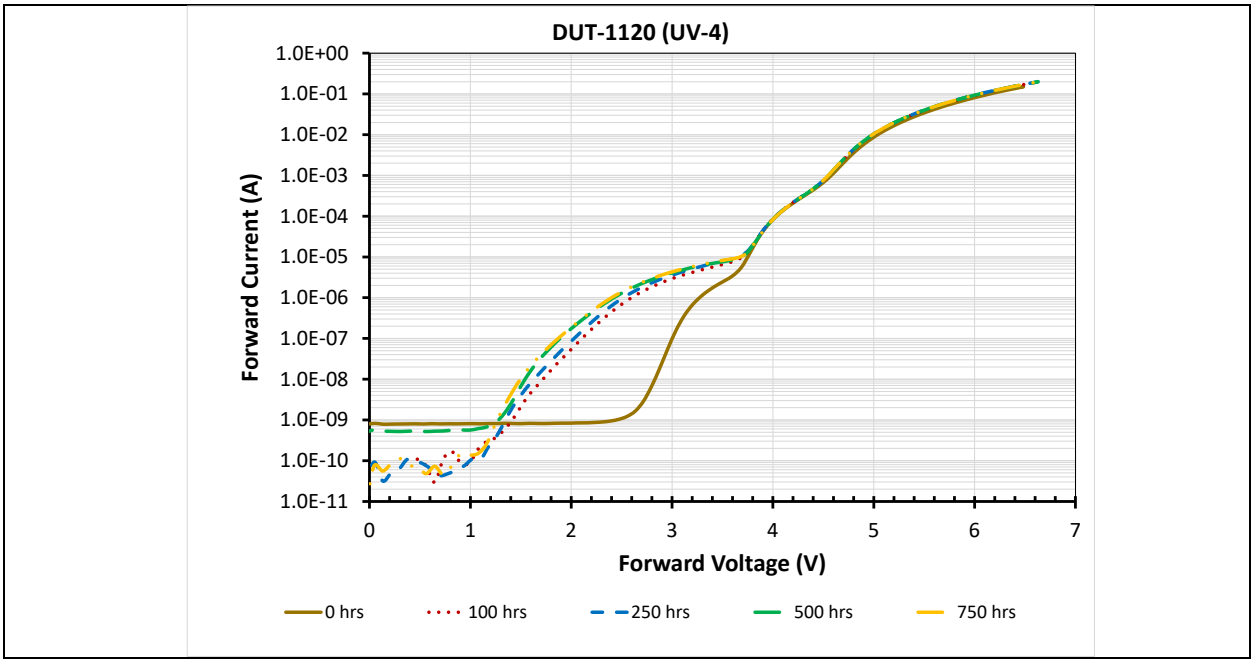

Figure 5-12. I-V measurements performed on DUT-1120 (UV-4) during the first 750 hrs of RTOL-2.

Likewise, the behavior of UV-6 and UV-12 were similar during RTOL-1 and RTOL-2. For UV-6, the same characteristic hump of a parasitic diode appeared in the DUTs during RTOL-1 and RTOL-2. This hump spanned the range from 0 V to 4.3 V during RTOL-1, whereas it only spanned the range from 1.0 V to 4.2 V during RTOL-2. An examination of the I-V curves at different times showed that the parasitic diode circuit caused the biggest change in the I-V profile during the first 100 hrs with subsequent changes much smaller. A similar behavior was found for UV-12 DUTs during RTOL-2. In this case, the voltage at which I_f exceeded 10^{-9} A

decreased from approximately 1.8 V to approximately 0.8 V during the 3,000 hrs of RTOL-2. This change in voltage and the accompanying change in the I-V curve are believed to coincide with the emergence of a parasitic, non-emitting diode circuit in parallel to the main UV diode circuit. Consistent with the previous examples, most of this change in the I-V curve occurred in the first 100 hrs of testing, as shown in **Figure 5-13**, with only minor changes thereafter.

A closer examination of the I-V curves for UV-8 (**Figure B-8**) demonstrated that there were at least three different sub-populations of this product that were tested during RTOL-2. These different sub-populations are likely the result of manufacturing process variations. Similar behavior was also exhibited by UV-8 during RTOL-1; however, the data are not shown here for brevity. This finding is further reinforced by an examination of the resistance versus voltage behavior (**Figure 5-14, Figure 5-15,** and **Figure 5-16**) for the three sub-populations of UV-8 DUTs. Sub-population 1, consisting of DUT-1262 and DUT-1267, exhibited a high resistance up to approximately 2.8 V, followed by a gradual decline until V_{th} was reached at approximately 5.50 V. This is typical behavior that can be expected of a properly functioning diode. As shown in **Figure 5-14**, there was little difference in the I-V curves for DUT-1262 and DUT-1267 as received and after 2,500 hrs of RTOL-2. The RFM for DUT-1267 showed a drop to 0.89 during the first 100 hrs of testing, and then showed a gradual decline to 0.80 after 2,500 hrs. Similar behavior was found for DUT-1262 and DUT-1267 at the times when all samples were measured (i.e., 500 hrs; 1,000 hrs; 2,000 hrs; and 2,500 hrs), suggesting that the RFM behavior of DUT-1262 was similar to that of DUT-1267.

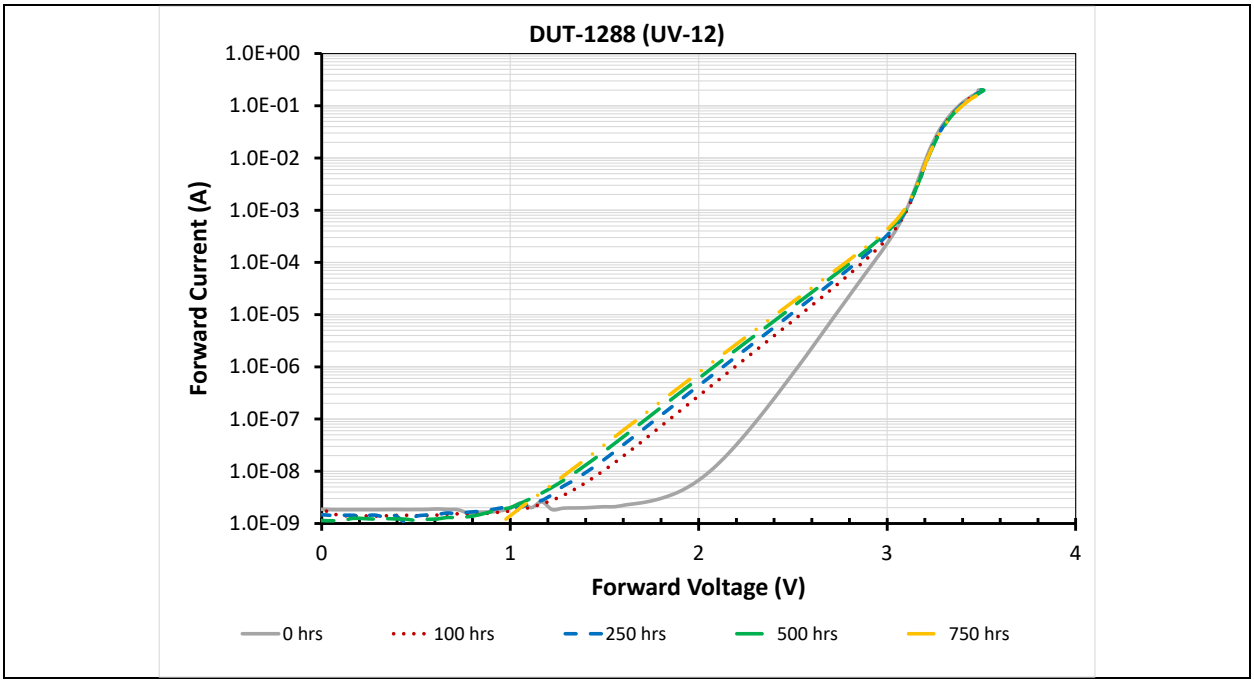

Figure 5-13. I-V measurements performed on DUT-1288 (UV-12) during the first 750 hrs of RTOL-2.

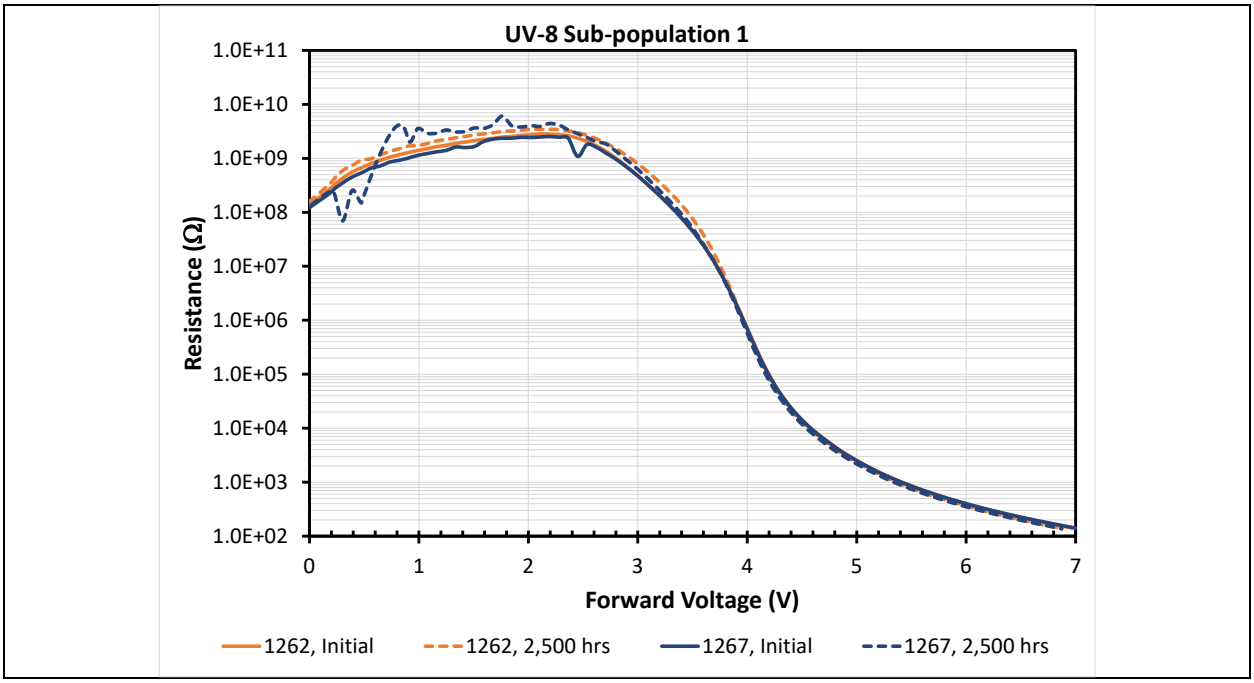

Figure 5-14. Resistance as a function of voltage for two UV-8 LEDs, DUT-1262 and DUT-1267, in initial state and after 2,500 hrs of RTOL-2.

Other UV-8 DUTs showed strong evidence of the emergence of a parasitic diode circuit as early as 100 hrs of RTOL-2 and continuing through the remainder of these tests. For example, Sub-population 2, consisting of DUT-1263 and DUT-1268, showed evidence of a deviation from typical diode behavior during RTOL-2 and the emergence of a parasitic diode that changes both the resistance and the I-V curves over the range from approximately 0.7 V to 4.6 V (**Figure 5-15**). The RFM value for DUT-1263 dropped to 0.87 after 100 hrs of operation, and then to 0.77 after 250 hrs of operation. After 250 hrs of operation, a more gradual decline in RFM was observed for DUT-1263, with the RFM value being 0.73 after 2,500 hrs of testing. Similar RFM values were observed for DUT-1263 and DUT-1268 at test times of 500 hrs; 1,000 hrs; 2,000 hrs; and 2,500 hrs, suggesting that their RFM behavior was similar throughout the test period. Although these RFM values are lower that those of Sub-population 1, they are still well above the parametric failure threshold (i.e., RFM < 0.50).

The other six UV-8 DUTs composed Sub-population 3, and they exhibited poorer resistance and I-V profiles than the other sub-populations. The resistance profiles of the six DUTs in their initial condition and after 2,500 hrs of RTOL-1 are presented in **Figure 5-16** and the similarities to **Figure 5-15** can be seen. Of particular note is the behavior of DUT-1264 and DUT-1269, which both demonstrated a parasitic diode in the initial state, as evidenced by the hump in the I-V and resistance curves between 2 V and 4.5 V (see **Figure B-8**). After 2,500 hrs of RTOL-2, these samples also demonstrated much lower resistance and higher current over the range from 0 V to 1 V. The RFM of DUT-1264 was tracked throughout the test, and it dropped from an initial value of 1.0 to 0.62 after 100 hrs; a second drop in RFM to 0.21 was recorded after 250 hrs. The sample was declared a parametric failure after 250 hrs of testing, the first detected for UV-8, but

continued during testing through 2,500 hrs, although the RFM value never exceeded 0.25 for the remainder of the test. The RFM values of the other five samples in Sub-population 3 (i.e., DUT-1261, DUT-1265, DUT-1266, DUT-1269, and DUT-1270) were similar to that of DUT-1264 at 500 hrs; 1,000 hrs; 2,000 hrs; and 2,500 hrs, suggesting that their RFM behaviors were similar throughout the test period.

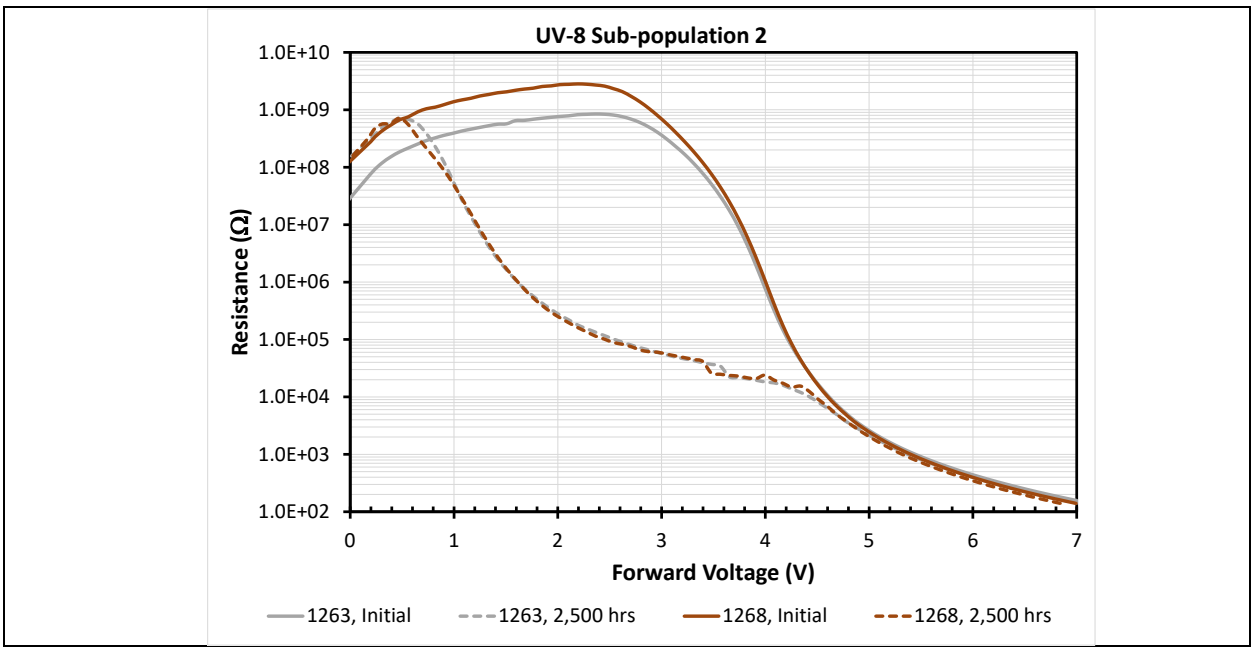

Figure 5-15. Resistance as a function of voltage for two UV-8 LEDs (i.e., DUT-1263 and DUT-1268) in initial state and after 2,500 hrs of RTOL-2.

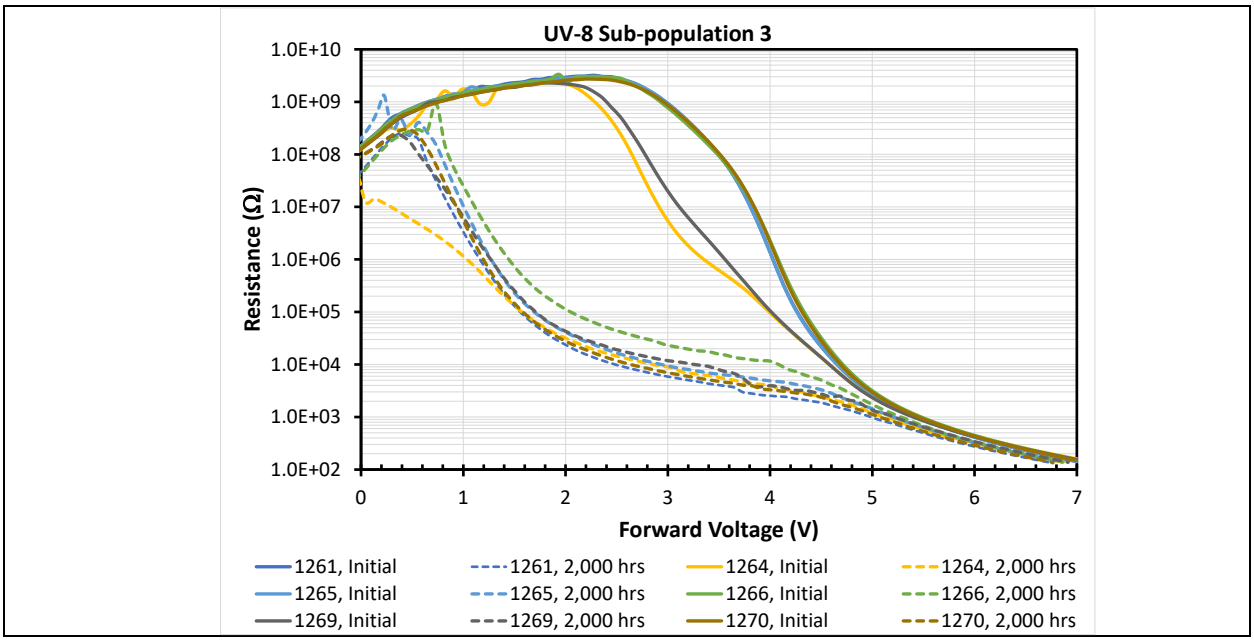

Figure 5-16. Resistance as a function of voltage for six UV-8 LEDs (DUT-1261, DUT-1264, DUT-1265, DUT-1266, DUT-1269, and DUT-1270) in initial state and after 2,000 hrs of RTOL-2.

5.3 T-H Storage Test

Three UV-C LED products (i.e., UV-4, UV-5, and UV-6) were chosen for the T-H storage test conducted at 50°C and 90% RH. Even though the UV LED products were not powered during the T-H storage test, the RFM values for the samples exhibited a steady decline as shown in **Figure 5-17**. Although this level of radiant flux decay is slower than observed during RTOL-2, it is still significant. The findings indicated that these three UV-C LED products, UV-4, UV-5, and UV-6, undergo radiant flux decay in an elevated temperature and humidity environment, even when not powered. Consequently, this finding is an indication that temperature and/or humidity exposure can affect the lifetime of UV-C LED products, even when they are in the off-state.

I-V measurements were also taken for the samples subjected to the T-H storage test. Except for one UV-6 device, there was minimal change in the I-V characteristics of the DUTs between the beginning value and after 148 hrs of T-H storage test. Specifically, the change in V_{th} was not statistically significant. This finding suggested that the decrease in RFM values occurring in the T-H storage test was likely not because of changes in the electrical properties of the DUTs. Other factors such as increased optical absorption potentially caused by several different factors (e.g., increased absorption in the p-type layer, deposition of organic residues on the lens) are possibly causes, although the exact mechanism is unknown at this time. The transmittance of the p-type layer is already low [7–11], and it is possible that added heat and humidity can reduce the transmittance further. Potential sources of organics outgassing inside the packages include the adhesive used for lid seal (UV-4 and UV-6), the silver-filled adhesive used to attach the protective diode (UV-4), and solder flux residues from the flip chip operation [27]. The only ways to verify the deposition of organics on the lens of the UV LED package would be to conduct UV transmittance tests of the lid when new and after use or perform chemical analysis (e.g., Fourier transform infrared spectroscopy) of any residues of the lens.

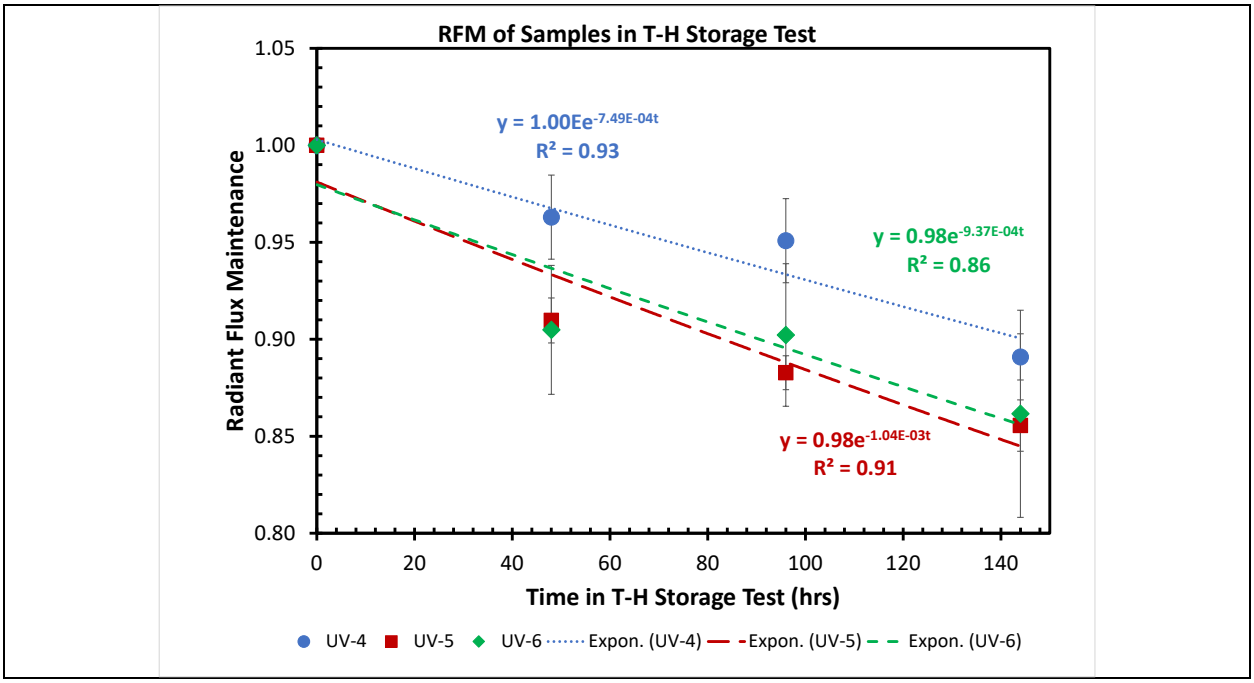

Figure 5-17. Average RFM values and standard deviation for unpowered samples in the T-H storage test.

6 Discussion

This study examined the performance of a matrix of 13 different UV LED products operating in a room temperature environment at a current near the rated maximum of each product (i.e., high current) and at a lower current. In addition, a subset of three products chosen from the test matrix was subjected to a storage test at 50°C and 90% RH in an unpowered state. These conditions were chosen to examine the impacts of current, temperature, and humidity on the lifetime of UV LED products. The failure rate of the UV LED products varied, depending on the environmental conditions and product design, although parametric failure was more common during these tests than abrupt failure.

RTOL-1 was conducted near the maximum rated I_f values for each UV LED, and efforts were made to keep the T_{sp} value below 60°C. This T_{sp} value was readily achieved by using a passive heat sink for all UV DUTs in the test matrix except for UV-13, which required water-chilled cooling plates to reduce T_{sp} below 60°C. Using the criteria that a parametric failure occurs when the RFM value is below 0.5 and abrupt failure occurs when no detectable radiation is emitted from the LED, a total of 57 failures (44% of the total population) were detected during RTOL-1. As shown in **Figure 5-1** and **Figure 5-2**, only seven were abrupt failures; the remaining 50 were parametric failures. As broken out in **Table 6-1**, the total failure percentage (i.e., the number of abrupt failures plus the number of parametric failures divided by the sample population) during RTOL-1 for the products with nominal λ_{max} of 365 nm (i.e., UV-11, UV-12, UV-13, and UV-14) was highest (63%) of any group, driven primarily by the high parametric failure rates in UV-12, UV-13, and UV-14. The total failure percentage for the products with nominal λ_{max} of 310 nm (i.e., UV-8 and UV-9) was 40% during RTOL-1. The total failure percentage for the products

with nominal λ_{max} of 275–280 nm (i.e., UV-1, UV-2, UV-3, UV-4, UV-5, UV-6, and UV-7), which had the largest population of samples being tested, was 39% during RTOL-1. However, the 275 nm exhibited a higher percentage of abrupt failures, driven mainly by the performance of UV-2.

Table 6-1. Percentage of Abrupt and Parametric Failures of the UV LED Products in RTOL-1 and RTOL-2 by λ_{max}

Nominal λ_{max}	RTOL-1		RTOL-2	
	Abrupt Failures	Parametric Failures	Abrupt Failures	Parametric Failures
275–280 nm	9%	30%	13%	7%
310 nm	0%	40%	5%	35%
365 nm	3%	60%	3%	23%

RTOL-2 was conducted at lower I_f values than RTOL-1, which resulted in a reduction in the T_{sp} value. Even though the RTOL-2 test was at least three times longer than RTOL-1, the milder environmental conditions resulted in a reduction of failure rates to 26% for the 365 nm products and to 20% for the 275–280 nm products. However, the 275–280 nm products again exhibited the highest abrupt failure rate of the products during RTOL-2, and this outcome was impacted heavily by the relatively poor performance of the UV-2 product.

Although the numbers of parametric failures were lower during RTOL-2, there were still some products (e.g., UV-8, UV-14) that exhibited high parametric failure rates during both RTOL-1 and RTOL-2. RTOL-1 lasted for 500 or 1,000 hrs depending on the sample, and no interim measurements were taken. In contrast, RTOL-2 lasted much longer, and interim measurements were taken on a sampling of the test population, which allows for a comparison of the findings for RTOL-1 with those for RTOL-2 at comparable test times. The RFM values at the end of RTOL-1, at an interim time during RTOL-2 corresponding to the duration of RTOL-1, and at the end of RTOL-2 are listed for each product in the test matrix in **Table 6-2**. In general, most products exhibited lower RFM values during RTOL-1 than at an equivalent time during RTOL-2, as would be expected from the milder conditions of RTOL-2. The only instances where this was not the case were UV-2, UV-3, and UV-9. These products generally have the lower maximum I_f ratings of those in this test matrix. UV-1, which is also a low I_f device, did not follow this trend for the lower power products, and its RFM value was slightly higher after 1,000 hrs of RTOL-2 than RTOL-1. UV-8, which is also a low I_f device, had comparable RFM values in RTOL-1 and RTOL-2. These findings for the lower power products indicate that current alone is not universally the sole determining factor for RFM. Other factors, such as T_j, semiconductor quality, and chip design, may also play a role.

In contrast, the higher power products exhibited higher RFM values in the milder conditions of RTOL-2 than in RTOL-1. This finding shows that reducing the I_f value and likely T_j can increase

the lifetime of some UV LED products. This rule appears to have a greater impact on the higher power UV LED products with rated maximum I_f values of 200 mA and above.

Table 6-2. Average RFM Values at the Completion of RTOL-1 and RTOL-2 for Each Product Tested[a]

Product	RTOL-1		RTOL-2			
	Final Test Time (hrs)	Final RFM Value	Interim Test Time (hrs)	Interim RFM Value	Final Test Time (hrs)	Final RFM Value
UV-1	1,000	0.77 (0.18)	1,000	0.84 (0.13)	2,500	0.73 (0.12)
UV-2	1,000	0.82 (0.03)	1,000	0.66[b] (0.01)	1,000	0.66[b] (0.01)
UV-3	500	0.88 (0.05)	500	0.82 (0.05)	2,500	0.81 (0.02)
UV-4	1,000	0.54 (0.11)	1,000	0.67 (0.06)	2,500	0.55 (0.07)
UV-5	1,000	0.55 (0.02)	1,000	0.92 (0.01)	3,000	0.77 (0.01)
UV-6	500	0.22 (0.04)	500	0.83 (0.02)	3,000	0.62 (0.02)
UV-7	500	0.06 (0.04)	500	0.64 (0.12)	3,000	0.52 (0.10)
UV-8	500	0.44 (0.36)	500	0.44 (0.33)	2,500	0.41 (0.39)
UV-9	1,000	0.82 (0.14)	1,000	0.69 (0.03)	2,500	0.63 (0.03)
UV-11	1,000	0.95 (0.04)	1,000	1.14 (0.02)	3,000	1.11 (0.02)
UV-12	500	0.47 (0.13)	500	0.88 (0.12)	3,000	0.73 (0.14)
UV-13	500	0.09 (0.03)	500	0.90 (0.10)	3,000	0.65 (0.05)
UV-14	500	0.38 (0.15)	500	0.80 (0.09)	3,000	0.51 (0.15)

[a] Standard deviations of RFM values are provided in parentheses.

[b] Testing of UV-2 RTOL was stopped at 1,000 hrs.

In contrast, no failures were observed during the T-H storage test, but it was the shortest duration test conducted during this study at 148 hrs. However, there was a significant depreciation in radiant flux ranging from 10% to 15% even though the DUTs were not powered during this test. This finding was true for both hermetic (i.e., UV-5) and non-hermetic (i.e., UV-4, UV-6) packages. Because the electrical performance of the UV LED products in the T-H storage test did not change after exposure to 5090, the reduction in RFM may be because of a change in the optical properties of the LED and/or the LED package [27].

6.1 Failure Mechanisms Involving Optical Degradation of UV LED Products

Optical degradation of the UV LED products in this test matrix resulted in some, but not all, of the parametric failures. Unfortunately, the definitive assignment of parametric failures during this test to either optical or electrical mechanisms would require additional study. However, the behavior of UV-4, UV-5, and UV-6 in the T-H storage test provided the strongest evidence that the degradation of the optical properties of the UV LED, the LED package, or both was occurring over time in an elevated temperature and humidity setting. The drop in RFM measured

for these samples (**Figure 5-17**) can only be caused by the effects of heat and humidity because of the following two reasons:

1. The DUTs were in an unpowered state during the T-H storage test.
2. The electrical properties of the DUTs were not changed by the T-H storage test as confirmed by the I-V measurements.

There are a few explanations for the degradation of optical performance caused by heat and/or humidity. However, these explanations are offered for consideration and none can be definitely proven as the root cause of initial RFM reduction at this time.

The first potential cause of this optical degradation was from the UV LED packaging process. Because the UV LED package is made from ceramic materials that have been gold plated, it is assumed that the package can withstand the modest temperatures of RTOL-1 and RTOL-2 without significant degradation. However, several sources of organic materials are used during package assembly. These organic materials include adhesives and solder fluxes used in flip chip bonding, die attach, protective diode attach, and attachment of the quartz lens. Such organic materials could outgas and could coat the interior surfaces of the package, including the LED chip, the reflectors, and the lens. The application of UV radiation could degrade these organic residues, which would decrease the reflectance or transmittance of any surface coated with the residues. For example, uncleaned solder flux residues are known to negatively impact the radiant flux emissions from flip chip LEDs [27], and conductive adhesive residues can negatively impact the resonant frequency of quartz crystal oscillators during their use [28].

Although a detailed study of potential sources of organic contamination in UV LEDs was beyond the scope of this work, some clues regarding potential sources were obtained with a visual inspection of the DUTs. **Figure 6-1** shows the potential sources of organic contamination for UV-13, and **Figure 6-2** shows the potential sources of organic contamination for UV-4 and UV-6. Similar sources of contamination occurred for all of the products with nominal λ_{max} of either 310 nm or 275–280 nm examined during this study because they have the same basic packaging structure as these LED products (albeit UV-13 has four die, whereas all of the other UV LED products only have a single die). Clearly, the surface cleanliness is sufficient at the wire bonding stage to form acceptable wire bonds, so die attach and protective diode attach processes may not be responsible for excessive organic residues. However, cleaning of the assembly is not possible after lid attach, and there is a significant amount of organic residues from the lid-seal adhesive on the gold plating on the top of the package. It is possible that these organic residues spread into the package and coated the lens and package structures. Furthermore, some designs (e.g., UV-4, UV-13) do not have a continuous lid-seal adhesive, which could allow for the escape of volatile components (as well as the ingress of outside contaminants), whereas others (e.g., UV-6) have a continuous adhesive on the lid seal. The impact of the lid-seal adhesive has been previously mentioned as a possible cause of reduced radiant flux during an examination of UV LED packaging methods [9]. Depending on the chemistry of this adhesive, its thickness, and its durability to UV exposure, these residues could be sufficient to attenuate UV radiation (e.g., a

UV curable lid-seal adhesive will absorb UV) in an operating diode, and the amount of attenuation would increase in time as more UV-induced degradation of the organic residues occurred. In addition, the composition and curing profile of the lid-seal adhesive is critical to minimizing outgassing and its deleterious effects [9].

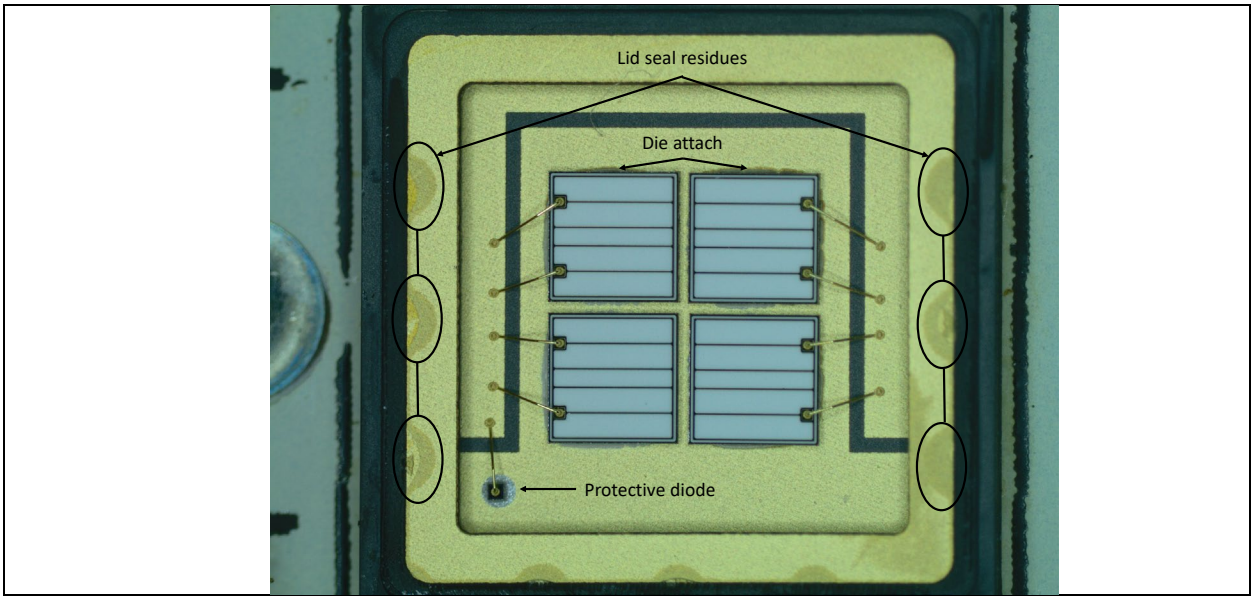

Figure 6-1. Potential sources of organic contamination for UV-13. The quartz lid had been removed from the sample. The presence of adhesive was also found on the lid of UV-13.

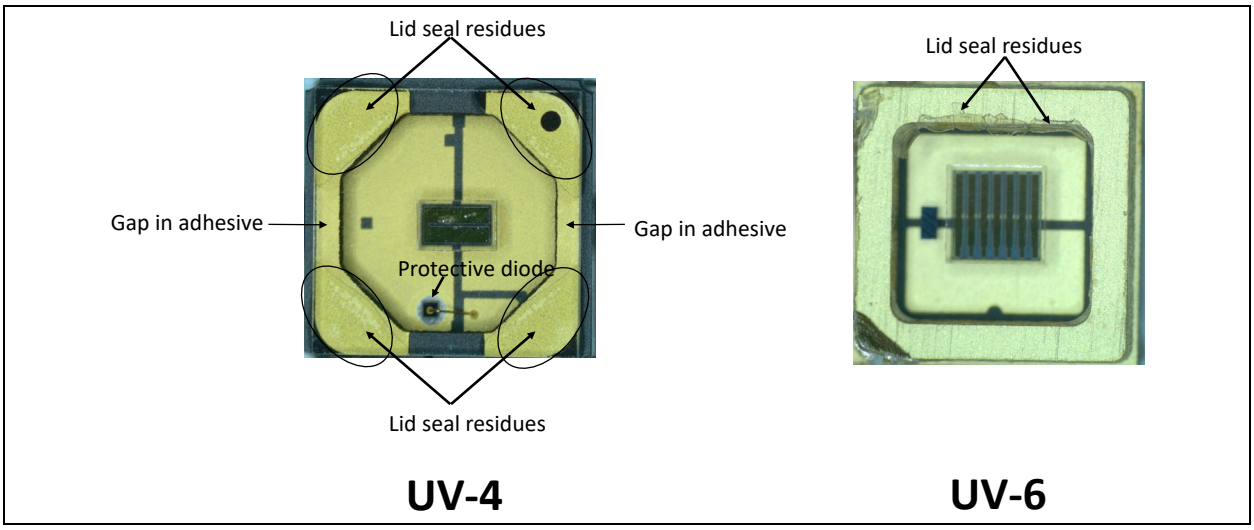

Figure 6-2. Potential sources of organic contamination for UV-4 and UV-6. The quartz lid was intact for UV-4 but had been removed for UV-6. Evidence of the adhesive was also found on the lid of UV-6.

Three of the UV-A LED products in the test matrix (i.e., UV-11, UV-12, and UV-14) have a packaging structure that was different from the other UV LED products. The package of UV-11 contained a silicone lens that was over molded onto the substrate—a package structure that is similar to a typical white high-power LED. The package of UV-12 consisted of the LED mounted in a shallow ceramic tub with the tub filled with a silicone encapsulant. This structure

was similar to that found in many mid-power LEDs (mp-LEDs) with the exception that the UV LED packages were made from ceramic, whereas most mp-LED packages are made from polymers. The package of UV-14 consisted of the LED mounted at the bottom of a cavity formed by a silver-plated reflector cup. A low viscosity substance (presumable a silicone) was used to fill the cavity, and a glass dome was placed on top.

The RFM value of UV-11 was maintained at a level greater than 0.95 for both RTOL-1 and RTOL-2, which is by far the best performance of any product in the test matrix. Although the test periods were limited, this finding demonstrated that some silicones can withstand UV-A radiation for prolonged periods of time. In fact, silicone chemistry has improved to the point where the transmittance in UV-A and UV-B is high for some silicone materials, although yellowing has been observed in some cases under UV radiation [29]. In contrast, for UV-12 and UV-14, silicone degradation (e.g., cracking, darkening) was a suspected cause for the rapid loss in RFM for these products during both RTOL-1 and RTOL-2. Evidence for silicone cracking was found in UV-14 DUTs after RTOL-1, and dark spots were found in the silicone layer for UV-12 after RTOL-1 but not after RTOL-2. This conclusion is based on general observations and knowledge of the impact of degradation of some silicones under UV radiation [9, 29–32]; however, confirmation of the impact of silicone yellowing on the high parametric failure rates for these products could not be determined within the scope of this study. For UV-13, the high parametric failure rate during RTOL-1 may be because of the high T_{sp} value during the first 92 hrs of operation, especially because acceptable RFM values were measured for UV-13 throughout RTOL-2 in which T_{sp} was much lower.

The second potential cause of optical degradation of the UV LED products lies within the LED itself. Changes in the optical properties of the UV LED semiconductor materials can increase internal absorption of radiation and reduce emitted radiation. Possible causes include changes in the reflectivity or absorbance of any material in the stack. The p-type layer contact, which is the last layer in the stack before emission from a flip chip diode, is one potential source of increased radiation adsorption over time. The p-type layer is known to have a higher than desired absorption for UV-B and UV-C radiation [11, 33].

6.2 Failure Mechanisms Involving Electrical Degradation of UV LED Products

Electrical degradation of UV LED products can result in both abrupt and parametric failures. Abrupt failures are straightforward to assign to electrical issues (e.g., shorting), whereas assignment of parametric failures to electrical degradation mechanisms caused by semiconductor defects is more complicated. In the current study, parametric failure was the dominant failure mechanism, accounting for 88% of the failures during RTOL-1 and 66% of the failures during RTOL-2. Abrupt failures were less common and accounted for 12% of the total failures during RTOL-1 and 34% of the failures during RTOL-2. Earlier studies demonstrated that the gradual decline of radiant flux in UV LED products depended primarily upon current, with temperature a secondary factor [34].

Abrupt failures of the UV LED products in this study occurred in 7 DUTs during RTOL-1 and 11 DUTs during RTOL-2. These 18 failures represent only 6.9% of the total test population of RTOL-1 and RTOL-2 (i.e., 260 DUTs). However, 11 out of 18 abrupt failures occurred in UV-2, with four failures occurring during 1,000 hrs of RTOL-1 and seven failures occurring during the first 1,000 hrs of RTOL-2. The other abrupt failures occurred in UV-3 (two DUTs during RTOL-2), UV-7 (two DUTs during RTOL-1), UV-9 (one DUT during RTOL-2), UV-13 (one DUT during RTOL-1), and UV-14 (one DUT at the end of RTOL-2). The abrupt failure found for UV-14 was an electrical short that occurred between radiometric and I-V testing after 3,000 hrs of operation during RTOL-2. This UV-14 sample is number 1318 in **Figure B-13**. The high failure rate of UV-2 suggests that this product had gross defects with epitaxial quality, which resulted in a high propensity of these DUTs to abruptly fail. Abrupt failures in UV LED products were previously associated with macroscopic defects in the alloy, including V defects [11, 34]. Other than UV-2, no other product in the test matrix demonstrated abrupt failure during both RTOL-1 and RTOL-2, suggesting that an abrupt failure was more of a random occurrence and not indicative of more systematic quality issues.

The role of defects in promoting the gradual decline of RFM values for UV LED products has been studied extensively [10, 12–15, 17, 20, 34–37]. A variety of analytical methods have been applied to investigating the causes of RFM loss in UV LED products. Some of the methods include electrical methods such as I-V [10, 12–15, 17, 20, 34–37] and capacitance-voltage measurements [20; 37]; spectroscopic methods such as deep-level transient spectroscopy (DLTS) [10, 13]; and chemical analysis methods such as secondary ion mass spectrometry (SIMS) [10, 17] and X-ray diffraction (XRD) [20]; imaging methods such as transmission electron microscopy (TEM) [10, 17, 37], atomic force microscopy (AFM) [20], and photoluminescence mapping [10]; and numerical simulations [35]. The conclusion from this prior research is that defects in the UV LED epitaxial structure create parallel circuits that provide tunneling pathways for non-radiative carrier recombination. The net result of the presence of these parallel and parasitic circuits is a reduction of radiative carrier recombination because carriers are lost to the parallel circuit, and reduced radiant emissions. These effects have been attributed by other researchers to trap-assisted tunneling (TAT) and have been assigned to the presence of various defects principally in the p-type layer [10, 12–15, 17, 20, 34–37].

Evidence for the emergence of a parallel diode circuit is found in previous studies, and this effect has been shown to be responsible for increases in non-radiative carrier recombination through modified SRH mechanisms. This behavior is identified by large increases (e.g., greater than 1,000-fold) in leakage current below V_{th}, culminating with the appearance of a hump on the I-V curve between 0 V and V_{th}. In the current work, evidence of the same increases in sub-threshold leakage currents occurred in many products during RTOL-1 and RTOL-2. In general, these features were absent or weak in the initial state of the DUTs but increased significantly in magnitude during operation.

However, such drastic changes in the I-V curves did not occur in all products or even within all DUTs of a given product. **Table 6-3** lists the percentage of DUTs for each product after the end of RTOL-1 and RTOL-2 that exhibited the characteristic hump at voltages below V_{th}, which indicates the presence of a parallel circuit. The behavior of UV-4 appears to be unique because only one device, DUT-1120, (out of 23 samples between RTOL-1, RTOL-2, and T-H test) displayed any evidence of a change in its I-V curve during RTOL-1 (**Figure 5-4**), the T-H storage test, or RTOL-2 (**Figure B-4**). Consequently, no UV-4 DUTs demonstrated TAT during RTOL-1, and only one (DUT-1120) exhibited TAT during RTOL-2. However, most products (e.g., UV-1, UV-3, UV-5, UV-8, UV-9) had some DUTs that showed minimal changes in the I-V measurements at the end of RTOL-2, whereas other DUTs of the same product displayed evidence of significant sub-threshold leakage currents. One of the best examples of this phenomenon was UV-8 (**Figure 5-16** and **Figure B-8**). During RTOL-2, DUT-1262 and DUT-1267 showed minimal changes in the I-V curves, and the RFM maintenance of these samples initially dropped to 0.89 by 100 hrs, but then showed a more gradual decline to 0.80 at the end of the test. In contrast, six UV-8 DUTs during RTOL-2 (i.e., DUT-1261, DUT-1264, DUT-1265, DUT-1266, DUT-1269, and DUT-1270) all exhibited a significant rise in TAT, which produced the characteristic hump in the I-V curve at sub-threshold voltages, and all DUTs were parametric failures in less than 500 hrs of testing. The same effect was also observed for UV-8 during 500 hrs of RTOL-1 test, in which four DUTs exhibited no change in the I-V curves, whereas the other six demonstrated strong evidence for TAT.

Table 6-3. Breakout of the Number of DUTs Exhibiting TAT Behavior During RTOL-1 and RTOL-2

Product Number	Percentage Showing TAT During RTOL-1	Percentage Showing TAT During RTOL-2
UV-1	70%	60%
UV-2	10%[a]	10%[a]
UV-3	60%	60%
UV-4	0%	10%
UV-5	40%	50%
UV-6	100%	100%
UV-7	90%	80%
UV-8	60%	80%
UV-9	10%	10%
UV-11	100%	100%
UV-12	100%	100%
UV-13	100%	0%
UV-14	100%	30%

[a] Only DUTs that exhibited TAT at the conclusion of RTOL-1 or RTOL-2 are counted. Abrupt failures are not counted.

This work also demonstrated that TAT typically appeared in a DUT within the first 100 hrs of testing. This phenomenon is demonstrated in this report by the behavior of one sample of UV-4 (**Figure 5-12**) and all samples of UV-12 **(Figure 5-13**). When TAT was present, the change in the I-V curve happened quickly for the first 100 hrs, and then the rate of change typically slowed, but a continual increase in the amount of TAT occurred throughout RTOL-2. This finding suggests that a short burn-in period (<500 hrs) can be used to identify products that will display a large amount of TAT and can be expected to show lower RFM performance.

Another key finding of this work was that the level of TAT was different between the InGaN UV LED products, which emit at approximately 365 nm, and the AlGaN UV LED products, which emit at approximately 310 nm or 275–280 nm. Only the AlGaN products exhibited a large, sub-threshold hump in the I-V curve, resulting in increases in leakage currents by a factor of 1,000-fold or more. In contrast, the amount of TAT occurring in the InGaN products was lower as indicated by the lack of the characteristic hump (**Figure 5-13**, **Figure B-10, Figure B-11**, and **Figure B-12**).

The higher levels of TAT found in the AlGaN LED products examined during this study suggest that electrical factors are the leading cause of parametric failure during these tests; this finding is in agreement with the literature [2, 6, 10, 11, 13–24, 28, 33–37]. These electrical factors, which are signaled by the appearance of a parasitic parallel circuit that reduces carrier concentrations, likely arose from defects in the epitaxial layer that produced a loss of carriers through modified SRH mechanisms. However, not all of the AlGaN DUTs exhibited this behavior because some DUTs within most of the tested products exhibited minimal evidence for the formation of the parasitic diode circuit and generally had higher RFM values. This finding is evidence of manufacturing process variability among the test products.

For the InGaN UV-A products, the conclusion was reached that the parametric failures observed for the 365 nm products were dominated by package effects such as silicone degradation (e.g., cracking, darkening) and the impact of residual organic residues following assembly processes that use adhesives (e.g., lid seal, die attach, protective diode attach). In addition, optical effects such as package degradation from organic residues may play a role in the drop in RFM over the first 100 hrs of operation of all the UV LED products examined during this study; therefore, this mechanism should not be ignored in any packaged UV products.

7 Conclusions

This work examined the long-term performance of a matrix of 13 commercially available, UV LED products, spanning the UV-A, UV-B, and UV-C bands of the electromagnetic spectrum. The intent of this report is to provide information to the lighting industry about the state of UV LEDs (as of mid-2021 when the tested products were purchased). Understanding the failure modes and failure rates of UV LEDs is important in improving UV product reliability at the LED, lamp, and luminaire level and is critical to developing products with higher efficiency, low carbon footprint, and significantly reduced environmental impact than LPMV lamps. Initial

benchmarks regarding the performance of these same products are provided in a previous report [1]. This current report examined the behavior of the UV LEDs in three different accelerated stress tests:

1. An RTOL-1 test conducted near the rate maximum I_f for each product
2. An RTOL-2 test conducted at a lower I_f value
3. A T-H storage test conducted in an unpowered state in an environmental chamber at 50°C and 90% RH.

Ten samples of each product were subjected to either 500 hrs or 1,000 hrs of RTOL-1, and separate populations of 10 samples of each product were subjected to 2,500 hrs or 3,000 hrs of RTOL-2. The samples were regularly checked for abrupt failure (i.e., produced zero UV radiation) and parametric failure (i.e., radiant flux was less than 50% of the initial value). Out of the 260 samples during RTOL-1 and RTOL-2, there were a total of 89 failures (34%), 57 of which occurred during RTOL-1. Parametric failure was the most common failure mode, accounting for 71 total failures. Parametric failure occurred through one of several mechanisms, including growth of defects in the LEDs that produced a parasitic diode circuit that reduced the number of carriers available for radiative recombination, and package effects arising from the use of polymers in the finished package (e.g., silicone encapsulants, lid-seal adhesives, die attach). Although both mechanisms are active in the tested products, the formation of parasitic diode circuits was judged to be more prevalent in AlGaN LED products than in InGaN LED products. Package effects were likely more significant in InGaN LED products, but package degradation, caused by UV-induced changes in the absorption of organic residues, may play a role in the initial drop in RFM values found in AlGaN products as well. Abrupt failures, likely caused by gross defects in the epitaxial layer account, accounted for only 18 total failures (20% of the failures). The abrupt failure mode was especially prominent in one product (i.e., UV-2).

The results of the study provided many key insights into the reliability of UV LED products:

1. The efficiency of InGaN LED products emitting at 365 nm was superior to that of AlGaN LED products emitting at 310 nm or 275 nm. However, in general, the efficiency of UV LEDs needs to be improved to at least the level of efficiency of LPMV lamps as described in a previous report [1].
2. The reliability of the tested products varied widely with some products (e.g., UV-5, UV-11), exhibiting no failures during tests, whereas others (e.g., UV-2, UV-14) exhibited very high failure rates. Reducing the parametric failure rate, and to a lesser extent the abrupt failure rate, is another long-term need for UV LED technology.
3. The reliability of UV LED products was, in general, poorer than the blue InGaN LED products used in SSL. However, one product that was tested (UV-11) exhibited performance similar to a common blue LED, including high flux maintenance during

testing. The structure and performance of UV-11 could serve as a blueprint for improving the quality of UV-A LEDs, at a minimum, and possibly UV-B and UV-C LEDs.

4. Not all DUTs of a given product exhibited the same long-term performance behavior. For some products, there were DUTs that exhibited minimal evidence of parasitic diode pathways and good RFM, whereas other DUTs of the same product exhibited strong parasitic diode pathways, which are correlated with reduced RFM. This outcome may be the result of sub-populations within a given product that are caused by manufacturing process variability. This finding suggests that additional improvement in the long-term reliability of UV LED products is possible with further epitaxial process optimization.
5. Monitoring the I-V characteristics of UV LEDs provides a simple screening tool to identify products that will form a diode circuit in parallel with the main diode during operation. The rise of such parallel circuits has been shown to reduce radiant carrier recombination, increase parasitic losses, and negatively impact efficiency. A simple burn-in test of less than 500 hrs followed by I-V measurements is usually sufficient to identify products with reduced reliability, especially in the UV-B and UV-C bands, as evidenced by significant increases in leakage currents below V_{th}.

In short, there appears to be a significant opportunity to improve the reliability of UV LED products with additional research into semiconductor manufacturing processes customized to AlGaN alloys, improved LED packaging technologies aimed at UV LED products, and advanced materials for use in UV LED products that have low absorption and low organic residues. Such an investment will likely help to improve the energy efficiency of UV LED products, which would accelerate their commercial use in industrial process, medical treatments, and disinfection applications. This investment will also reduce energy consumption and the carbon footprint of UV sources used in industrial, medical, and building technologies. In addition, replacing LPMV lamps with the more environmentally benign UV LEDs will eliminate a significant source of mercury contamination in the environment and provide benefits to ground water and the food chain.

References

1. Davis, J. L., Rountree, K., Pope, R., Clayton, C., Dart, A., McCombs, M., & Wallace, A. (2021). *Initial benchmarks of UV LEDs and comparisons with white LEDs.* U.S. Department of Energy—Lighting R&D Program. https://www.energy.gov/sites/default/files/2022-01/ssl-rti-uv-leds-nov2021.pdf
2. Young, A. R., Moan, J., Bjorn, L. O., & Nultsch, W. (Eds.). (1993). *Environmental UV photobiology*. Springer. https://doi.org/https://doi.org/10.1007/978-1-4899-2406-3
3. Mukish, P. (2021, June 7). *Has COVID-19 pandemic initiated the spark for UVC LED to shine?* 2021 International Ultraviolet Association (IUVA) World Congress, Online.
4. DOE BTO Lighting R&D Program. (2022). *2022 Solid-state lighting R&D opportunities*. U.S. Department of Energy—Lighting R&D Program. https://www.energy.gov/sites/default/files/2022-02/2022-ssl-rd-opportunities.pdf
5. Maxson, P., Bender, M., & Culver, A. (2010). *Mercury in fluorescent lighting: Unnecessary health risks and actionable solutions*. Clean Lighting Coalition. https://cleanlightingcoalition.org/wp-content/uploads/sites/96/Mercury-in-Fluorescent-Lighting_FINAL.pdf
6. Schubert, E. F. (2006). *Light-Emitting Diodes* (Second ed.). Cambridge, UK: Cambridge University Press. https://www.ifsc.usp.br/~lavfis2/BancoApostilasImagens/ApConstantePlanck/ApCtePlanck2013/LIGHT-EMITTING%20DIODES.e-0521865387-2e.pdf
7. Krames, M. (2021, March 23). *Webinar: UV-C advancements enable innovative germicidal uses displacing lamps in some scenarios*. LEDs Magazine.
8. Kneissl, M., Seong, T.-Y., Han, J., & Amano, H. (2019). The emergence and prospects of deep-ultraviolet light-emitting diode technologies. *Nature Photonics, 13*(4), 233–244. https://doi.org/10.1038/s41566-019-0359-9
9. Peng, Y., Liang, R., Mou, Y., Dai, J., Mingxiang, C., & Luo, X. (2019). Progress and perspective of near-ultraviolet and deep-ultraviolet light-emitting diode packaging technologies. *Journal of Electronic Packaging, 141*. https://doi.org/10.1115/1.4044624
10. De Santi, C., Caria, A., Piva, F., Meneghesso, G., Zanoni, E., & Meneghini, M. (2021). Degradation mechanisms of InGaN visible LEDs and AlGaN UV LEDs. In R. W. Herrick & O. Ueda (Eds.), *Reliability of Semiconductor Lasers and Optoelectronic Devices* (pp. 273-312). Woodhead Publishing. https://doi.org/10.1016/b978-0-12-819254-2.00001-1
11. Mondal, R. K., Adhikari, S., Chatterjee, V., & Pal, S. (2021). Recent advances and challenges in AlGaN-based ultra-violet light emitting diode technologies. *Materials Research Bulletin, 140*, 111258. https://doi.org/https://doi.org/10.1016/j.materresbull.2021.111258
12. Monti, D., M., M., De Santi, C., Meneghesso, G., & Zanoni, E. (2016). Degradation of UV-A LEDs: Physical origin and dependence on stress conditions. *IEEE Transactions on Device and Materials Reliability, 16*(2), 213–219. https://doi.org/10.1109/TDMR.2016.2558473
13. Wang, Y.-Z., Zheng, X.-F., Zhu, J.-D., Li, P.-X., Ma, X.-H., & Hao, Y. (2019). New view on the variation of forward conduction mechanisms derived from electrical stress in UV-A light emitting diodes. *Superlattices and Microstructures, 130*, 208–214. https://doi.org/https://doi.org/10.1016/j.spmi.2019.04.038

14. Arques-Orobon, F. J., Vazquez, M., & Nuñez, N. (2020). Lifetime analysis of commercial 3 W UV-A LED. *Crystals, 10*(12), 1083. https://www.mdpi.com/2073-4352/10/12/1083. PMID: doi:10.3390/cryst10121083
15. Monti, D., Meneghini, M., De Santi, C., Meneghesso, G., Zanoni, E., Glaab, J., Rass, J., Einfeldt, S., Mehnke, F., Enslin, J., Wernicke, T., & Kneissl, M. (2017). Defect-related degradation of AlGaN-based UV-B LEDs. *IEEE Transactions on Electron Devices, 64*(1), 200–205. https://doi.org/10.1109/TED.2016.2631720
16. Fujioka, A., Asada, K., Yamada, H., Ohysuka, T., Ogawa, T., Kosugi, T., Kishikawa, D., & Mukai, T. (2014). High-output-power 255/280/310 nm deep ultraviolet light-emitting diodes and their lifetime characteristics. *Semiconductor Science and Technology, 29*(084005). https://iopscience.iop.org/article/10.1088/0268-1242/29/8/084005
17. Ma, Z., Cao, H., Lin, S., Li, X., & Zhao, L. (2019). Degradation and failure mechanism of AlGaN-based UVC-LEDs. *Solid-State Electronics, 156*, 92–96. https://doi.org/https://doi.org/10.1016/j.sse.2019.01.004
18. Trivellin, N., Monti, D., Piva, F., Buffolo, M., De Santi, C., Zanoni, E., Meneghesso, G., & Meneghini, M. (2019). Degradation processes of 280 nm high power DUV LEDs: impact on parasitic luminescence. *Japanese Journal of Applied Physics, 58*, SCCC19. https://doi.org/10.7567/1347-4065/ab1393
19. Wang, Y.-Z., Zheng, X.-F., Shu, J.-D., Xu, L.-L., Xu, S.-R., Liang, R.-L., … Hao, Y. (2020). Degradation in AlGaN-based UV-C LEDs under constant current stress: A study on defect behaviors. *Applied Physics Letters, 116*(203501). https://doi.org/10.1063/5.0010540
20. Dalapati, P., Yamamoto, K., Egawa, T., & Miyoshi, M. (2020). Current-induced degradation process in (In)AlGaN-based deep-UV light-emitting diode fabricated on AlN/sapphire template. *Optical Materials, 109*, 110352. https://doi.org/https://doi.org/10.1016/j.optmat.2020.110352
21. Ruschel, J., Glaab, J., Susilo, N., Hagedorn, S., Walde, S., Ziffer, E., … Kneissl, M. (2020). Reliability of UVC LEDs fabricated on AlN/sapphire templates with different threading dislocation densities. *Applied Physics Letters, 117*(24), 241104. https://doi.org/10.1063/5.0027769
22. Trivellin, N., Fiorimonte, D., Piva, F., Buffolo, M., De Santi, C., Meneghesso, G., … Meneghini, M. (2022). Reliability of commercial UVC LEDs: 2022 state-of-the-art. *Electronics, 11*(5), 728. https://www.mdpi.com/2079-9292/11/5/728. PMID: doi:10.3390/electronics11050728
23. Dal Lago, M., Meneghini, M., Trivellin, N., Meneghesso, G., & Zanoni, E. (2011). Degradation mechanisms of high-power white LEDs activated by current and temperature. *Microelectronics Reliability, 51*(9), 1742–1746. https://doi.org/https://doi.org/10.1016/j.microrel.2011.06.057
24. RTI International. (2013). *Hammer test findings for solid-state lighting luminaires*. RTI International. https://www1.eere.energy.gov/buildings/publications/pdfs/ssl/hammer-testing_Dec2013.pdf
25. ANSI (American National Standards Institute), & IES (Illuminating Engineering Society). (2019). *ANSI/IES LM-79-19, Approved method: Optical and electrical measurements of solid state lighting products*. IES.

26. ANSI (American National Standards Institute), & IES (Illuminating Engineering Society). (2020). *ANSI/IES LM-85-20, Approved method: Optical and electrical measurements of LED packages and arrays*. IES.
27. Herrick, N. G., Kumar, S., Siebenhuhner, M., Patel, A., Dutt, G., & Pandher, R. (2017, November). Solder flux cleaning, reliability, and optical performance of UV flipchip LEDs. 2017 Surface Mount Technology Association (SMTA) Assembly, Reliability, and Testing Conference, Durham, NC.
28. IQD Frequency Products. (n.d.). *Quartz crystal ageing.* IQD Frequency Products. https://www.iqdfrequencyproducts.com/media/pg/1589/1459502414/quartz-crystal-ageing.pdf
29. de Buyl, F., & Yoshida, S. (2022). Degradation mechanisms of silicones. In W. D. van Driel & M. Yazdan Mehr (Eds.), *Reliability of organic compounds in microelectronics and optoelectronics: From physics-of-failure to physics-of-degradation* (pp. 1–31). Springer International Publishing. https://doi.org/10.1007/978-3-030-81576-9_1
30. Nagasawa, Y., & Hirano, A. (2019). Review of encapsulation materials for AlGaN-based deep-ultraviolet light-emitting diodes. *Photonics Research, 7*(8), B55–B65. https://doi.org/10.1364/PRJ.7.000B55
31. Kim, H.-Y., Lee, J.-W., Jun, D.-J., Song, S.-J., Oh, J.-T., Jeong, H.-H., … Amano, H. (2020). Effects of ultraviolet wavelength and ambient temperature on reliability of silicones in InAlGaN-based light-emitting-diode package. *ECS Journal of Solid State Science and Technology, 9*(3), 035005. https://doi.org/10.1149/2162-8777/ab7c40
32. Fan, J., Jing, Z., Cao, Y., Ibrahim, M. S., Li, M., Fan, X., & Zhang, G. (2021). Prognostics of radiation power degradation lifetime for ultraviolet light-emitting diodes using stochastic data-driven models. *Energy and AI, 4*, 100066. https://doi.org/https://doi.org/10.1016/j.egyai.2021.100066
33. Ryu, H.-Y. (2014). Numerical study on the wavelength-dependence of light extraction efficiency in AlGaN-based ultraviolet light-emitting diodes. *Optical and Quantum Electronics, 46*(10), 1329–1335. https://doi.org/10.1007/s11082-014-9877-3
34. Gong, Z., Gaevski, M., Adivarahan, V., Sun, W., Shatalov, M., & Khan, M. A. (2006). Optical power degradation mechanisms in AlGaN-based 280nm deep ultraviolet light-emitting diodes on sapphire. *Applied Physics Letters, 88*(12), 121106. https://doi.org/10.1063/1.2187429
35. Sakowski, K., Marcinkowski, L., Krukowski, S., Grzanka, S., & Litwin-Staszewska, E. (2012). Simulation of trap-assisted tunneling effect on characteristics of gallium nitride diodes. *Journal of Applied Physics, 111*(12), 123115. https://doi.org/10.1063/1.4730772
36. Jung, E., Lee, J. K., Kim, M. S., & Kim, H. (2015). Leakage current analysis of GaN-based light-emitting diodes Uusing a parasitic diode model. *IEEE Transactions on Electron Devices, 62*(10), 3322–3325. https://doi.org/10.1109/TED.2015.2468581
37. Xiu, H., Zhang, Y., Fu, J., Ma, Z., Zhao, L., & Feng, J. (2019). Degradation behavior of deep UV-LEDs studied by electro-optical methods and transmission electron microscopy. *Current Applied Physics, 19*(1), 20–24. https://doi.org/https://doi.org/10.1016/j.cap.2018.10.019

Appendix A: Ultraviolet Light-Emitting Diode Products Examined During This Study

The ultraviolet (UV) light-emitting diode (LEDs) products examined during this study were classified by semiconductor chemistry (e.g., indium gallium nitride [InGaN], aluminum gallium nitride [AlGaN]) and major features of the LED package. **Figure A-1** provides a summary of these features, along with a photograph of each UV LED package. Additional details are provided in the initial benchmark report of the LEDs in this test matrix [1].

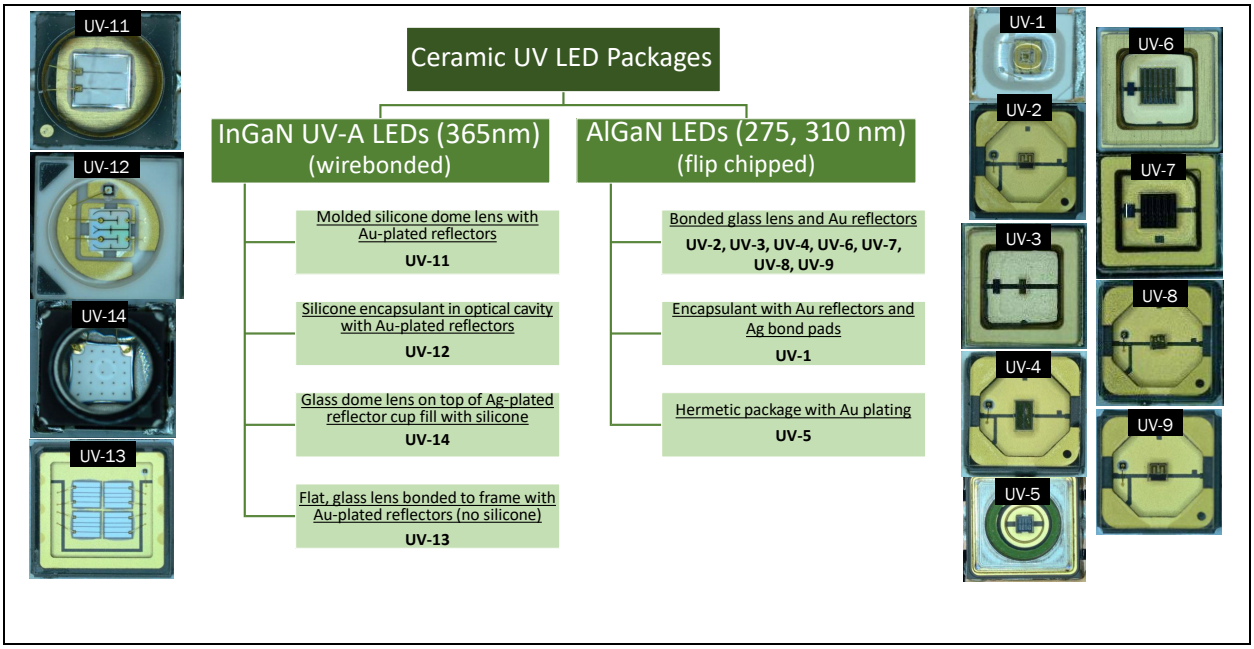

Figure A-1. The UV LED products studied, with details of their LED packages: (left) InGaN UV-A LEDs and (right) AlGaN LEDs.

Note: Ag = silver; Au = gold; nm = nanometer.

Appendix B: Current-Voltage Measurement (I-V) of Ultraviolet (UV) Light-Emitting Diodes (LEDs) in This Study

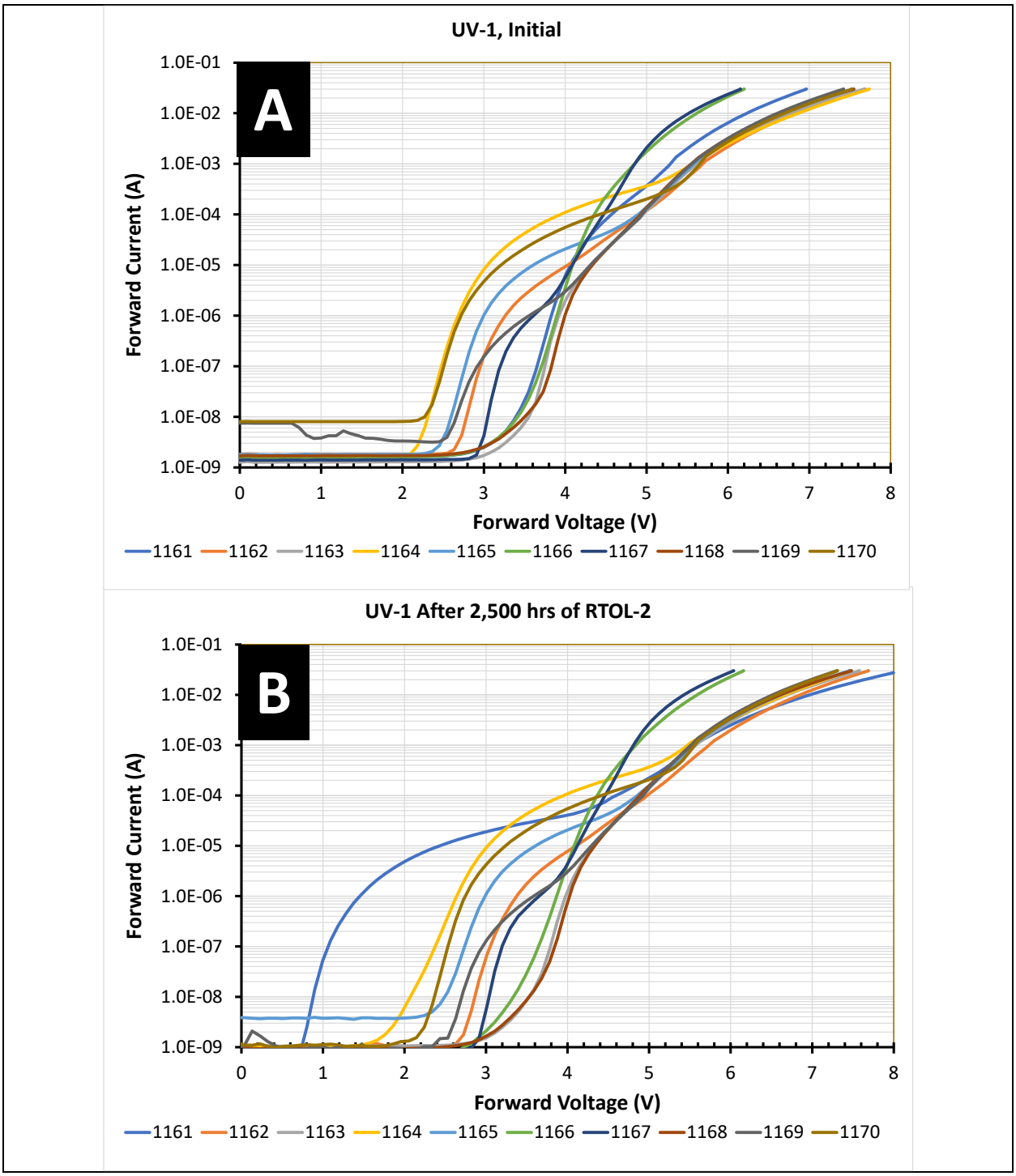

Figure B-1. I-V curves of the UV-1 DUTs under test (DUTs) during room temperature operating life (RTOL)-2: (A) the I-V curves as received in the initial condition; (B) the I-V curves after 2,500 hours (hrs) of RTOL-2.

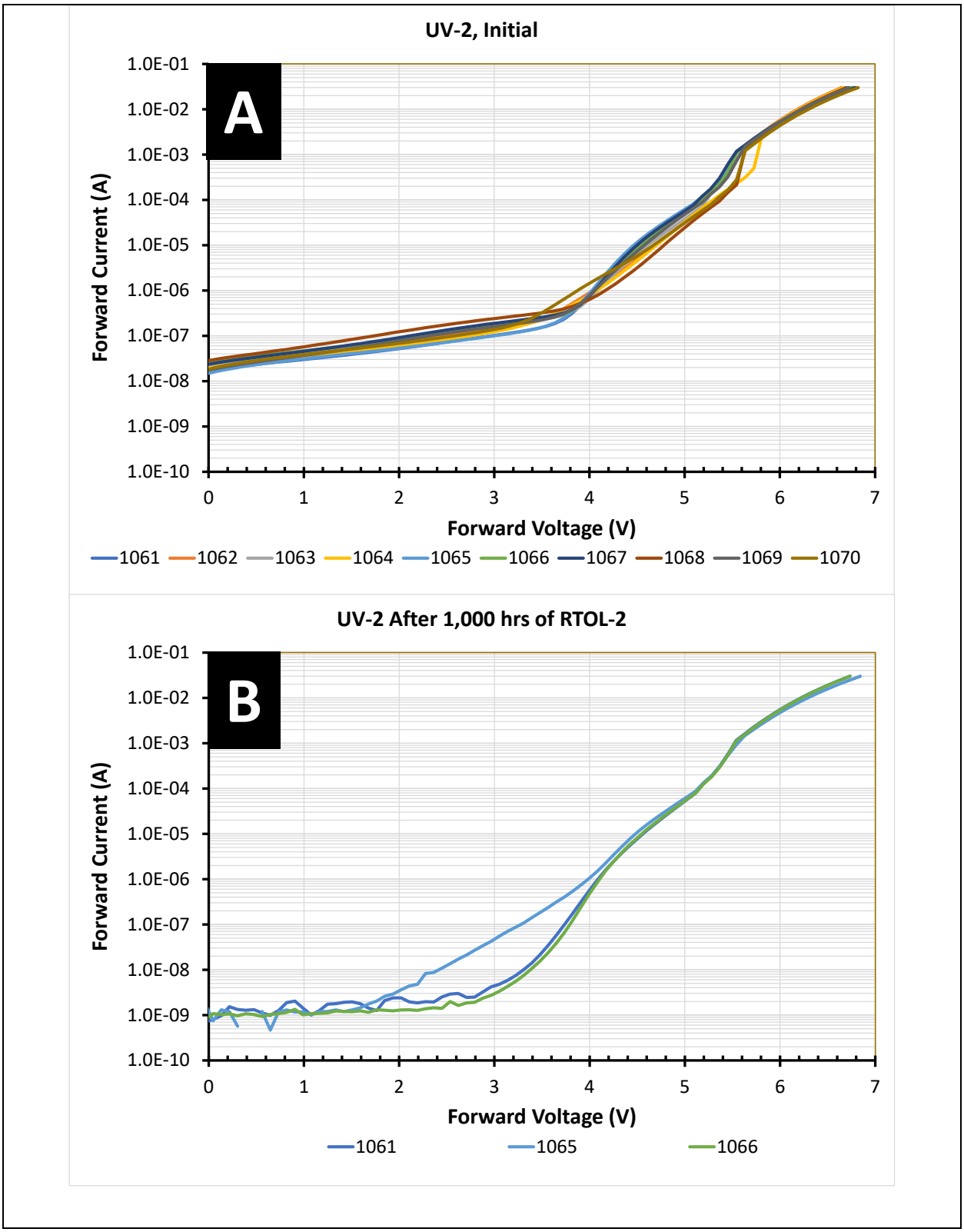

Figure B-2. I-V curves of the UV-2 DUTs during RTOL-2: (A) the I-V curves as received in the initial condition; (B) the I-V curves after 2,500 hrs of RTOL-2.

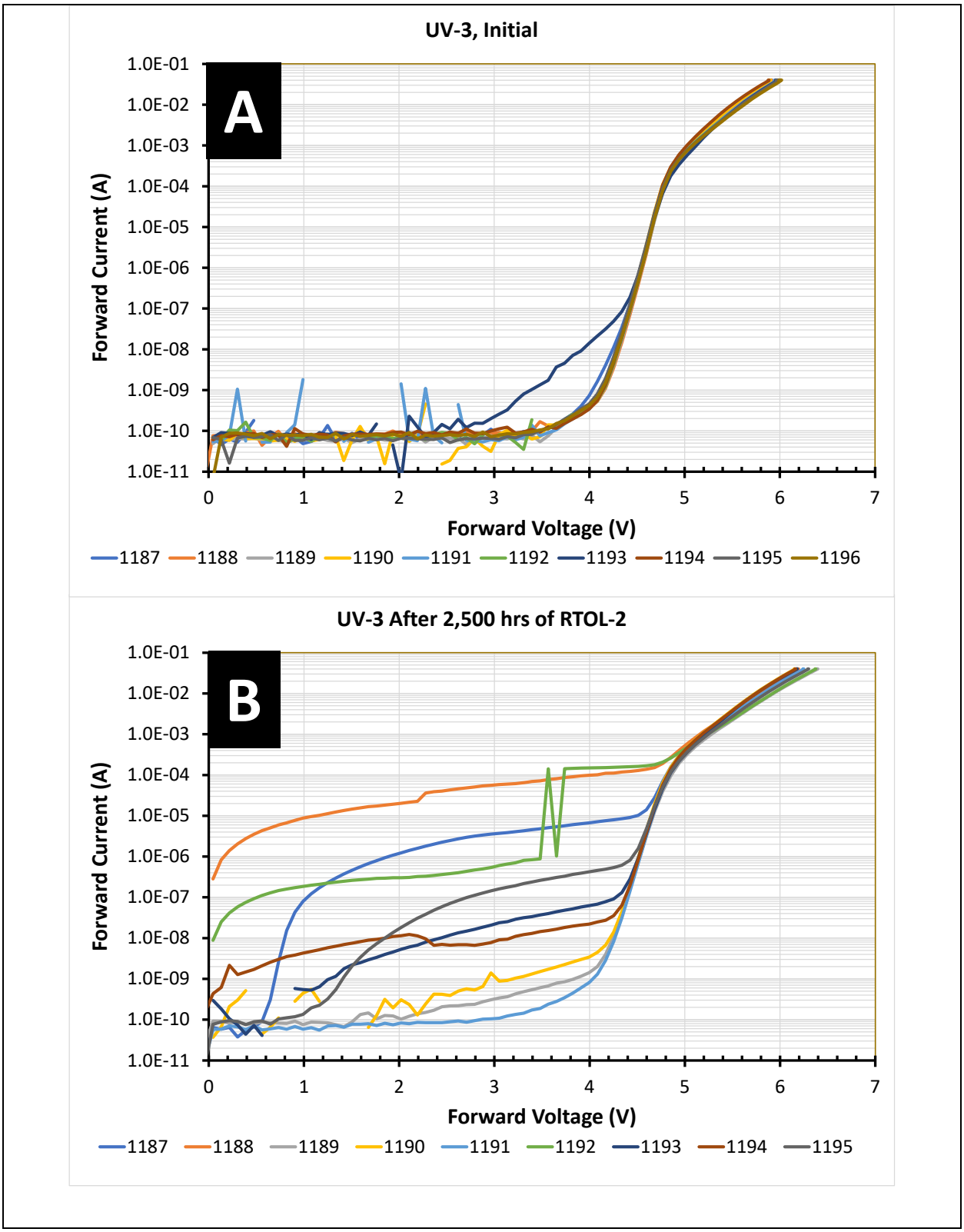

Figure B-3. I-V curves of the UV-3 DUTs during RTOL-2: (A) the I-V curves as received in the initial condition; (B) the I-V curves after 2,500 hrs of RTOL-2.

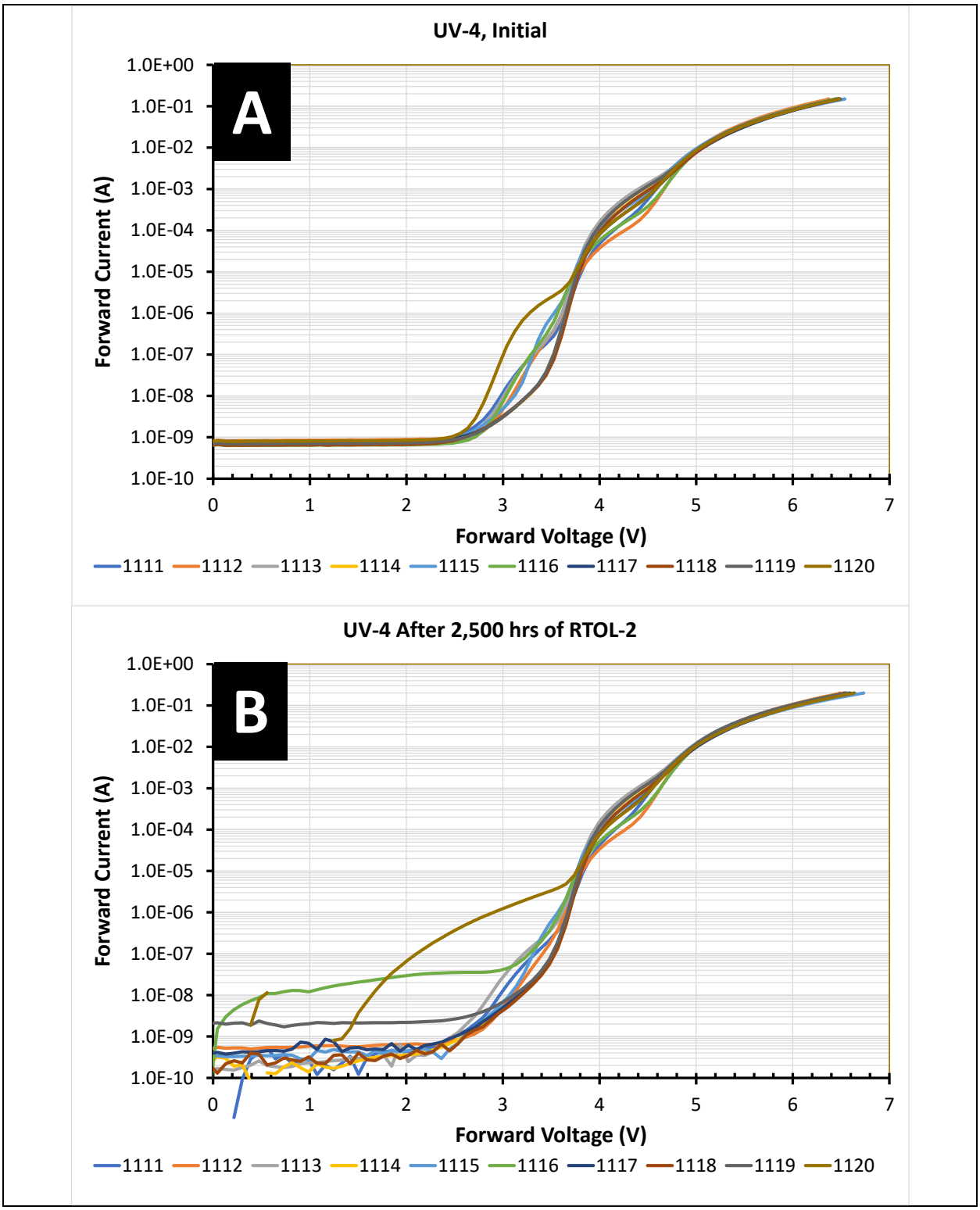

Figure B-4. I-V curves of the UV-4 DUTs during RTOL-2: (A) the I-V curves as received in the initial condition; (B) the I-V curves after 2,500 hrs of RTOL-2.

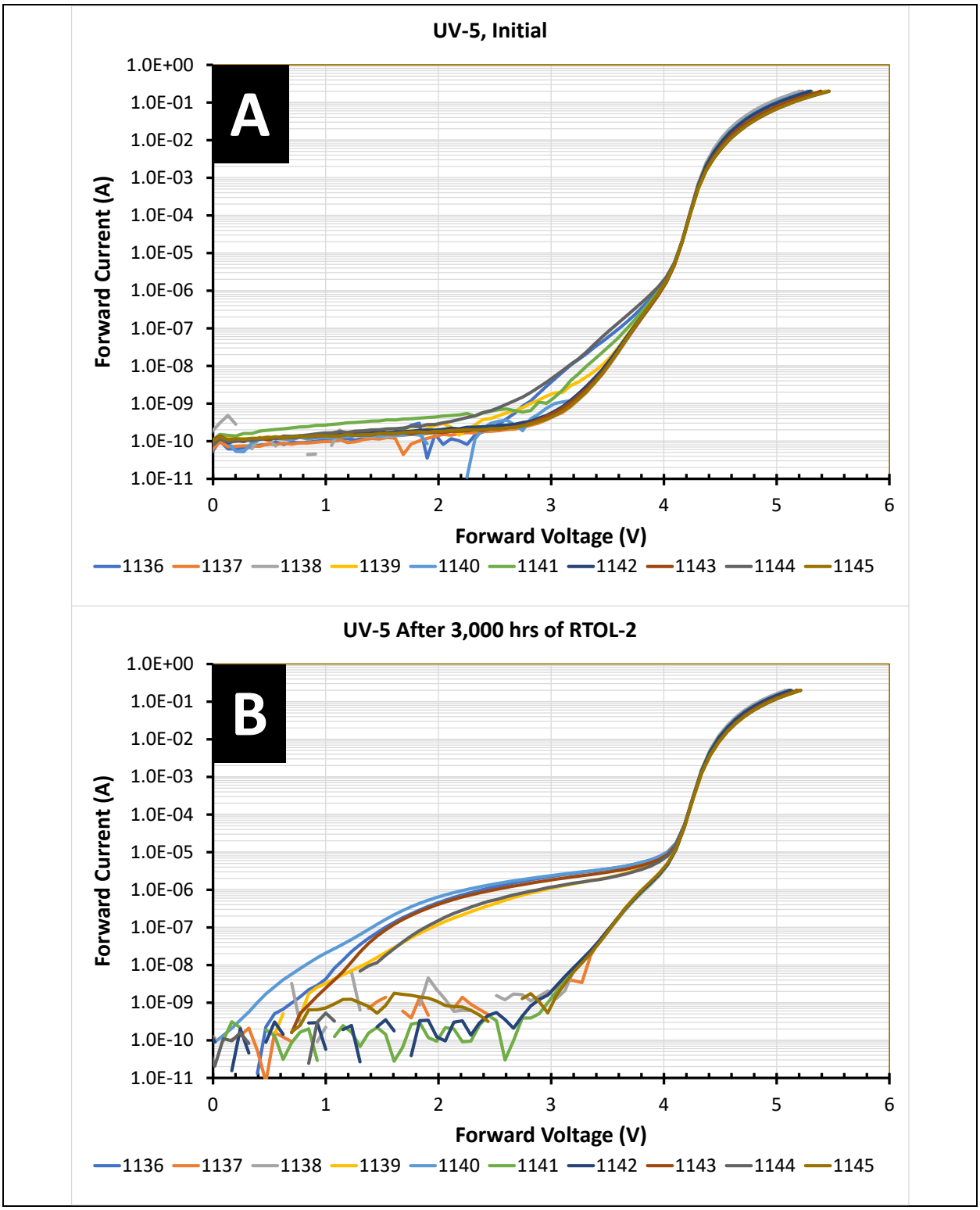

Figure B-5. I-V curves of the UV-5 DUTs during RTOL-2: (A) the I-V curves as received in the initial condition; (B) the I-V curves after 3,000 hrs of RTOL-2.

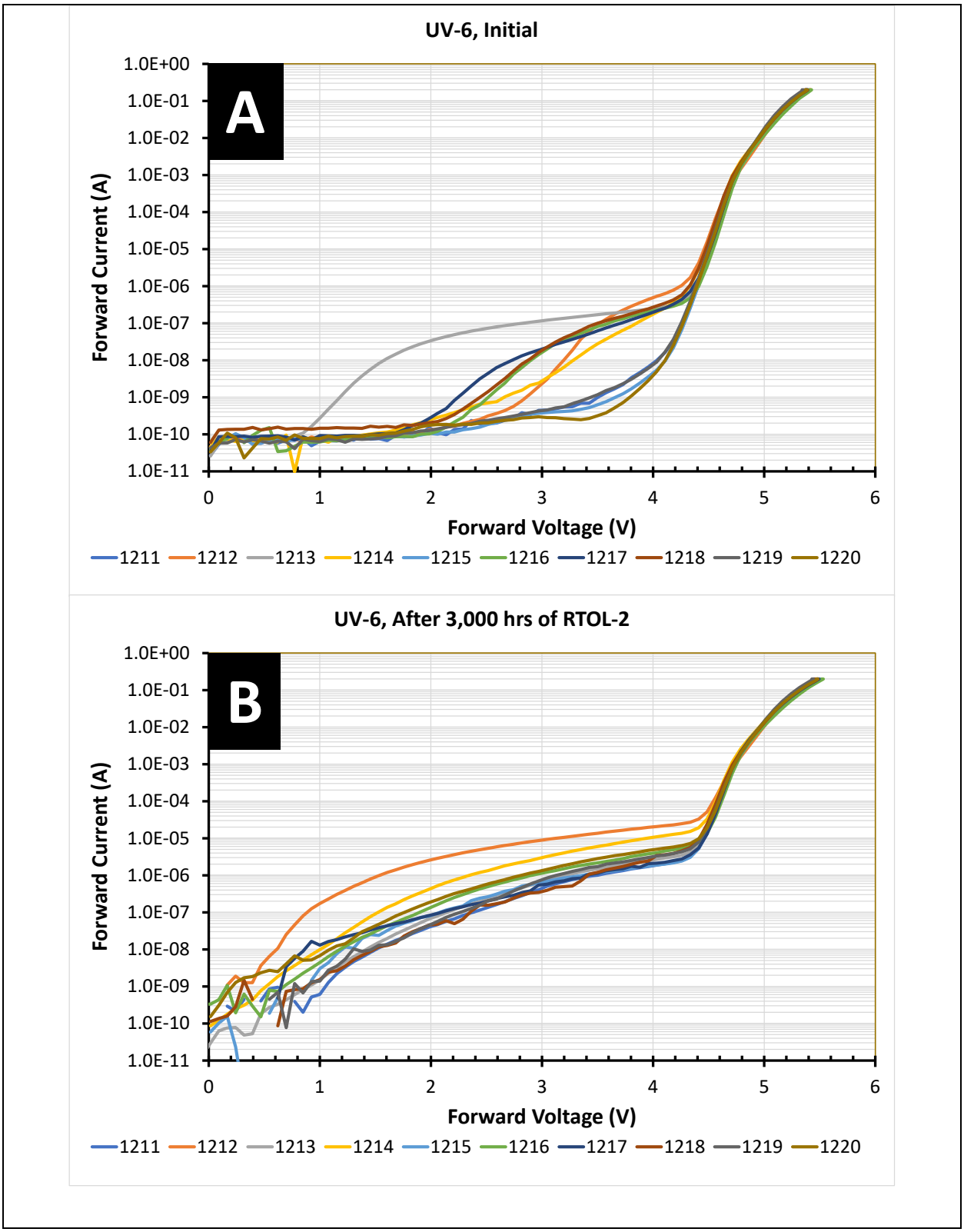

Figure B-6. I-V curves of the UV-6 DUTs during RTOL-2: (A) the I-V curves as received in the initial condition; (B) the I-V curves after 3,000 hrs of RTOL-2.

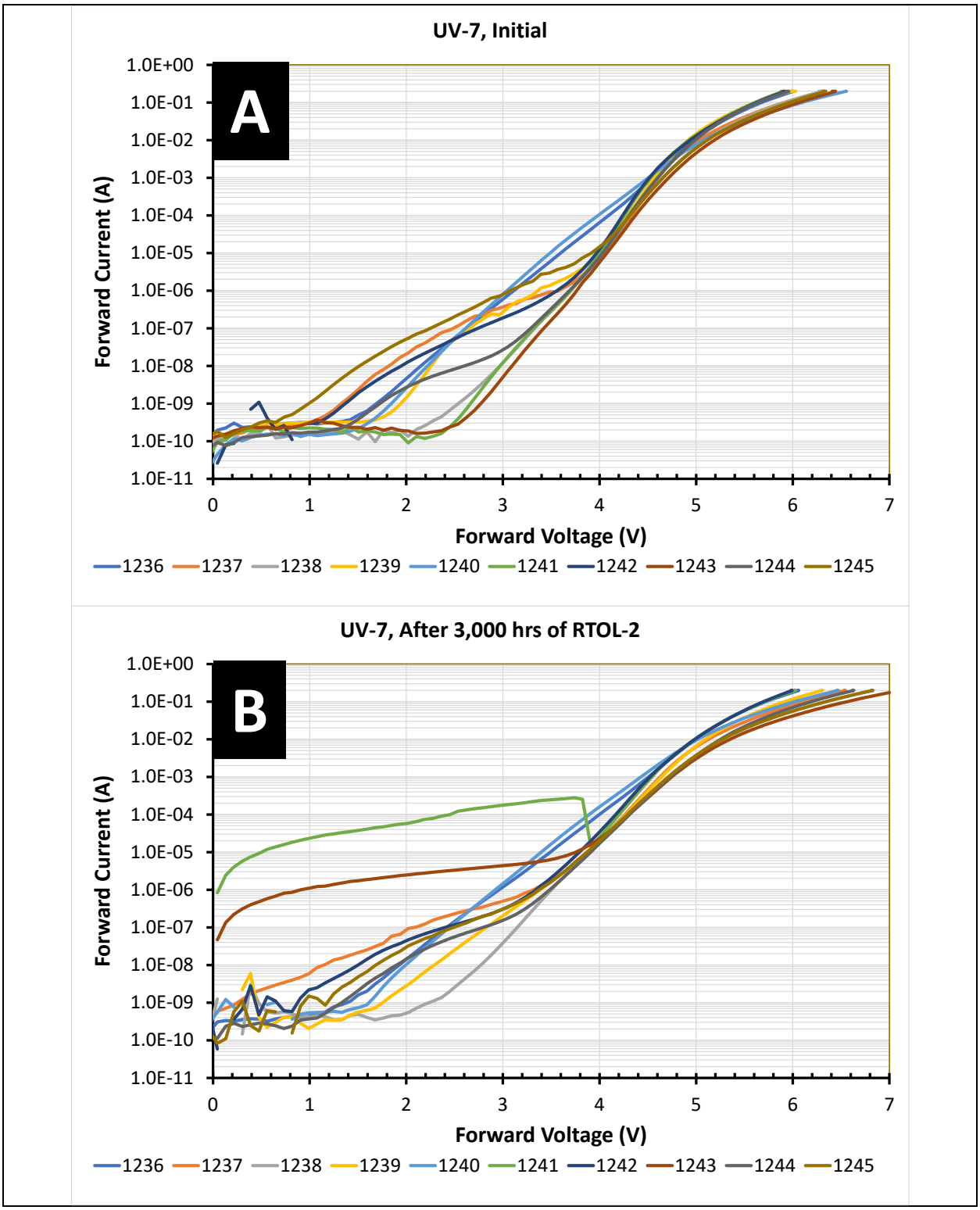

Figure B-7. I-V curves of the UV-7 DUTs during RTOL-2: (A) the I-V curves as received in the initial condition; (B) the I-V curves after 3,000 hrs of RTOL-2.

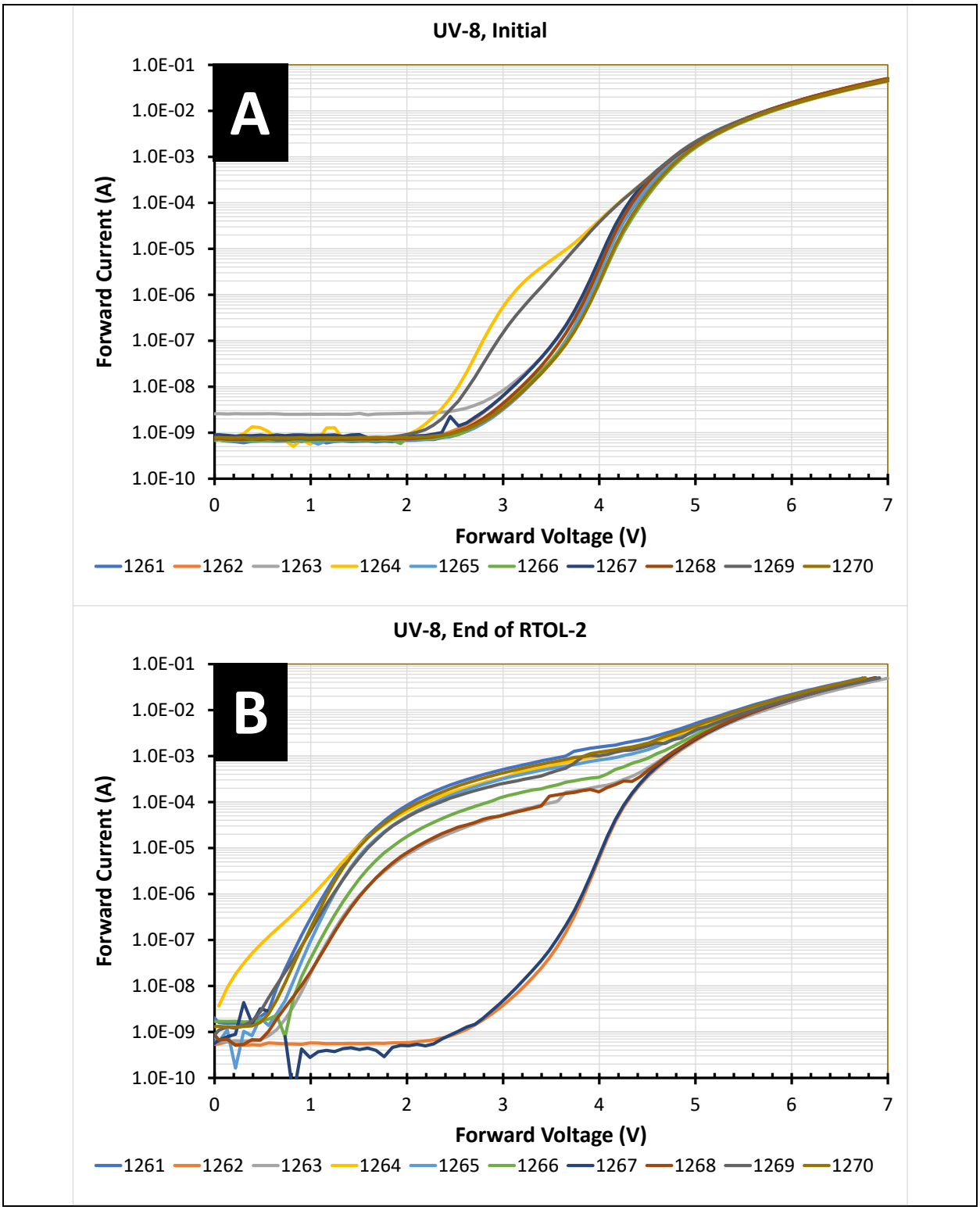

Figure B-8. I-V curves of the UV-8 DUTs during RTOL-2: (A) the I-V curves as received in the initial condition; (B) the I-V curves after 2,000 hrs of RTOL-2 for DUT-1261, DUT-1264, DUT-1265, DUT-1266, DUT-1269, and DUT-1270 and 2,500 hrs for DUT-1262, DUT-1263, DUT-1267, and DUT-1268.

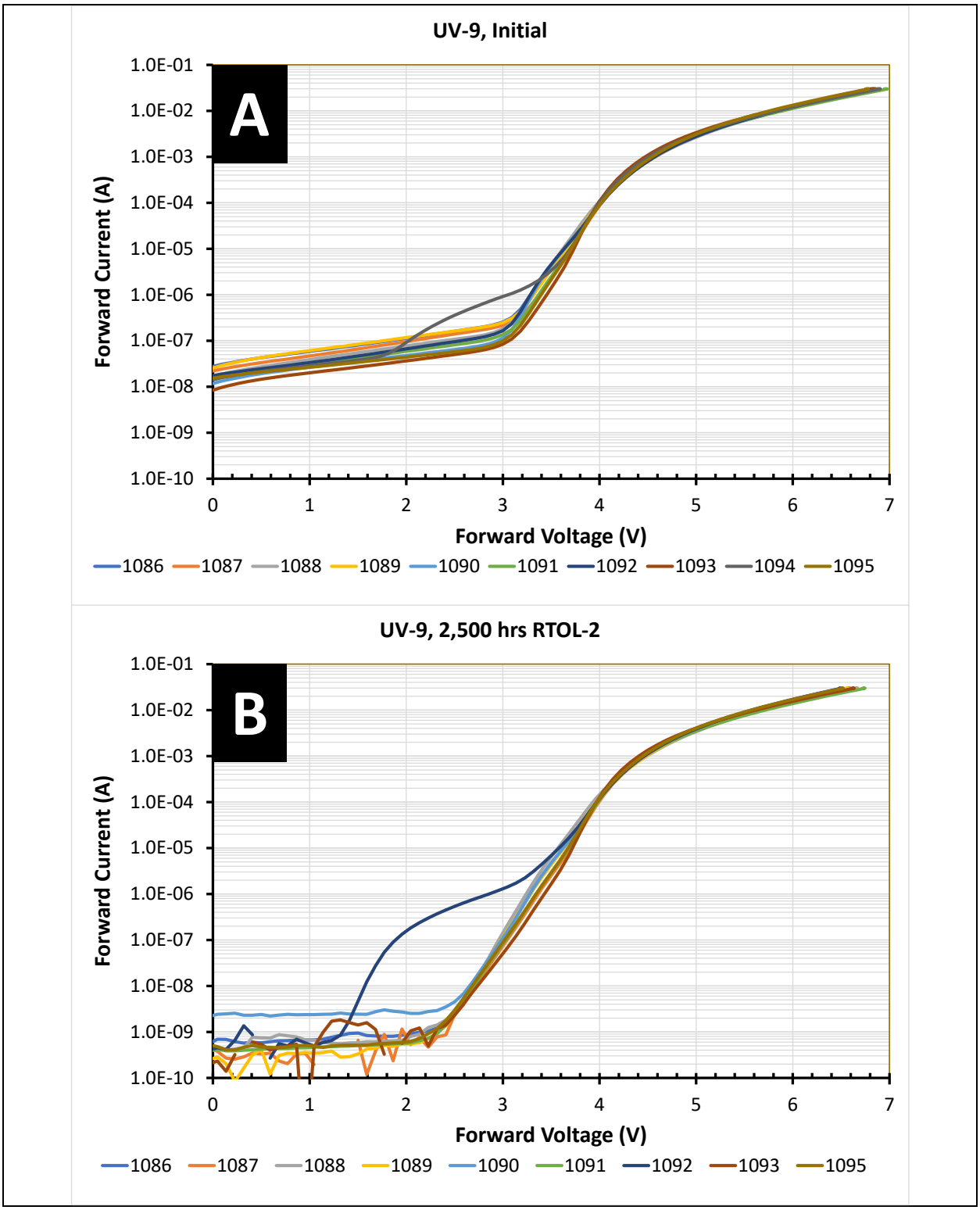

Figure B-9. I-V curves of the UV-9 DUTs during RTOL-2: (A) the I-V curves as received in the initial condition; (B) the I-V curves after 2,500 hrs of RTOL-2.

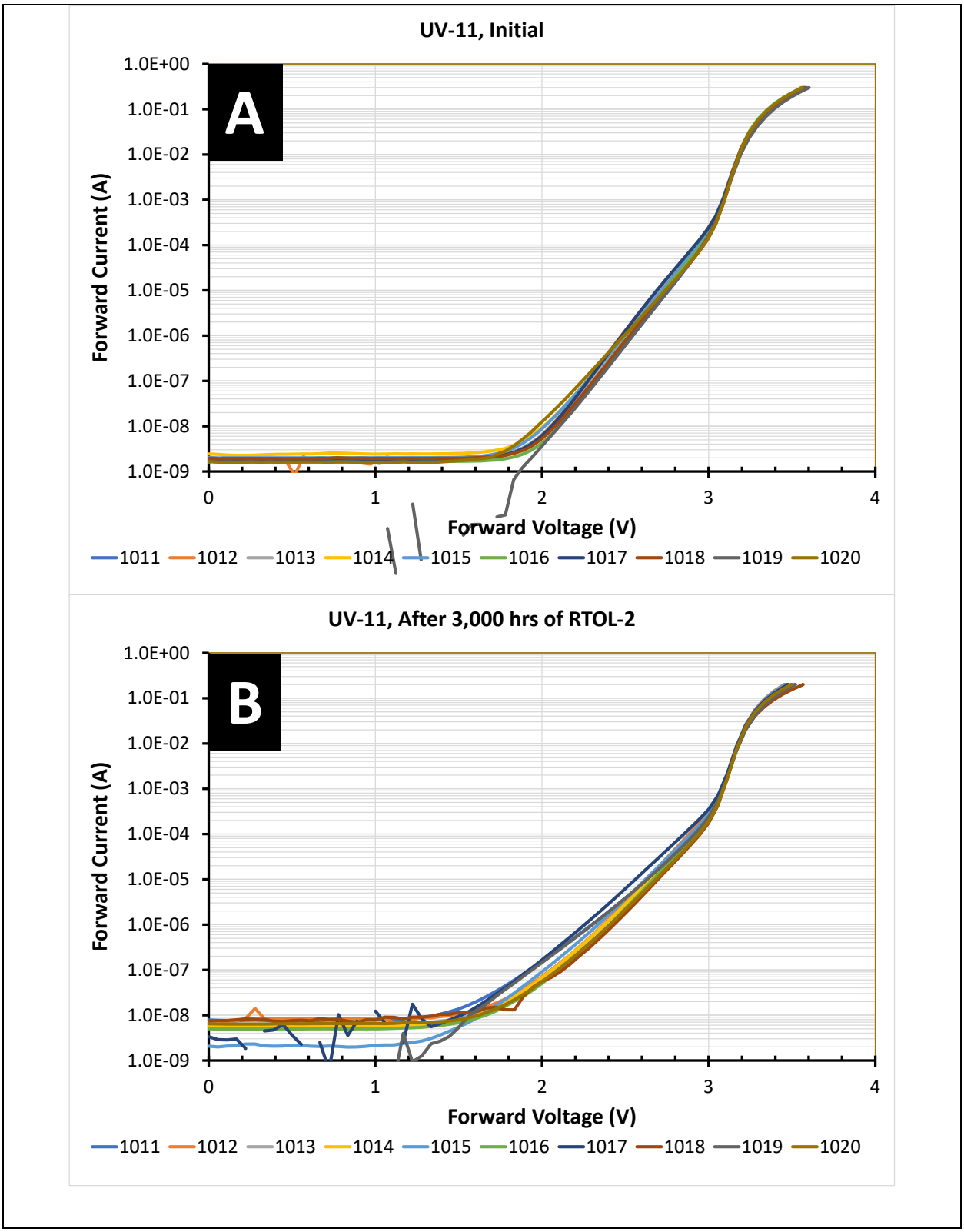

Figure B-10. I-V curves of the UV-11 DUTs during RTOL-2: (A) the I-V curves as received in the initial condition; (B) the I-V curves after 3,000 hrs of RTOL-2.

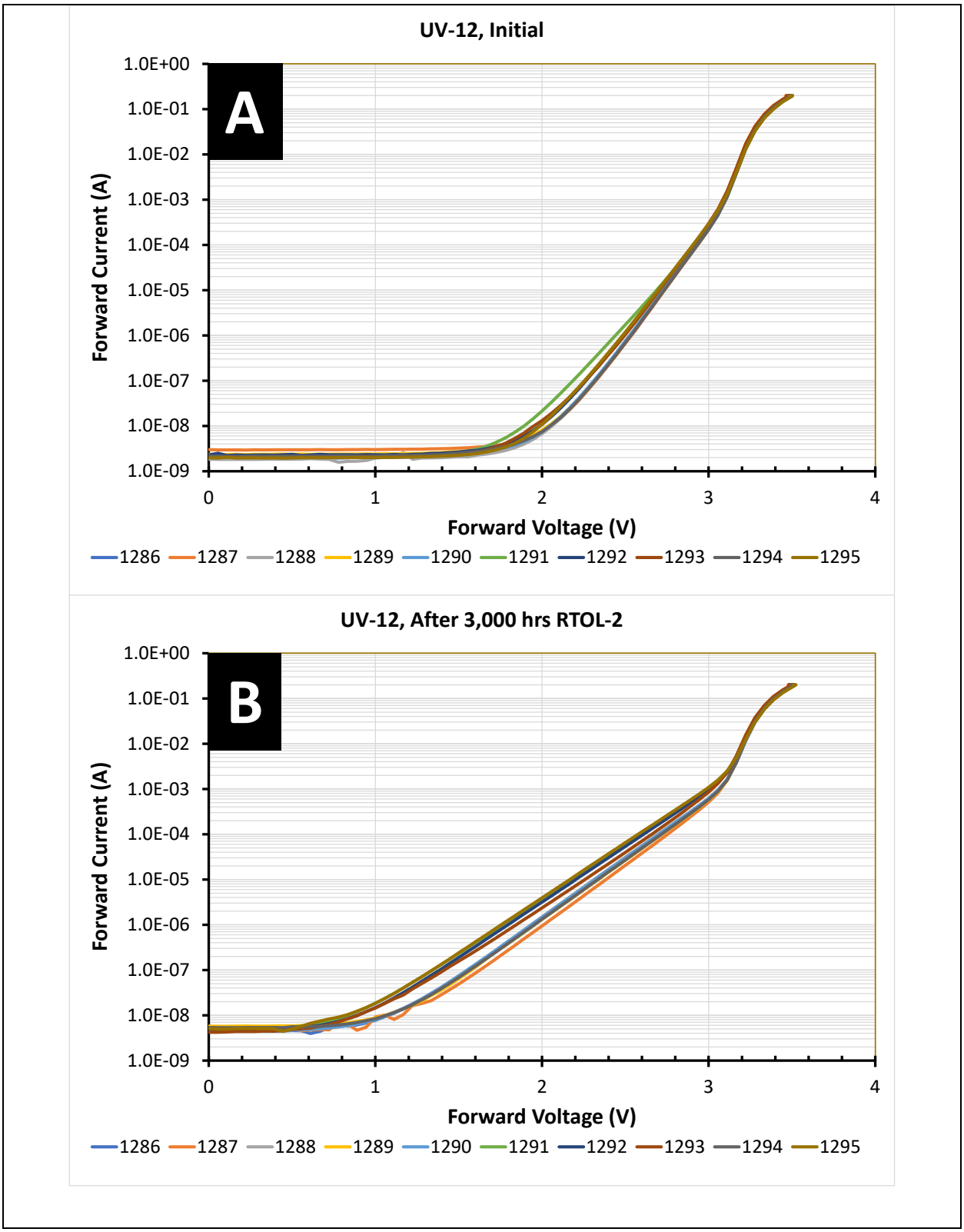

Figure B-11. I-V curves of the UV-12 DUTs during RTOL-2: (A) the I-V curves as received in the initial condition; (B) the I-V curves after 3,000 hrs of RTOL-2.

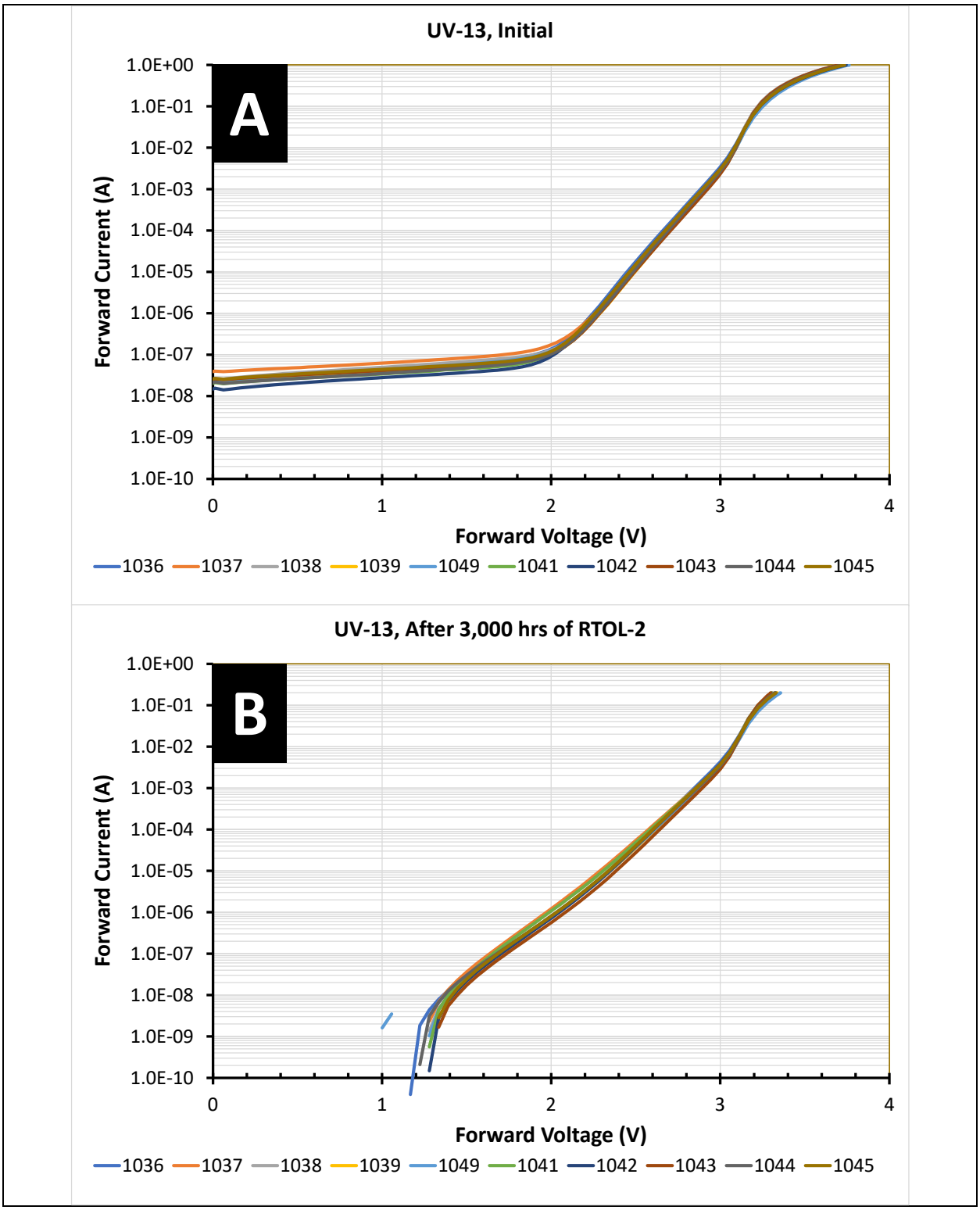

Figure B-12. I-V curves of the UV-13 DUTs during RTOL-2: (A) the I-V curves as received in the initial condition; (B) the I-V curves after 3,000 hrs of RTOL-2.

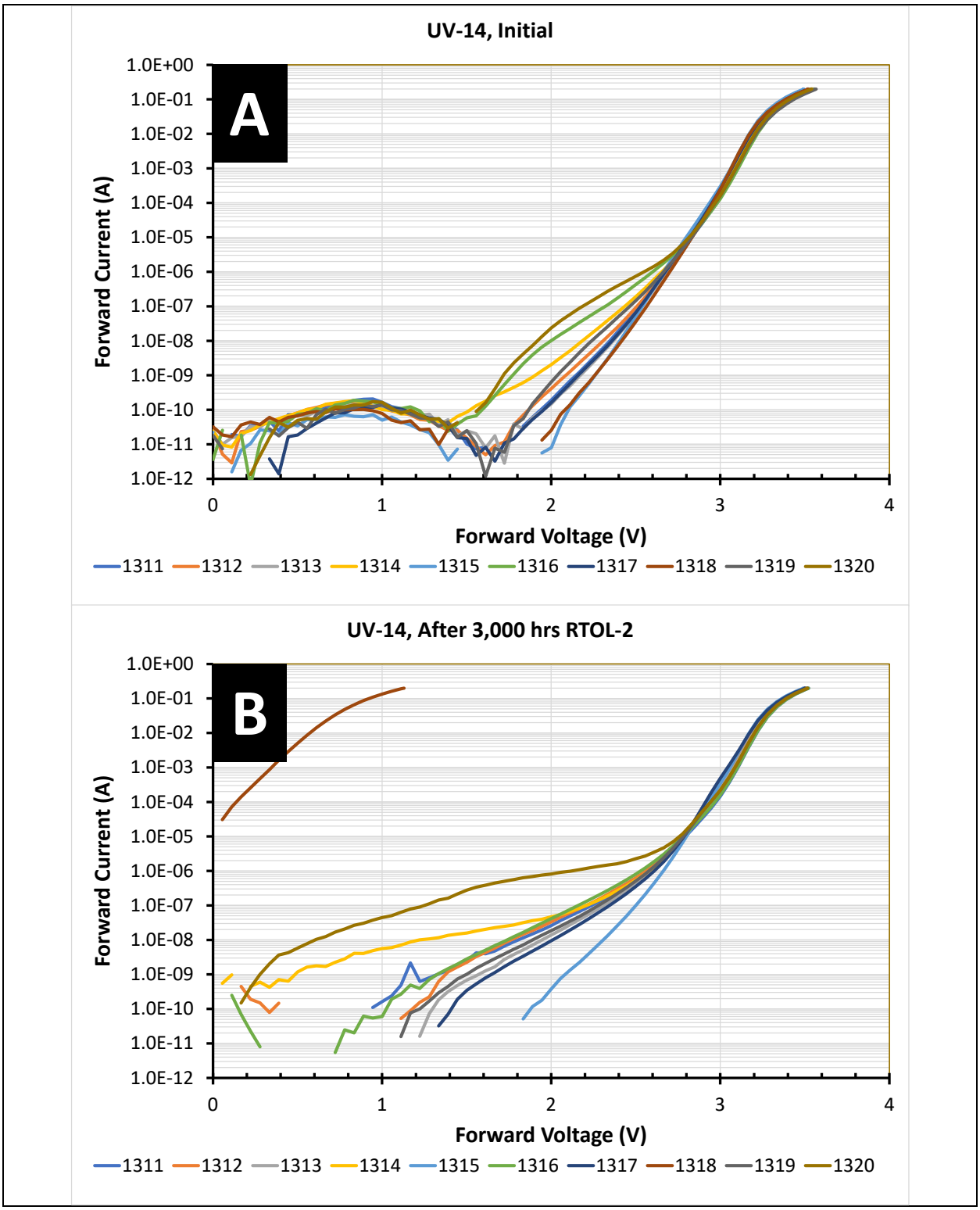

Figure B-13. I-V curves of the UV-14 DUTs during RTOL-2: (A) the I-V curves as received in the initial condition; (B) the I-V curves after 3,000 hrs of RTOL-2.

(This page intentionally left blank)

U.S. DEPARTMENT OF
ENERGY

Office of
ENERGY EFFICIENCY &
RENEWABLE ENERGY

For more information,
visit: energy.gov/eere/ssl

DOE/EE-2592 • April 2022